STRATIFICATION LIMITED VERTICAL VENTILATION: EFFECTS OF WATER COLUMN STABILITIES ON THE FORMATION OF HYPOXIA ON THE TEXAS-LOUISIANA SHELF

A Dissertation

by

BO LI

Submitted to the Office of Graduate and Professional Studies of
Texas A&M University
in partial fulfillment of the requirements for the degree of

DOCTOR OF PHILOSOPHY

Chair of Committee,	Steven F. DiMarco
Committee Members,	Robert D. Hetland
	George A. Jackson
	Xiaopei Lin
	Antonietta S. Quigg
Head of Department,	Piers Chapman

December 2013

Major Subject: Oceanography

ABSTRACT

I examine the vertical structure of water-column stability and its relationship to near-bottom dissolved oxygen (DO) concentration in the hypoxic zone of the Texas-Louisiana Shelf using observations collected between year 2003 and 2009. A threshold of N=0.06 s^{-1} is defined to represent the lower limit of the stratification strength for existence of hypoxia. An idealized one-dimensional model with parameterized respiration was applied to study stratification structure associated hypoxia development. The simulation results showed that the bottom mixed layer could enhance the bottom DO depletion and favor the development of hypoxia. A secondary pycnocline was above the bottom mixed layer and performed as a barrier to inhibit the vertical extension of hypoxia and vertical DO flux through it. Furthermore, I discussed possible mechanisms causing bottom mixed layer on the continental shelf, including return flow caused by upwelling, inertial motions and tidal currents.

Diapycnal diffusivity was calculated using hourly continuous observations in the hypoxic zone on the Texas-Louisiana Shelf. The estimated time-averaged diapycnal diffusivity was 3×10^{-6} m^2 s^{-1} along the pycnocline. Averaged cross-pycnocline vertical dissolved oxygen flux was calculated in a two-layer stratified water column with subpycnocline hypoxia. The estimated cross-pycnocline dissolved oxygen flux was 156.8 ml l^{-1} d^{-1}, which resupplied 45% dissolved oxygen consumption in the subpycnocline layer.

Continuous observations at the South Marsh Mooring showed the first highly resolved observations of short timescale fluctuations in the DO concentrations in the seasonal hypoxic waters on the Louisiana Shelf. There were 19 ventilation events in the DO records with a time period of 1~3 days. Analysis of the time series of DO, salinity and temperature at different levels of the mooring demonstrated that most of the ventilation-intervals were associated with increased vertical mixing, which contributed 58% of the total ventilation intervals. It suggests that mixing events dominate the ventilation-intervals. Comparison of the time derivative of the low-frequency part of the near-bottom DO concentration to observations of the wind and significant wave height suggests that local wind events are responsible for the enhanced vertical mixing.

DEDICATION

To my parents Mingji Li and Xiuping Kang

and

my wife Lifei Liu

ACKNOWLEDGEMENTS

I would like to thank my committee chair, Dr. Steven DiMarco, for his excellent assistance and guidance in my research, for giving me several opportunities to join research cruises and attend national conferences, and for all the other support in the last five years to help me finish my research. I also want to express my thanks to my other committee members: Dr. Robert Hetland, for his help in turbulence theory and dynamical analysis; Dr. George Jackson for his assistance in the model study and very helpful advice in my research and writing; Dr. Xiaopei Lin, for all his invaluable suggestions and comments on my research; Dr. Antonietta Quigg, for her helpful comments of the knowledge in biological sciences.

I also want to express my thanks to the Geochemical and Environmental Research Group (GERG) for instrument deployments and sample analysis.

Thanks also go to my friends and colleagues and the department faculty and staff for making my time at Texas A&M University a great experience.

I would like to thank the National Oceanic and Atmospheric Administration (NOAA) Center for Sponsored Coastal Ocean Research, whose funding for the Mechanisms Controlling Hypoxia (MCH) Project on the Texas-Louisiana shelf under contract Nos. NA03N0S4780039, NA06N0S4780198 and NA09N0S4780208 support this study.

At last, I want to thank the China Scholarship Council (CSC) for the financial support to help me finish my study in Texas A&M University.

TABLE OF CONTENTS

ABSTRACT ii

DEDICATION iv

ACKNOWLEDGEMENTS v

TABLE OF CONTENTS vi

LIST OF FIGURES viii

LIST OF TABLES xiv

CHAPTER I INTRODUCTION 1

1.1. Background 1
1.2. Hypoxia in the Northern Gulf of Mexico along the Texas-Louisiana Shelf 3
1.3. Physical description of the Texas-Louisiana Shelf 10
1.4. Study objectives 14
1.5. Organization 15

CHAPTER II DATA AND METHODOLOGIES 17

2.1. Observations 17
2.1.1. Historical observations 18
2.1.2. Survey cruises 21
2.1.3. Continuous CTD observations 23
2.1.4. South Marsh Mooring 24
2.2. Methodologies 24
2.2.1. Data methods 24
2.2.2. One dimension models 34

CHAPTER III STRATIFICATION STRUCTURE AND VERTICAL DISTRIBUTION OF DO 42

3.1. Results 46
3.1.1. Horizontal distribution of hypoxia 46
3.1.2. Vertical distribution of hypoxia from Acrobat transects 49
3.1.3. Stratification strength and development of hypoxia 54
3.1.4. Observed stratification structure and vertical distribution of hypoxia 57
3.1.5. Modeling hypoxia development under different stratification structures 62

3.2. Discussion 76
3.2.1. Stratification limit and hypoxia 76
3.2.2. Stratification structure and vertical distribution of hypoxia 77
3.2.3. Bottom mixed layer and hypoxia 79
3.2.4. Secondary pycnocline 80
3.2.5. Water column respiration and benthic respiration 81
3.2.6. Mechanisms causing bottom mixed layer 83

CHAPTER IV ESTIMATION OF VERTICAL EDDY DIFFUSIVITY AND CROSS-PYCNOCLINE DO FLUX 86

4.1. Results 86
4.1.1. Temporal changes of the stratification structure and vertical distribution of hypoxia 86
4.1.2. Estimation of K_Z 95
4.1.3. Vertical DO flux through pycnocline 97
4.2. Discussion 98
4.2.1. Temporal changes of DO concentration 98
4.2.2. Diapycnal diffusivity and vertical DO flux through pycnocline 99

CHAPTER V INTERMITTENT VENTILATION IN THE HYPOXIC ZONE ON TEXAS-LOUISIANA SHELF 102

5.1. Results 102
5.1.1. Observation results from the raw time series 102
5.1.2. Intermittent ventilation in the hypoxic zone 110
5.1.3. Mixing induced intermittent ventilation 114
5.1.4. Wind induced mixing 119
5.2. Discussions 120
5.2.1. DO budget 120
5.2.2. Fast DO depletion after ventilation-intervals 121
5.2.3. Ventilation mechanisms 121

CHAPTER VI CONCLUSIONS 123

REFERENCES 126

LIST OF FIGURES

Page

Figure 1.1 Study area and bathymetry for the MCH program on the Texas-Louisiana Shelf in northern Gulf of Mexico. The 10, 20, 30, 40, 50, 100, 200, 500, 1000, 2000 m isobaths are shown. 11

Figure 2.1 CTD stations (black dots) for MCH cruises (M00-M14). The 10, 20, 30, 40, 50 m isobaths are shown. 20

Figure 2.2 Top: The mean (solid) and standard deviations (dashed) of the estimated bottom (left) and surface (right) mixed layer thickness from the all CTD stations between 2003 and 2009 as a function of the choice of $\Delta\rho$. Bottom: The mean (solid) and standard deviations (dashed) of N in the bottom (left) and surface (right) layer as a function of the choice of $\Delta\rho$ for the same data set. 27

Figure 2.3 A typical CTD profile with double-pycnocline structure. The black vertical solid line is the threshold of $N = 0.05\ s^{-1}$. Surface-layer, mid-layer and bottom-layer are marked in the grey band. Main-pycnocline and secondary-pycnocline are marked in white band. 29

Figure 2.4 The averaged N at each bin above bottom for all the CTD profiles from MCH cruises between 2003 and 2009. 30

Figure 2.5 Estimated mean (solid) and standard deviations (dashed) of the height of the weakly stratified layer above bottom as a function of the choice of critical N. 32

Figure 2.6 Schema for the one-dimensional subpycnocline box model of DO. Vertical axis is marked on the left. 0 depth and $-b$ stand for sea surface and bottom, respectively. h and d are the thickness of subpycnocline layer and pycnocline respectively. R is the subpycnoline water-column oxygen consumption rate. 33

Figure 2.7 The water column respiration (upper panel) and benthic respiration (bottom panel) at 25 °C used in the model. 36

Figure 2.8 Simulated DO profiles changing with time with different K_Z: (a) $K_Z = 1 \times 10^{-6}\ m^2s^{-1}$; (b) $K_Z = 1 \times 10^{-5}\ m^2s^{-1}$; (c) $K_Z = 1 \times 10^{-4}\ m^2s^{-1}$; (d) $K_Z = 1 \times 10^{-3}\ m^2s^{-1}$. Hypoxia formation time in bottom layer with different K_Z is shown in (e). 38

Figure 2.9 The vertical profile of K_Z of the three cases: single main pycnocline, single near-bottom pycnocline and double pycnoclines (from left to right). 40

Figure 3.1 Near bottom DO concentration during MS2 cruise, 2-7 August 2010, using optimal interpolation of CTD and "Acrobat" data. Black dots represent the location of CTD casts and bottom measurements from "Acrobat". Hypoxic (DO < 1.4 ml l^{-1}) regions are in deep blue and circled out by white lines (S. F. DiMarco unpublished). 42

Figure 3.2 DO concentration during MS4 cruise, 8-15 August 2011, using optimal interpolation of CTD data. Black dots represent locations of CTD casts (S. F. DiMarco unpublished). 43

Figure 3.3 Vertical DO (ml l^{-1}) distributions along the "Acrobat" transects on the Texas-Louisiana Shelf during MS2 cruise in August 2010. Coastlines and bathymetry are included. 44

Figure 3.4 Vertical salinity (PSU) distributions along the "Acrobat" transects on the Texas-Louisiana Shelf during MS2 cruise in August 2010. Coastlines and bathymetry are included. 45

Figure 3.5 Vertical DO (ml l^{-1}) distributions along the "Acrobat" transects on the Texas-Louisiana Shelf during MS4 cruise in August 2011. Coastlines and bathymetry are included. 47

Figure 3.6 Vertical Salinity (PSU) distributions along the "Acrobat" transects on the Texas-Louisiana Shelf during MS4 cruise in August 2011. Coastlines and bathymetry are included. 48

Figure 3.7 Cross-shore transect during the MS2 cruise in August 2010. Top: the color map denotes DO concentration, the red contour lines denote the boundary of the hypoxia and the black contour lines denote salinity. Bottom: contour plot of N for the same section in unit of s^{-1} while the red contour lines denote $N = 0.05$ s^{-1}. Black lines below the color map show the bottom in both panels. 49

Figure 3.8 Cross-shore transect during MS2 cruise, August 2010. Top: the color map denotes DO concentration, the red contour lines denote the boundary of hypoxia, and the black contour lines denote salinity. Bottom: contour plot of N for the same transect in unit of s^{-1} while the red contour lines denote $N = 0.05$ s^{-1}. Black lines below the color map show the bottom in both panels. 51

Figure 3.9 Cross-shore transect during the MS4 cruise in August 2011. Top: the color map denotes DO concentration, the red contour lines denote the boundary of the hypoxia, and the black contour lines denote salinity. Bottom: contour plot of N for the same section in unit of s^{-1} while the red contour lines denote N = 0.05 s^{-1}. Black lines below the color map show the bottom in both panels. 52

Figure 3.10 Upper panel: near-bottom DO concentration versus N_{max} for all the CTD profiles from MCH cruises between 2003 and 2009. The threshold of 1.4 ml l^{-1} for hypoxia are shown with horizontal solid line. Bottom panel: histogram of the number of hypoxic stations at different N_{max}. 53

Figure 3.11 Accumulation lines of hypoxic station numbers in percentage along with the N_{max} for CTD profiles from MCH cruises between 2003 and 2009 (solid) and CTD profiles from the cruises made by LUMCON to estimate the hypoxic area size between 1998 and 2007 (dashed). The horizontal solid line denotes the 1% cut-off. 55

Figure 3.12 Averaged N at each height above bottom for all the profiles (solid) and hypoxic profiles (dashed lines). 56

Figure 3.13 Histogram of the thicknesses of the hypoxic layers (or heights of the hypoxic layers above bottom) for all the profiles from the MCH cruises between 2003 and 2009 58

Figure 3.14 Histograms of thicknesses of the bottom (top) and surface mixed layers observed in the CTD profiles from MCH cruises between 2003 and 2009. 59

Figure 3.15 Scatter plot of the height of the 1.4 ml l^{-1} DO concentration isopleth above the bottom against the height of the main (red dots) and secondary (blue dots) pycnocline for the CTD profiles from MCH cruises between 2003 and 2009. (a) CTD profiles with single pycnocline (n=132). (b) CTD profiles with double-pycnocline (n=113). (c) CTD profiles with hypoxia below the secondary-pycnocline (n=57). (d) CTD profiles with hypoxia top interface between the main and secondary-pycnoclines (n=56). 60

Figure 3.16 Simulation results from the one-dimension DO model. Three cases are shown by rows from top to bottom: single mid-depth pycnocline (a1, a2, a3), single near-bottom pycnocline (b1, b2, b3), and double-pycnocline (c1, c2, c3). Figures in the left, middle and right columns are the K_Z profiles, DO concentration changes with time at bottom, 7

m and 15 m above bottom, and contour plots of DO concentration changes with time for each case. 63

Figure 3.17 Simulation results of experiment A from the one-dimension DO model. Three cases are shown by rows from top to bottom: no bottom mixed layer (A1a, A1b, A1c), moderately mixed bottom layer (A2a, A2b, A2c), and well mixed bottom layer (A3a, A3b, A3c). Figures in the left, middle and right columns are the K_Z profiles, DO concentration changes with time at bottom, 7 m and 15 m above bottom, and contour plots of DO concentration changes with time for each case. 67

Figure 3.18 Simulation results of experiment B from the one-dimension DO model. Three cases are shown by rows from top to bottom: weak secondary pycnocline (B1a, B1b, B1c), moderately strong secondary pycnocline (B2a, B2b, B2c), and strong secondary pycnocline (B3a, B3b, B3c). Figures in the left, middle and right columns are the K_Z profiles, DO concentration changes with time at bottom, 7 m and 15 m above bottom, and contour plots of DO concentration changes with time for each case. 69

Figure 3.19 Simulation results of experiment C from the one-dimension DO model. Three cases are shown by rows from top to bottom: Benthic respiration only (C1a, C1b, C1c), half water column respiration and half benthic respiration (C2a, C2b, C2c), and water column respiration only (C3a, C3b, C3c). Figures in the left, middle and right columns are the K_Z profiles, DO concentration changes with time at bottom, 7 m and 15 m above bottom, and contour plots of DO concentration changes with time for each case. 72

Figure 3.20 Simulation results of experiment D from the one-dimension DO model. Three cases are shown by rows from top to bottom: 3 m bottom mixed layer (D1a, D1b, D1c), 4 m bottom mixed layer (D2a, D2b, D2c), and 5 m bottom mixed layer (D3a, D3b, D3c). Figures in the left, middle and right columns are the K_Z profiles, DO concentration changes with time at bottom, 7 m and 15 m above bottom, and contour plots of DO concentration changes with time for each case. 75

Figure 3.21 Ratio between benthic respiration and total respiration changing with local DO concentrations with a subpycnocline layer of 3 m, 5 m, and 10 m thick. 83

Figure 4.1 Hourly CTD profiles at station CAS1, March 2007. Local DO concentration, $\log_{10}(N^2)$, $\log_{10}(s^2)$ and $\log_{10}(K_Z)$ are shown in each

panel from top to bottom. The black contour lines circle out hypoxia (DO concentration < 1.4 ml l^{-1}). Black dots denote the measurement position of CTD casts. 87

Figure 4.2 Hourly CTD profiles at station CAS2, July 2007. Local DO concentration, $\log_{10}(N^2)$, $\log_{10}(s^2)$ and $\log_{10}(K_Z)$ are shown in each panel from top to bottom. The black contour lines circle out hypoxia (DO concentration < 1.4 ml l^{-1}). Black dots denote the measurement position of CTD casts. 89

Figure 4.3 Hourly CTD profiles at station CAS3, September 2007. Local DO concentration, $\log_{10}(N^2)$, $\log_{10}(s^2)$ and $\log_{10}(K_Z)$ are shown in each panel from top to bottom. The black contour lines circle out hypoxia (DO concentration < 1.4 ml l^{-1}). Black dots denote the measurement position of CTD casts. 91

Figure 4.4 Hourly CTD profiles at station CAS4, July 2008. Local DO concentration, $\log_{10}(N^2)$, $\log_{10}(s^2)$ and $\log_{10}(K_Z)$ are shown in each panel from top to bottom. The black contour lines circle out hypoxia (DO concentration < 1.4 ml l^{-1}). Black dots denote the measurement position of CTD casts. 93

Figure 4.5 Hourly CTD profiles at station CAS5, August 2010. Local DO concentration, $\log_{10}(N^2)$, $\log_{10}(s^2)$ and $\log_{10}(K_Z)$ are shown in each panel from top to bottom. The black contour lines circle out hypoxia (DO concentration < 1.4 ml l^{-1}). Black dots denote the measurement position of CTD casts. 94

Figure 4.6 Magnitude of horizontal current (top) and wind speed (bottom) at station CAS5. 96

Figure 5.1 Observations at South Marsh mooring in the year 2010: (a) DO concentration (ml l^{-1}); (b) salinity; (c) temperature (°C); (d) density, σ_t. The curves marked by blue, green and red show the data at 1.5 m, 8 m and 12 m above the bottom. Grey bands are the stratification times. 104

Figure 5.2 Spectra of the raw DO (a1, a2, and a3), salinity (b1, b2 and b3) and temperature (c1, c2 and c3) time series at each depth (surface, mid, and bottom) at South Marsh Mooring. Green dash lines show the 95% confidence level. 106

Figure 5.3 Low-pass filtered Observations at South-Marsh mooring in the year 2010: (a) DO concentration (ml l^{-1}); (b) salinity; (c) temperature (°C); (d) density, σ_t. The curves marked by blue, green and red show the

data at 1.5 m, 8 m and 12 m above the bottom. Grey bands shows the time with stratification. 108

Figure 5.4 (a) The rate of change of the low-pass filtered bottom DO concentration (ml l^{-1} d^{-1}); (b) The rate of change of low-pass filtered bottom salinity; (c) The rate of change of low-pass filtered bottom temperature; (d) Low-pass filtered bottom density (kg m^{-3}). Grey bands show the ventilation-intervals. 109

Figure 5.5 (a) Low-pass filtered bottom DO concentration (ml l^{-1}); (b) low-pass filtered bottom-surface salinity difference; (c) low-pass filtered bottom-surface temperature difference; (d) low-pass filtered bottom-surface density difference (kg m^{-3}). Grey bands show the ventilation-intervals. 112

Figure 5.6 (a) The rate of change of low-pass filtered bottom-surface salinity difference; (b) the rate of change of low-pass filtered bottom-surface temperature difference; (c) the rate of change of low-pass filtered bottom-surface density difference (kg m^{-3}). Grey bands show the ventilation-intervals..... 115

Figure 5.7 (a) u component of the wind speed (m s^{-1}); (b) v component of the wind speed (m s^{-1}); (c) Magnitude of the wind speed (m s^{-1}); (d) significant wave height (m) at the South Marsh mooring. Grey bands show the ventilation-intervals. 118

LIST OF TABLES

Page

Table 2.1 Research cruises for the Mechanisms Controlling Hypoxia (MCH) project during years 2003-2009. 19

Table 2.2 Survey cruise identifiers and their corresponding dates. Total number of acrobat transects and CTD stations are also included. 22

Table 2.3 Continuous stations' ID and their corresponding dates. Research vessel and number of CTD casts are also included. 23

Table 3.1 Simulation results of experiment A. K_Z values in the bottom layer, time of bottom and mid layer becoming hypoxia are listed for each case. 68

Table 3.2 Simulation results of experiment B. K_Z values at the secondary pycnocline, time of bottom and mid layer becoming hypoxia are listed for each case. 71

Table 3.3 Simulation results of experiment C. Water column respiration and benthic respiration in percentage, time of bottom and mid layer becoming hypoxia are listed for each case. 73

Table 3.4 Simulation results of experiment D. Height of secondary pycnocline, time of bottom and mid layer becoming hypoxia are listed for each case. 76

Table 5.1 Correlations between the time-series of DO & AOU and other different parameters at the South Marsh Mooring. All the P values for the correlation is much smaller than 0.0001. Each calculated correlation coefficient is significant. 113

CHAPTER I

INTRODUCTION

In Chapter I, I review the previous studies about hypoxia on the Texas-Louisiana Shelf and set up the problems to be solved in this dissertation. I will determine the relationship between the stratification structure of the water-column and the vertical distribution of low dissolved oxygen conditions; estimate the vertical eddy diffusivity and the vertical DO flux though the pycnocline; and describe the intermittent ventilation events in the hypoxic zone.

1.1. Background

Sufficient oxygen is a fundamental requirement for most living organisms to survive on the earth. In the marine environment, hypoxia is defined as a condition in which the dissolved oxygen (DO) concentration falls below 1.4 ml l^{-1} (or equivalently 2.0 mg l^{-1}, 2 ppm, or 62 μM), low enough to impact the normal function of living organisms. Hypoxia has existed in the ocean throughout geological time (Diaz and Rosenberg 1995). Hypoxic conditions have been increasing in both severity and frequency since the 1960s in shallow, costal and estuarine areas due to worldwide coastal eutrophication fueled by riverine runoff of fertilizers and the burning of fossil fuels (Bianchi et al. 2010; Diaz and Rosenberg 2008; Conley et al. 2009). Hypoxia can lead to dramatic consequences for coastal ecosystems and local economies, including changes in the relative importance of various trophic pathways within food webs (Caddy 1993), reduction in the economic value of fisheries (Lipton and Hicks 2003), and

reduced production of commercially and recreationally valuable fish and shellfish (Breitburg 2002).

Two principal factors, water-column stratification and DO consumption below the pycnocline, are required for the development and maintenance of hypoxia. The stratification of the water-column inhibits the DO exchange between low-oxygen subpycnocline water and high-oxygen surface water. Microbial decomposition of organic matter in the sub-pycnocline layer consumes oxygen during the decay process and decreases the DO concentration to the hypoxic level.

Hypoxia has been observed all over the world. Occurrences of hypoxia have been documented near the mouths of the world's major river systems, such as the Mississippi and Atchafalaya River System in the Gulf of Mexico (Rabalais et al. 2002a), the Pearl River (Yin et al. 2004) and Changjiang River (Wei et al. 2007) in China. Many estuaries and bays around the world have experienced hypoxic or anoxic conditions, including the Chesapeake Bay (Cooper 1995), Erka estuary in the Adriatic Sea (Legovic et al. 1991), Florida Keys (Lapointe and Matzie 1996), Long Island Sound (Welsh and Eller 1991), New York Bight (Waldhauer et al. 1985), northern Adriatic Sea (Justic et al. 1993), Virginia estuaries (Kuo and Neilson 1987), the York River (Diaz et al. 1992), and the Texas coast (DiMarco et al. 2012). Hypoxia conditions have also been observed in the open oceans (Helly and Levin 2004; Kamykowski and Zentara 1990), such as in the Pacific Ocean off the coast of Oregon (Grantham et al. 2007) and the oxygen minimum zone (OMZ) in the eastern Pacific Ocean (Fuenzalida et al. 2009; Ulloa and Pantoja

2009), the southeast Atlantic off West Africa (Karstensen et al. 2008), and in the northern Indian Ocean (Paulmier and Ruiz-Pino 2009).

1.2. Hypoxia in the Northern Gulf of Mexico along the Texas-Louisiana Shelf

The Texas-Louisiana Shelf in the northern Gulf of Mexico has the largest area of hypoxic water in the western Atlantic Ocean and the second largest worldwide (Dale et al. 2010; Diaz 2001; Rabalais et al. 2002a). Hypoxic conditions have been found in the bottom water during the summer months since 1970s as a consequence of environmental changes on the Texas-Louisiana Shelf (Pokryfki and Randall 1987; Dale et al. 2010). The areal extent of the hypoxic zone on the continental shelf averaged more than 15,000 km^2 for the years 1993-2006 and reached 20,500 km^2 in the year 2007 (Rabalais et al. 2007). Hypoxia occurs in the region shallower than 30 m between 89.5°W and 94°W and is typically found in the lower half to two thirds of the water column (Rabalais et al. 1999). Osterman et al. (2005) reconstructed the history of low oxygen events on the Texas-Louisiana continental shelf over the past 180 years using the relative abundance of low oxygen tolerant benthic foraminifera in the sediment cores. Osterman et al.'s (2005) results supported the conclusion that hypoxia was a natural phenomenon whose extent and duration have increased over the past 50 years (Rabalais et al. 2002a) and indicated that the hypoxic events of the past few decades had become more extreme than during the past 180 years.

Nutrient enhanced productivity and strong local stratification are the two principal factors required for the development and maintenance of coastal hypoxia on

the Texas-Louisiana Shelf (Bianchi et al. 2010; Dale et al. 2010). In late spring, high phytoplankton growth, fueled by riverine nutrient flux, increases the flux of organic material to the lower water-column driven by sinking cells and zooplankton fecal pellets. The supply of organic material is decomposed, consuming oxygen in the subpycnocline water by water column and benthic respiration (Rabalais et al. 1999; 2002b). Strong local density stratification can separate the stratified water-column into two vertical regions at the pycnocline. The resupply of DO from the surface to the bottom layer is inhibited by this vertical stratification. DO below the pycnocline is depleted when respiration rate exceeds the ventilation rate in that layer (Wiseman et al. 1997).

Fresh water derived from the Mississippi and Atchafalaya River System and seasonally warmed surface water floating above the denser salty and cool oceanic water control the strength of stratification on the Texas-Louisiana Shelf. Hypoxic conditions persist during the summer until the fall, when river water input and solar heating decrease and stratification breaks down (Rabalais et al. 2002b). The result is a seasonal cycle that has hypoxia and strong stratification during the summer and non-hypoxia with weak stratification during the winter (Bianchi et al. 2010; Wiseman et al. 1997). This seasonal cycle is caused by the strength and spread of fresh water discharge, by air-sea heat exchange, by local circulation and by wind mixing (Cochrane and Kelly 1986; Cho et al. 1998; Nowlin et al. 2005).

Hypoxia has been observed to harm the living organisms and coastal ecosystems in the northern Gulf of Mexico. Gaston (1985) found the population of most macrobenthos species were significantly reduced during the hypoxia on the inner shelf

south off Cameron, Louisiana, during the summer of 1981. Harper et al. (1981) documented a decrease in species diversity and abundance over the Texas Shelf associated with the 1979 summer hypoxia off Freeport, Texas. Thronson and Quigg (2008) found that low DO concentration was the leading cause of fish kills in coastal Texas from 1951 to 2006. Fish mortality event was observed in 2005 on Texas's upper coast by McInnes and Quigg (2010), which was caused by large amounts of detritus from a cyanobacterial bloom in conjunction with strong stratification and hypoxic bottom water.

Because of its severe consequences, the hypoxia on the Texas-Louisiana Shelf has received increasing study since it was first documented (Pokryfki and Randall 1987; Boesch and Rabalais 1991; Rabalais et al. 2002b). Most of the studies have focused on the nutrient loading and resulting eutrophication. Turner and Rabalais (1994) and Rabalais et al. (2002a) suggested that the hypoxia on the Texas-Louisiana Shelf was the result of extensive nutrient loading with the river runoff into the continental shelf. They argued that the extent and intensity of hypoxia could be reduced by limiting the nutrient input.

While eutrophication due to nutrient loading has traditionally been regarded as the most important element controlling hypoxia on the northern Gulf of Mexico continental shelf, water-column stability and wind forcing also play important roles in controlling its formation and spatial distribution (Feng et al. 2012; Forrest et al. 2011). Wiseman et al. (1997) noted that fresh water in the surface prevents oxygen-rich surface water mixing downward into the near-bottom water, where respiration dominates. They

demonstrated that when the vertical density gradient reaches critical levels, mixing from the surface no longer refreshes the bottom water and leads to hypoxia condition on time scales from weeks to months. Belabbassi (2006) and Kiselkova (2008) found hypoxia occurs when local stratification exceeds a Brunt-Väisälä (or stability) frequency > 40 h^{-1}. It is commonly accepted that strong local stratification can limit the DO transport from the surface to the bottom. However, the processes controlling vertical oxygen ventilation or the vertical oxygen flux to the bottom water during stratified conditions have not been fully investigated there.

DO concentrations in the water column are affected by fluxes at the top and bottom boundary across the air-sea and sediment-water interfaces. Within the water column, DO is influenced by several sinks and sources. Oxygen budgets have been constructed in several previous studies (Rowe 2001; Justic et al. 2002; O'Donnell et al. 2008; Dale et al. 2010) and have been expressed using the following DO balance model:

$$\frac{\partial O_2}{\partial t} + u\frac{\partial O_2}{\partial x} + v\frac{\partial O_2}{\partial y} + w\frac{\partial O_2}{\partial z} = \frac{\partial}{\partial z}\left(K_Z\frac{\partial O_2}{\partial z}\right) + K_H\left(\frac{\partial^2 O_2}{\partial x^2} + \frac{\partial^2 O_2}{\partial y^2}\right) - r + p \qquad (1)$$

The first term describes the local rate of change of oxygen concentration with time, the second and third terms describe the effect of horizontal advection, the fourth term describes the effect of vertical advection, the fifth term describes the effect of vertical mixing in which K_Z is the vertical eddy diffusivity, and the sixth and seventh terms describe horizontal mixing where K_H is the horizontal eddy diffusivity. All the biological and chemical processes that consume oxygen in the water column are collectively represented by *r*, including respiration, denitrification and bacterial organic matter

remineralization. Processes producing oxygen, such as photosynthesis, are represented by p.

The vertical mixing term, described using $K_Z \frac{\partial^2 O_2}{\partial z^2}$, plays a key role in the local oxygen balance (Pena et al. 2010). Its magnitude depends on the value of K_Z and the vertical oxygen gradient. The value of K_Z is highly variable in both space and time. A strong vertical density gradient (stratification) and weak vertical shear can limit K_Z and favor hypoxia formation. Several factors can affect vertical density gradients, including freshwater inputs from river, precipitation and solar radiation. Factors that increase vertical shear include tidal and wind-driven current, internal waves, and Langmuir circulation. Few field studies using microstructures to measure the turbulent dissipation rates of velocity, salinity and temperature fluctuations have been reported for the northern Gulf of Mexico. An investigation of the vertical eddy diffusivity is necessary for a full understanding of the formation, duration, extent, and break down of hypoxia on the Texas-Louisiana Shelf.

A number of statistical and modeling studies have been conducted to understand the hypoxic zone dynamics and to enhance the predictive capabilities:

Rowe (2001) developed a time-dependent numerical simulation model to compare biological and physical processes that introduce and consume oxygen. He incorporated shipboard measurements and continuous near-bottom in-situ observations. He incorporated biological processes that consume and produce oxygen. This DO budget model was used to estimate the extent to which consumption in deep waters and in

sediments exceeds net production and to calculate the time needed to reach hypoxia. He used a constant K_Z in the simulation, which implies that vertical ventilation depends only on the oxygen gradient and is independent of changes in K_Z.

Justic et al. (1996, 2002) used a vertical two-layer model to simulate hypoxia on the Texas-Louisiana Shelf. Simulation results suggested that hypoxia has intensified in recent years as a consequence of increased net productivity and resulting increase in vertical flux of organic carbon. They asserted that the long-term increase in riverine nutrient fluxes has been the primary factor controlling this decline in DO concentration. However, Justic et al. (2002) assumed a constant energy dissipation rate to calculate K_Z for strongly stratified conditions to run the model. They calculated the vertical density gradient between the lower and upper water column using a multiple regression with surface salinity and temperature to estimate their K_Z. Their mixing rate was assumed to be relatively small and dependent only on the vertical density gradient.

Scavia et al. (2003, 2006) used a one-dimensional DO model driven by the May-June total nitrogen loading from the Mississippi and Atchafalaya Rivers to reproduce the hypoxic area. Turner et al. (2005) found a statistical relationship between freshwater discharge and near-shore nitrogen concentrations and correlated discharge to the area of the hypoxic region. Turner et al. (2006) used a multiple linear regression model to correlate the size of summertime hypoxic zone with the Julian year and the loading by various forms of nitrogen, phosphorus, dissolved silicate and their molar ratios. They included Julian year as an independent variable and interpreted it later as a proxy for carbon stored in the sediments (Turner et al. 2008). Greene et al. (2009) used a multiple

linear regression model to predict the hypoxic area using riverine nitrate and phosphate concentrations and river volumetric discharge. All these studies conclude that riverine nutrient fluxes, via their influence on the net productivity of the upper water column, play a major role in controlling bottom water hypoxia. However, all of these models ignored the physical factors limiting aeration of near-bottom waters.

Other factors, such as the wind-driven currents and topographic influences can change the distribution of hypoxic zone. Hetland and DiMarco (2008) applied simple, idealized models of biological respiration to a complex three-dimensional hydrodynamic model of coastal circulation. They showed that the formation of hypoxia is primarily a vertical process dependent on the local respiration and vertical mixing. After analyzing the spatially detailed observations along and cross the continental shelf in the central and western areas of coastal Louisiana, DiMarco et al. (2010) suggested that the along-shelf variability of DO has a characteristic wavelength of approximately 50 km that is phase-locked to the fresh water meander at locations of three shallow shoals along the coastline. Changes in the winds can alter the horizontal distribution of the river plume on the continental shelf and thereby the vertical stratification.

Forrest et al. (2011) examined the relationship between the hypoxic area and the average east-west wind speed. Their correlation was weak ($r^2 = 0.16$), but statistically significant. Feng et al. (2012) used duration of westerly wind instead of the east-west wind speed in their statistical analysis. Both of their statistical relationships reflected the movement and changes in horizontal river plume position associated with the wind and

the influence of stratification on hypoxic area. However, the mechanisms by which wind influences the extent of hypoxia on the continental shelf are still not clear.

1.3. Physical description of the Texas-Louisiana Shelf

This dissertation focuses on the physical mechanisms that control the formation and maintenance of hypoxia on the Texas-Louisiana Shelf. A brief review of the physical background of the Texas-Louisiana Shelf is given in this section.

The Texas-Louisiana Shelf is west of the Mississippi delta on the northern shelves of the Gulf of Mexico (Figure 1.1). The Gulf of Mexico is a semi-closed basin with broad and narrow continental shelves surrounding a deep abyss that reaches 3800 m. It is connected to the open ocean through the Yucatan Channel and the Florida Straits. The width of the Texas-Louisiana Shelf, defined as the distance between the coast and the 200-m isobaths, varies from 200 km near the Texas-Louisiana border to 90 km off the Rio Grande Delta and ends at the Mississippi Delta near the mouth of the Mississippi River (Etter et al. 2004).

The quasi-annual low-frequency circulation over the Texas-Louisiana Shelf is driven primarily by the wind. The dominant feature of the prevailing circulation on this shelf is a cyclonic elongated gyre, with inshore westward flow near the coast and eastern flow near the shelf break at about the 200-m isobath (Cochrane and Kelly, 1986; Cho et al. 1998; Nowlin et al. 2005). The downwelling-favorable non-summer (from September to next June) winds drive the currents downcoast (westward), and transport the freshwater from Louisiana to Texas. The direction of the mean wind in June changes

from predominantly westward to north and northeast, resulting in a current reversal to eastward flow over the shelf (Cochrane and Kelly 1986; Nowlin et al. 1998; Wang et al. 1998).

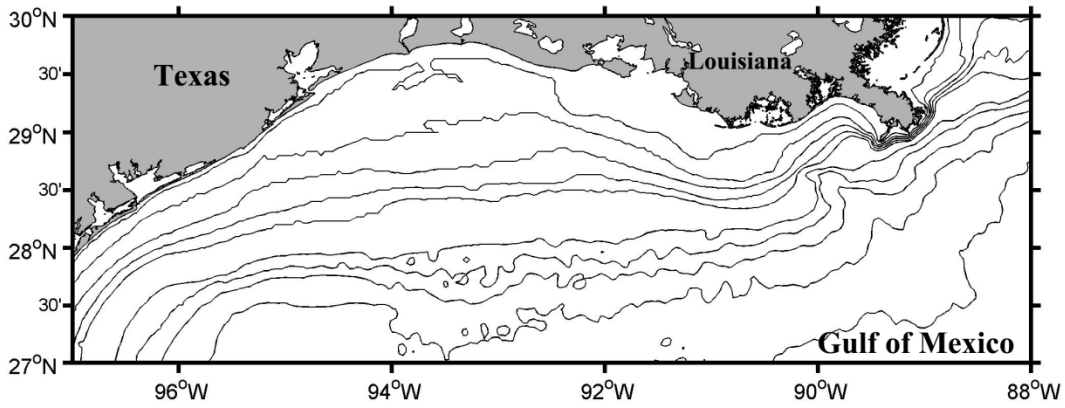

Figure 1.1 Study area and bathymetry for the MCH program on the Texas-Louisiana Shelf in northern Gulf of Mexico. The 10, 20, 30, 40, 50, 100, 200, 500, 1000, 2000 m isobaths are shown.

The circulation patterns of the outer shelf in the northern Gulf of Mexico are influenced by the Loop Current and its eddies (Nowlin et al. 2001; Sturges et al. 2005; Nowlin et al. 2005). The Loop Current is a part of the Atlantic western boundary current that flows northward through the Yucatan Channel and makes a sharp 90° clockwise reversal at approximately 26°N and exits the Gulf at the Florida Straits (Leben 2005).

Loop Current Eddies, with a diameter up to 400 km, separate from the Loop Current at an average frequency of 11 months and travel westward in the Gulf of Mexico (Sturges and Leben 2000). The current velocities of Loop Current Eddies are up to 2.5 m s^{-1} and can affect the currents on the outer edge of the Texas-Louisiana Shelf. The offshore circulation features are episodic in nature due to the chaotic character of the Loop Current intrusions into the northern Gulf of Mexico and the separation periods of the Loop Current Eddies (Sturges and Leben 2000; Leben 2005).

The tides on the Texas-Louisiana Shelf are small. DiMarco and Reid (1998) studied the eight principal tidal current constituents by analyzing the current measurements collected by 81 current meters deployed on the Texas-Louisiana Shelf from 1992-1994. Tides in the region are predominantly diurnal, and the dominant tidal constituents are K1, O1, and M2. The tidal surface current is about 9 cm s^{-1} at the northeast corner of the shallow shelf near the Atchafalaya Bay and decreases to about 2 cm s^{-1} at the shelf edge (DiMarco and Reid 1998).

The average annual outflow of the Mississippi-Atchafalaya River System is about 530 km^2 (Milliman and Meade 1983), which constitutes 55% of the total freshwater input to the Gulf of Mexico (Solis and Powell 1999). The Mississippi River discharges onto the Louisiana Shelf through the bird-foot delta with a mean annual discharge of 13,500 m^3 s^{-1}

, half of which goes west and enters the Texas-Louisiana Shelf (Dinnel and Wiseman 1986; Etter et al. 2004). The Atchafalaya River discharges onto the Louisiana Shelf through Atchafalaya Bay near Morgan City, LA, and contributes approximately 30% of

the total fresh water inflow. The huge amount of fresh water input from the Mississipi-Atchafalaya River system can significantly influence the physical and biochemical activities on Texas-Louisiana Shelf. The discharge has an annual cycle that is dominated by the spring flood (Dinnel and Wiseman 1986). Maximum and minimum shelf freshwater volume occurs approximately one month after peak spring runoff and just prior to the spring maximum, respectively.

Near-inertial motions on the Texas-Louisiana Shelf are driven by the passage of atmospheric fronts, hurricanes and tropical storms (Nowlin et al. 1998; Nowlin et al. 2005). Weak front passage lead to inertial oscillations that can reach 15 cm s^{-1} and surface trapped above the pycnocline (Chen et al. 1996; DiMarco et al. 2000). Zhang et al. (2009, 2010) studied the spatial structure and temporal evolution of sea breeze and the latitudinal distribution of propagation and mixing of sea breeze driven near-inertial ocean response in the Gulf of Mexico using comprehensive data sets and a non-linear numerical model. They found that near 30°N, inertial oceanic response is significantly enhanced by a near-resonant condition between inertial and diurnal forcing frequencies.

Synoptic frontal passages can affect the stratification of the water column through shear mixing processes. The strength and frequency of synoptic frontal passages increase during the non-summer months and break down the stratification of the water column (Nowlin et al. 1998). In summer, lack of atmospheric fronts allows the shelf to remain stratified and inhibits vertical mixing. Zhang et al. (2009) demonstrated that sea breezes, which peak in summer, can act as a substitute for winter frontal passages and can drive significant near-inertial motions in the water column and enhance the vertical

mixing in the summer months. The sea breeze driven near-inertial motions also provide a potential mechanism to ventilate seasonally occurring near-bottom hypoxic waters of the coastal ocean.

1.4. Study objectives

Although previous studies addressed the fact that stratification is one of the two factors controlling hypoxia on the Texas-Louisiana Shelf in northern Gulf of Mexico, there are still many fundamental questions to study, including:

1. What is the magnitude and spatial (horizontal and vertical) variability of K_Z and buoyancy frequency, N, in the stratified water column of the Texas-Louisiana Shelf?
2. What is the DO flux to the lower layer under hypoxic conditions?
3. How do high-frequency wind events enhance mixing and affect the vertical distribution of DO?

To solve these problems, I set up the primary objectives of this dissertation:

1. To quantify the vertical distribution of hypoxia associate with the local stratification structure on the Texas-Louisiana Shelf;
2. To estimate K_Z and vertical DO flux through pycnocline at hypoxic conditions;
3. To examine the formation of hypoxia using a one-dimension model with the estimated K_Z; and,
4. To discuss physical processes controlling DO dynamics, including wind, advection and mixing.

1.5. Organization

This dissertation is organized into five chapters.

Chapter I has presented an introduction to hypoxia on the Texas-Louisiana Shelf, and reviews the previous studies associate with hypoxia on Texas-Louisiana Shelf. Study objectives are also given in this chapter.

In Chapter II, I provide an overview of the data and research method used in this dissertation.

In Chapter III, I describe the horizontal and vertical distribution of hypoxia and discuss its relationship with local stratification structure and other processes using observational data. A threshold of N=0.05 s^{-1} is found to represent the lower limit of the stratification strength for existence of hypoxia. A double-pycnocline structure is observed in 56% of all the hypoxic stations. An idealized one-dimensional model with parameterized respiration is applied to study stratification structure associated hypoxia development.

In Chapter IV, Diapycnal diffusivity is calculated based on 24 hours continuous observations in the hypoxic zone on the Texas-Louisiana Shelf. Averaged cross-pycnocline vertical DO flux is calculated in a two-layer stratified water column with subpycnocline hypoxia.

In Chapter V, I show continuous observations at the South Marsh Mooring. 19 ventilation events are observed in the DO records with a time period of 1~3 days. Analysis of the time series of DO, salinity and temperature at different levels of the mooring demonstrates that 58% of the total ventilation intervals are induced by

increased vertical mixing. Comparison of the time derivative of the low-frequency part of the near-bottom DO concentration to observations of the wind and significant wave height suggests that local wind events are responsible for the enhanced vertical mixing.

Chapter VI summarizes the results in the previous chapters and provides the conclusions of this study.

This dissertation study increases our understanding of the mechanisms, especially physical processes, which control and affect hypoxia on the Texas-Louisiana Shelf. Results from this study provide helpful input for hypoxia predictions, management and action plans.

CHAPTER II

DATA AND METHODOLOGIES

A combination of in-situ observations and numerical modeling is used to accomplish the study objectives presented in Chapter I. In Chapter II, I describe the field observations used in this study, including historical observations, survey cruises, processes cruises and moorings. Methods to estimate the vertical eddy diffusivity and diapycnal DO flux are introduced in this chapter. A one-dimension idealized model is developed to simulate the formation and maintenance of hypoxia under different stratification structures as a supplement of the observations.

2.1. Observations

Oceanographic and meteorological observations used in this study were made during the program "Mechanisms Controlling Hypoxia on the Louisiana Shelf" (MCH), which was sponsored by the National Oceanic and Atmosphere Administration (NOAA) Center for Sponsored Coastal Ocean Research. Historical hypoxia observations (2003 to 2009) are introduced in section 2.1.1. Field data were collected from April 2010 through August 2011. Data includes water properties (conductivity, temperature and DO) collected with a CTD with a SBE 43 DO sensor, vertical sections of water property data (temperature, salinity, and DO) collected with a towed vehicle (Acrobat), and observations of salinity, temperature and DO collected from moorings. Observational data collected during survey cruises and process cruises are introduced in the sections

2.1.2 and 2.1.3, respectively. Section 2.1.4 introduces the long time-series data collected by the MCH South Marsh mooring located on the Texas-Louisiana Shelf.

2.1.1. Historical observations

The historical data was collected by the MCH program from September 2003 to July 2009. A total of 15 cruises were conducted. All the CTD profiles collected are used in this study. A summary of the cruises, which include the start and end dates, are given in Table 2.1. The timing of the cruises was planned in the summer according to the temporal scales of hypoxia, including periods typical for the onset, duration, and dissipation of the hypoxic conditions on the shelf.

The sampling plan was designed to test a hypothesis proposed by Rowe and Chapman (2003), stating that different biological processes controlled hypoxia in different physical regimes. The cruise tracks for M0-M14 cruises were similar and designed to obtain measurements from the three regions of the shelf. The actual CTD/bottle stations for all cruises are shown in Figure 2.1.

Table 2.1 Research cruises for the Mechanisms Controlling Hypoxia (MCH) project during years 2003-2009.

Cruise ID	Start date	End date	CTD stations
M00	13 Sep 2003	16 Sep 2003	37
M01	01 Apr 2004	08 Apr 2004	63
M02	25 Jun 2004	01 Jul 2004	125
M03	19 Aug 2004	26 Aug 2004	142
M04	23 Mar 2005	29 Mar 2005	201
M05	19 May 2005	26 May 2005	192
M06	07 Jul 2005	12 Jul 2005	156
M07	17 Aug 2005	24 Aug 2005	234
M08	22 Mar 2007	29 May 2007	238
M09	16 Jul 2007	19 Jul 2007	125
M10	06 Sep 2007	09 Sep 2007	146
M11	16 Apr 2008	19 Apr 2008	86
M12	17 Jul 2008	20 Jul 2008	137
M13	07 Apr 2009	10 Apr 2009	74
M14	28 Jul 2009	31 Jul 2009	62

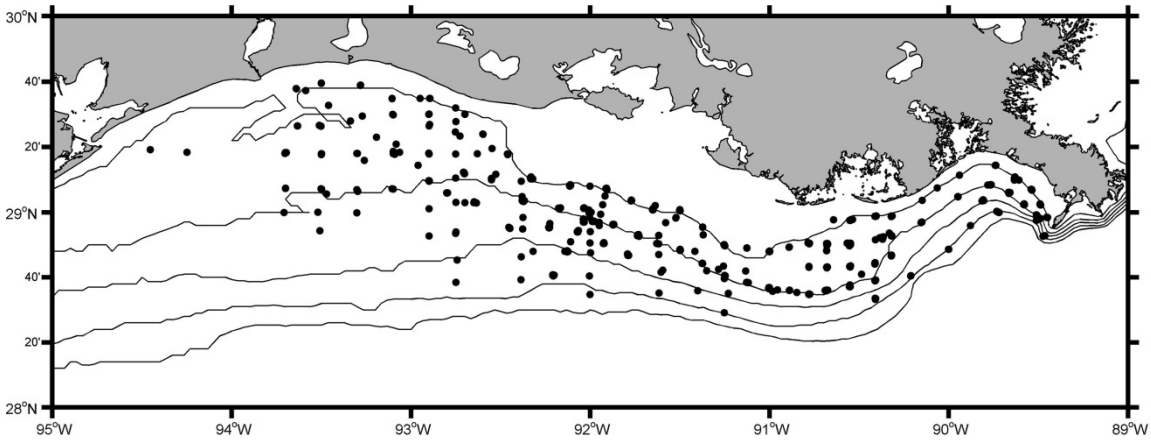

Figure 2.1 CTD stations (black dots) for MCH cruises (M00-M14). The 10, 20, 30, 40, 50 m isobaths are shown.

Vertical profiles of salinity, temperature, pressure, and DO concentrations were made using a SBE 911 CTD with a SBE43 oxygen sensor. The vertical separation of data of these profiles after processing raw records is 0.5 m. Water samples were taken using Niskin bottles on a 12-bottle rosette. DO concentration of the water sample were analyzed at sea using the Winkler titration method (Carpenter 1965; Williams and Jenkinson 1982). Water samples were analyzed in the lab and compared to the CTD observations to calibrate the electronic probe measurements. A shipboard 150-kHz ADCP (Acoustic Doppler Current Profiler) was used on all cruises to provide measurements of current velocity along the ship track.

2.1.2. Survey cruises

Four shelf-wide survey cruises (Table 2.2) of the Texas-Louisiana Shelf were conducted in June and August of 2010 and 2011 to estimate the horizontal areal extent of hypoxia and the vertical distribution of DO and other hydrographic properties.

An "Acrobat" (SeaSciences Inc.) towed vehicle was used to measure water properties along cross-shelf transects during each cruise (Table 2.2). The Acrobat was designed to undulate vertically behind the ship to make continuous profiles of water properties. It was equipped with a Sea-Bird SBE 43 DO sensor, RINKO DO sensor, Sea-Bird 55 CTD, WET-labs Fluorometer/Turbidity and CDOM sensors. The system sampled every 0.25 second. The Acrobat was towed between 2 m above the bottom and 2 m below the surface. During each transect, the ship maintained a constant heading and a tow velocity of 5 knots. Cross-shelf transect was designed to be roughly perpendicular to the local bathymetric lines. It took 4-6 hours to accomplish a cross-shelf transect. The measured parameters were compared with the measurement in the lab from the water samples as mentioned in the previous section 2.1.1 to calibrate the electronic probe measurements.

The designed cross-shelf transects were not accomplished in cruise MS1 and MS3. MS1 cruise was terminated at the half way caused by the engine problem on the R/V Manta in June 2010. MS3 cruise was suffering large wave conditions induced by the storm in June 2011, under which it is not safe to tow the "Acrobat". Therefore, only towed transects in MS2 and MS4 cruise were used in this study.

Table 2.2 Survey cruise identifiers and their corresponding dates. Total number of acrobat transects and CTD stations are also included.

Cruise ID	Start date	End date	Transacts	CTD stations
MS1	14 Jun 2010	19 Jun 2010	5	19
MS2	02 Aug 2010	07 Aug 2010	15	64
MS3	23 Jun 2011	01 Jul 2011	6	73
MS4	07 Aug 2011	15 Aug 2011	15	66

Vertical profiles of current velocity were recorded by a 300-kHz shipboard RDI ADCP while towing "Acrobat". The ADCP measured the current velocity relative to the ship. Current vectors (u, v) relative to the bottom were calculated and averaged in two-meter vertical bins by using the bottom track speed (ship speed relative to the bottom) to adjust the ADCP data to a fixed spatial frame. The current measurements were averaged every five minutes (i.e. approximately 600 m of horizontal distance).

CTD casts were made at the inshore and offshore ends of each cross-shelf transect. Water samples from surface, mid-depth, and bottom were collected and analyzed for nutrients, DO concentrations. The Winkler titration method was used to measure DO concentration of the water samples and the results were used to calibrate the SBE 43 electronic sensors. Data collected by the CTD casts were also used to increase horizontal coverage of the cruises.

2.1.3. Continuous CTD observations

A series of hourly CTD observations had been made during the MCH project since the year 2005. One special station, located at 29°N, 92°W on the inner shelf of the Louisiana coast, was also the location of the South Marsh mooring. It had been revisited five times at different seasons between 2007 and 2010 (Table 2.3). CTD casts were made every an hour to collect hydrography data with a total duration from 12 hours to 36 hours for different stations. A 600-kHz bottom mounted RDCP (CAS1 to CAS4) or a 600-kHz shipboard ADCP (CAS5) was used to collect the current velocity profiles while on station. Measured velocities were averaged into 2-m vertical depth bins and 5-min time bins.

Table 2.3 Continuous stations' ID and their corresponding dates. Research vessel and number of CTD casts are also included.

Station ID	Time	Research Vessel	CTD Casts
CAS1	Mar 2007	R/V Pelican	25
CAS2	Jul 2007	R/V Pelican	14
CAS3	Sep 2007	R/V Pelican	37
CAS4	Jul 2008	R/V Pelican	25
CAS5	Aug 2010	R/V Pelican	25

2.1.4. South Marsh Mooring

The South Marsh Mooring, located at 29°N, 92°W on the inner shelf of the Louisiana coast, made hourly observations of DO concentration, temperature, and salinity profiles from May 2010 to Nov 2010. Averaged total water depth at the mooring was 20 meters. Sea-Bird SBE 37 sensors were positioned 1.5 m, 8 m, and 12 m above the bottom to measure conductivity, temperature and DO concentrations. A 600-kHz RDCP was mounted in the bottom to observe current and wave conditions. The RDCP failed to collect the current velocity profiles during the deployment of the mooring. Wave condition data was obtained during May 2010.

2.2. Methodologies

In this section, the methodologies applied to the data listed in Section 2.1 are described and explained. The methodologies include descriptions of how metrics such as Brunt-Väisälä frequency (N), Richardson number (Ri), and vertical eddy diffusivity (K_Z) are estimated in this dissertation. The definition of double-pycnocline structure is also described in this section.

2.2.1. Data methods

a) Brunt-Väisälä frequency

The Brunt-Väisälä (or buoyancy) frequency, N, is often used to quantify the local density stratification, with large values of N corresponding to a strong stratification or,

equivalently, high stability. The term is a function of the vertical density gradient and is defined by

$$N = \sqrt{-\frac{g}{\rho}\frac{\partial \rho}{\partial z}}, \quad (1)$$

where ρ is water density, g is gravity acceleration, and z is the depth from the water surface. N characterizes the highest frequency of small-amplitude free oscillations that occur naturally following a disturbance in a stable stratified fluid. In this dissertation, N is calculated from density profiles determined using temperature and salinity observations collected by Acrobat and CTD casts. The investigated N is used to determine how stratification controls the distribution of low DO water.

b) Gradient Richardson number (Ri)

The gradient Richardson number is a dimensionless number that expresses the ratio of potential energy to kinetic energy. It is a measure of relative importance of the mechanical (shear flow) and density effects (density gradient or N) in the water column:

$$Ri = \frac{N^2}{S^2}. \quad (2)$$

In this study, the gradient Richardson number is used as an indicator of mixing. Miles (1961) and Howard (1961) have demonstrated that $Ri > 0.25$ is a sufficient condition for stability in a shear layer for which velocity and density vary linearly with depth. When $Ri < 0.25$, velocity shear is sufficient to overcome the stratification and lead to mixing.

The Gradient Richardson number can be calculated using density and ADCP current velocity profiles. Density profiles collected by Acrobat were averaged vertically in one-meter vertical bins and averaged in a five minutes time window to investigate the *N*. Vertical velocity shear (*S*) was calculated from the ADCP current measurements in a one-meter vertical bin too. Gradient Richardson number was calculated using the values of *N* and *S* at one-meter vertical intervals.

c) Vertical eddy diffusivity

Vertical eddy diffusivity K_Z was calculated as a function of Γ, ε ,and N^2 (Osborn 1980):

$$K_Z = \frac{\Gamma\varepsilon}{N^2} \quad , \tag{3}$$

Dissipation is the process of converting kinetic energy into potential and thermal energy. The turbulence dissipation rate is the rate of dissipation of turbulent kinetic energy in a turbulent flow. Different methods have been used to estimate the dissipation rate for stable ($Ri > 0.25$) and unstable conditions ($Ri < 0.25$). Kunze et al. (1990a, 1990b) proposed an estimate of the mean turbulence dissipation rate in a turbulent flow for $Ri < 0.25$:

$$\varepsilon = (\Delta z)^2 \left\langle \left(\frac{S^2 - 4N^2}{24}\right)\left(\frac{S - 2N}{4}\right) \right\rangle , \tag{4}$$

where ε_0 is the averaged dissipation rate during the observation, $N_0 = S_0 = 3$ cph, and $\varepsilon_0 = 6.9\times10^{-10}$ at a stratified condition ($Ri > 0.25$). Parameter values were obtained

from cruise averaged microstructure measurements on the outer of New England shelf in the late summer of 1996 (Mackinnon and Gregg 2003).

The calculated vertical eddy diffusivity was used to estimate the vertical DO flux through the pycnocline and thereby make the DO budget below the pycnocline.

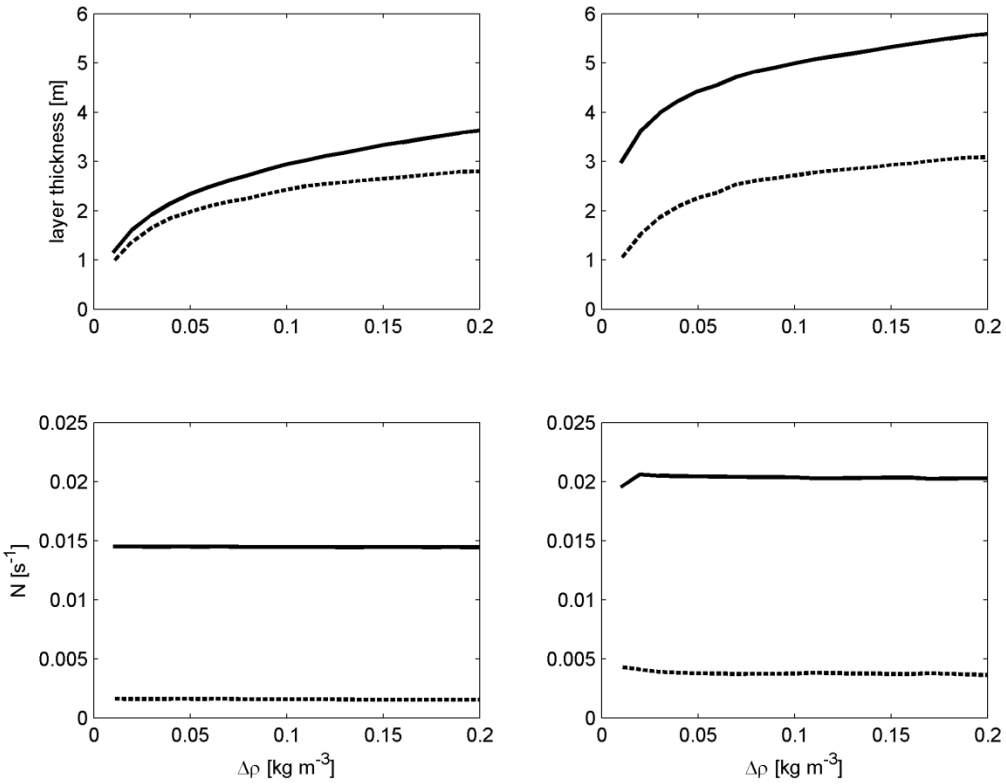

Figure 2.2 Top: The mean (solid) and standard deviations (dashed) of the estimated bottom (left) and surface (right) mixed layer thickness from the all CTD stations between 2003 and 2009 as a function of the choice of Δρ. Bottom: The mean (solid) and standard deviations (dashed) of *N* in the bottom (left) and surface (right) layer as a function of the choice of Δρ for the same data set.

d) Definition of mixed layer

The mixed layer is a layer in which active turbulence has homogenized some range of depths. Bottom mixed layer is defined as the distance from the bottom over which density decrease for a certain $\Delta\rho$ from its bottom value. Surface mixed layer is defined as the distance from the surface over which density increase for a certain $\Delta\rho$ from its surface value. The estimated surface/bottom mixed layer thickness depends on the choice of $\Delta\rho$. The mean and standard deviations of the estimated bottom and surface mixed layer thickness from the all CTD stations between 2003 and 2009 as a function of the choice of $\Delta\rho$ are shown in the top panels of Figure 2.2. In these two figures, the rapid fall off for small $\Delta\rho$ is probably underestimation of the mixed layer thickness due to instrument noise. The more slowly varying region for larger $\Delta\rho$ is overestimation of the mixed layer due to the choice of a finite $\Delta\rho$ in combination with the background vertical density gradient (Lentz and Trowbridge, 1991). The mean N in the bottom and surface mixed layer are almost constant and small in the bottom panels of Figure 2.2. It suggests that there are only small vertical density gradients inside of the mixed layer. For this study, $\Delta\rho$ was chosen to be 0.1 kg m^{-3} to define both the bottom and surface mixed layer.

e) Definition of the double-pycnocline structure

In the CTD profiles from the MCH cruises between 2003 and 2009, a strongly stratified layer is usually observed below the surface mixed layer and a weakly stratified layer is usually observed above the bottom mixed layer. A typical CTD profile is given in Figure 2.3. The strongly stratified layer below the surface mixed layer is at 8 meter

depth with the largest N of 0.12 s^{-1}. The weakly stratified layer above the bottom mixed layer is located at 15 m depth with a peak of $N = 0.06$ s^{-1}. Both salinity and temperature show the largest vertical gradient at the main-pycnocline, and a relatively weak vertical gradient at the secondary-pycnocline.

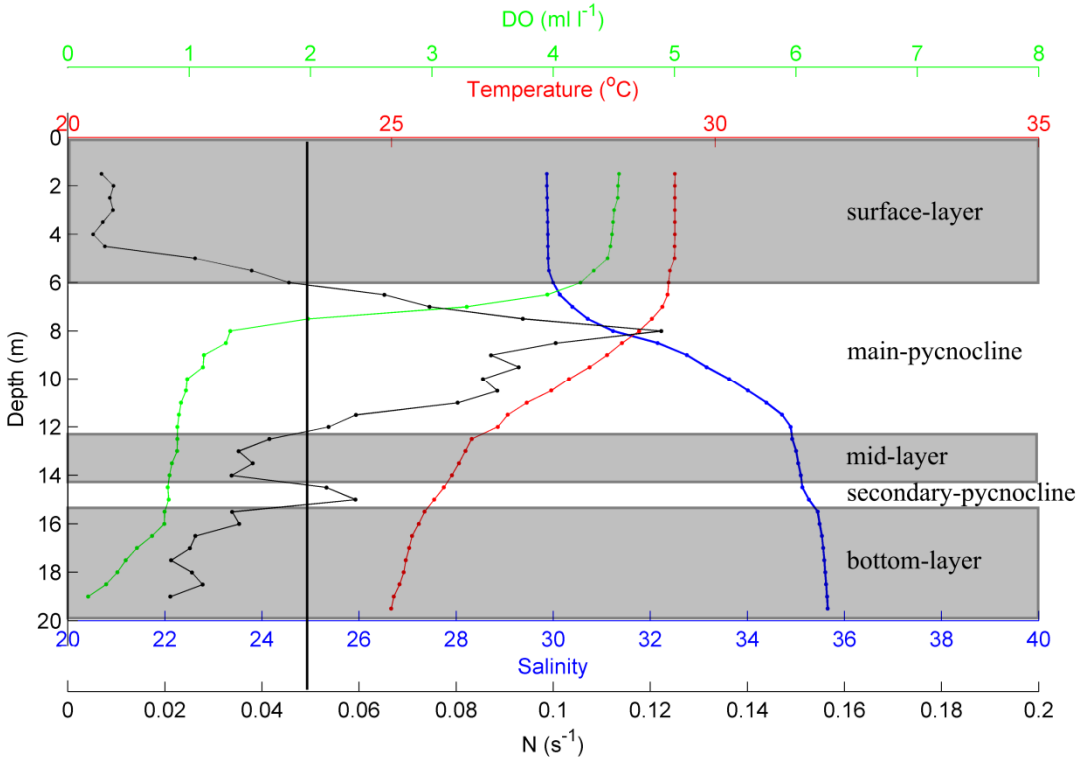

Figure 2.3 A typical CTD profile with double-pycnocline structure. The black vertical solid line is the threshold of $N = 0.05$ s^{-1}. Surface-layer, mid-layer and bottom-layer are marked in the grey band. Main-pycnocline and secondary-pycnocline are marked in white band.

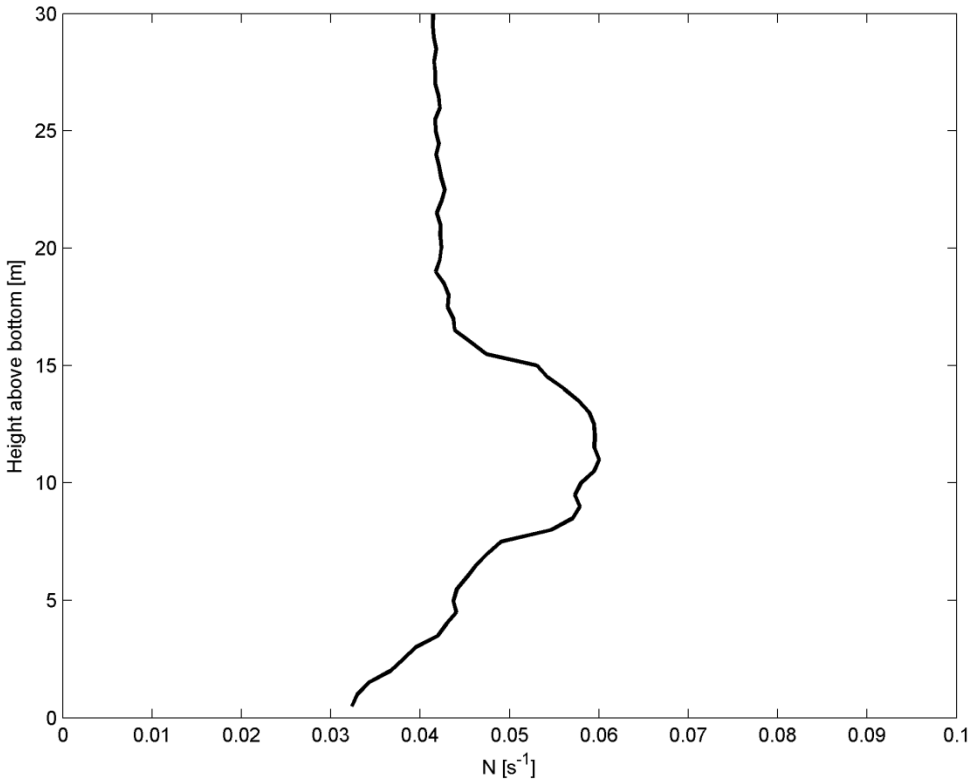

Figure 2.4 The averaged N at each bin above bottom for all the CTD profiles from MCH cruises between 2003 and 2009.

To define these two stratified layers and their thickness, a critical value of N is needed to identify the stratified layer from the background stratification. The averaged N at each bin above bottom is shown in Figure 2.4. The back ground stratification is around $N = 0.04$ s^{-1}. N in the strongly stratified layer from eight to fifteen meters above bottom is around 0.06 s^{-1}. The near bottom averaged N is even smaller than 0.04 s^{-1}. The critical value of N should be sufficiently large enough to identify the stratified layers

from the back ground stratification and small enough to identify the weakly stratified layer above the bottom mixed layer. Based on visual comparison among the CTD individual profiles, $N = 0.05\ s^{-1}$ was chosen to be the critical value in this study. Estimated mean and standard deviations of the height of the weakly stratified layer above bottom as a function of the choice of critical N is shown in Figure 2.5. When critical N equals to $0.05\ s^{-1}$, the height of the weakly stratified layer is about 4.5 m above the bottom and is closely to cap the bottom mixed layer (about 3.0 m above the bottom, Figure 2.2). There is a 1.5 m difference between these two heights, which is considered to be caused by the thickness of the stratified layer above bottom mixed layer.

With the definition of this critical N, the vertical profile of N is separated into 5 segments marked in white and grey bands in Figure 2.3. I define the segment with largest peak of N as the main-pycnocline, which is marked in the white band near surface. The white segment with the second largest peak of N near the bottom is defined as the secondary-pycnocline. The double-pycnocline structure separates the water column into three layers, marked in grey bands: surface, mid, and bottom. In the surface-layer, both salinity and temperature are relatively homogeneous with $N < 0.02\ s^{-1}$. In the mid-layer, salinity is homogeneous, while the temperature profile shows a slow decrease with depth. The N value at the mid-layer is around $0.04\ s^{-1}$. Salinity profile is relatively homogeneous in the bottom layer, with a slightly decrease in the temperature profile. The N in the bottom layer is around $0.03\ s^{-1}$. The DO concentration is $4.5\ ml\ l^{-1}$ in the surface-layer, decreasing sharply to $1.0\ ml\ l^{-1}$ in the lower part of the main-pycnocline. In the mid-layer, DO concentration drops to $0.8\ ml\ l^{-1}$, and is homogeneous in the mid-

layer. DO concentrations keep decreasing in the bottom-layer and drops to 0.1 ml l^{-1} at the bottom.

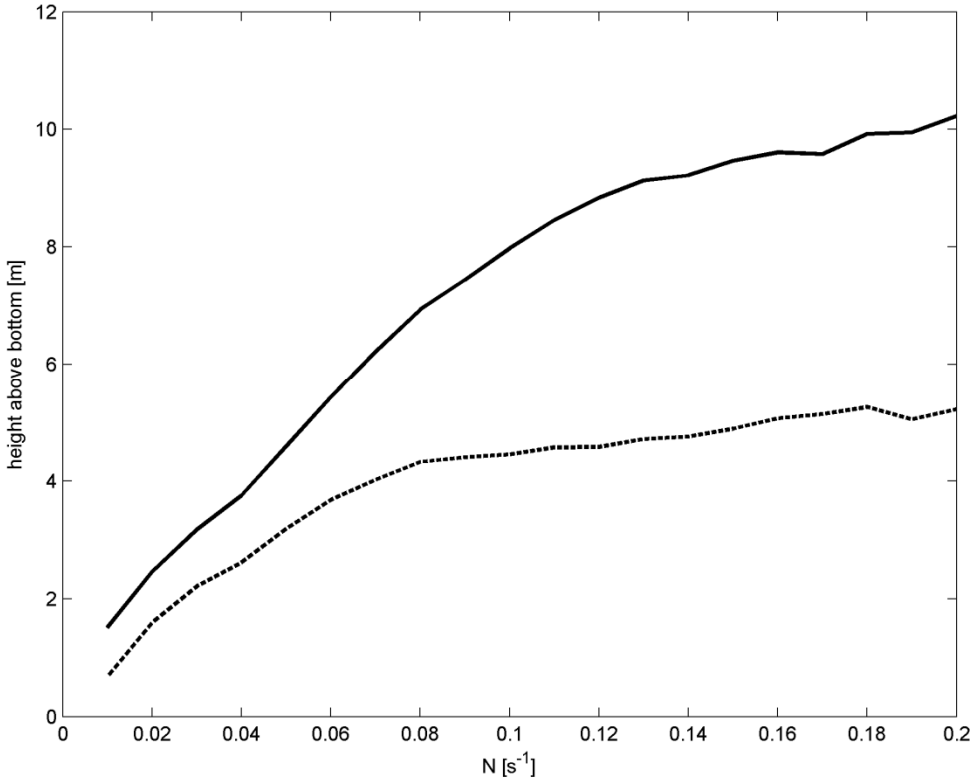

Figure 2.5 Estimated mean (solid) and standard deviations (dashed) of the height of the weakly stratified layer above bottom as a function of the choice of critical *N*.

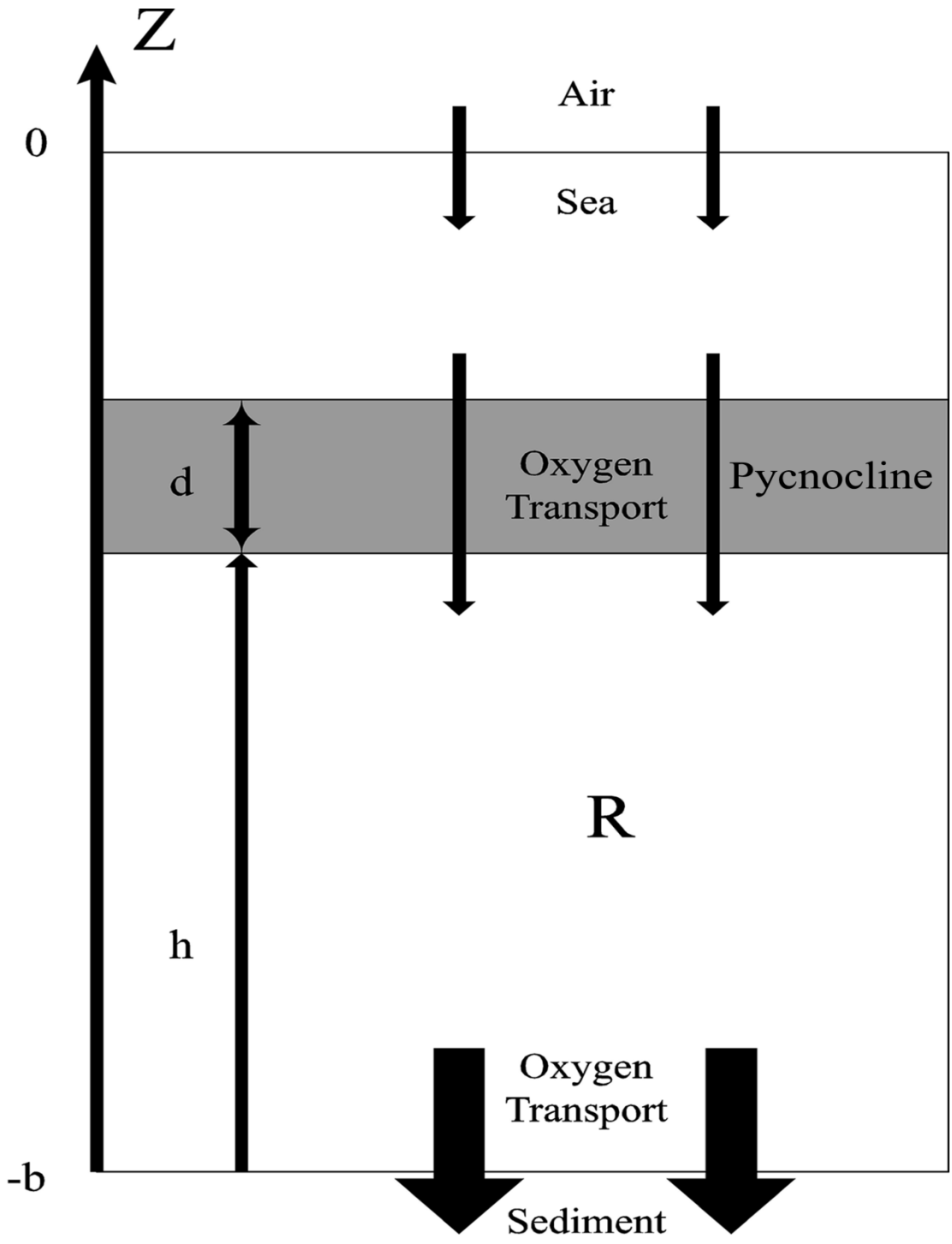

Figure 2.6 Schema for the one-dimensional subpycnocline box model of DO. Vertical axis is marked on the left. 0 depth and *–b* stand for sea surface and bottom, respectively. *h* and *d* are the thickness of subpycnocline layer and pycnocline respectively. *R* is the subpycnoline water-column oxygen consumption rate.

2.2.2. One dimension models

a) One-dimensional subpycnocline model for DO

To study the relationship between the vertical structure of stratification and vertical distribution of hypoxic water, I developed a one-dimensional DO model of sub-pycnocline DO dynamics (Figure 2.6). I made the following assumptions: (1) horizontal DO concentration gradients are negligible during hypoxia formation (Rowe 2001); (2) the effect of vertical advection on DO concentrations is negligible under stratified conditions; (3) DO changes are determined by the differences between local respiration and vertical mixing (Hetland and DiMarco 2010). With the above assumptions, the simplified equation from Eqn. 1 for vertical DO dynamics is

$$\frac{\partial O_2}{\partial t} = K_Z \frac{\partial^2 O_2}{\partial z^2} - r + p\,. \tag{5}$$

Eqn. 7 is vertically integrated from the seabed to the base of the pycnocline, $[-b, -b+h]$, where h is the thickness of the subpycnocline layer,

$$h\frac{\partial \overline{O_2}}{\partial t} = K_Z \left.\frac{\partial O_2}{\partial z}\right|_{-b+h} - B - hR\,, \tag{6}$$

where $\overline{O_2} = \frac{1}{h}\int_{-b}^{-b+h} O_2 dz$, $R = \frac{1}{h}\int_{-b}^{-b+h} (r-p)dz$ are the vertically averaged DO concentration and the integrated respiration rate, respectively. The oxygen flux at the bottom boundary is expressed as $B = K_Z \left.\frac{\partial O_2}{\partial z}\right|_{-b}$. The change of DO is then a sum of the vertical turbulent flux through the pycnocline, and biogeochemical processes that consume oxygen in the water-sediment boundary and the subpycnocline water.

The subpycnocline DO model is used to estimate the averaged respiration rate in the subpycnocline layer. Year-long bottom DO concentration data observed from the mooring is used to investigate the bottom DO concentration decrease rate. Vertical eddy diffusivity, pycnocline thickness and vertical DO gradient investigated from a 24-h anchor station at the same location as the mooring are used to estimate the vertical turbulent flux of oxygen.

b) One-dimensional DO model

To study stratification structure associated near-bottom hypoxia formation, a one-dimensional model is developed. The same assumptions are made as the one-dimensional subpycnocline DO model described in section 2.2.2 (a). The control equation is given as

$$\frac{\partial O_2}{\partial t} = \frac{\partial}{\partial z}(K_z \ \frac{\partial O_2}{\partial z}) - R. \tag{7}$$

where K_Z is the vertical eddy diffusivity, R is the respiration rate. This equation is solved numerically as following,

$$O_2 \ (z)_{t+\Delta t} = \left[\frac{1}{\Delta z}\left(\frac{K_z(z+\Delta z)+K_z(z)}{2} \times \frac{O_2 \ (z+\Delta z)_t - O_2 \ (z)_t}{\Delta z} - \frac{K_z(z)+K_z(z-\Delta z)}{2} \times \frac{O_2\,(z)_t - O_2\,(z-\Delta z)_t}{\Delta z}\right) - R(z)_t\right] \times \Delta t + O_2 \ (z)_t, \tag{8}$$

where $\Delta z = 0.5m$, $\Delta t = 300s$. The surface DO concentration was assumed to be held

constant by atmosphere exchange at the saturated value of 25 °C. The model was initialized with a saturated DO concentration at each bin from surface to 20 m at the bottom. The model was run for 60 days to allow the DO concentration to reach steady state.

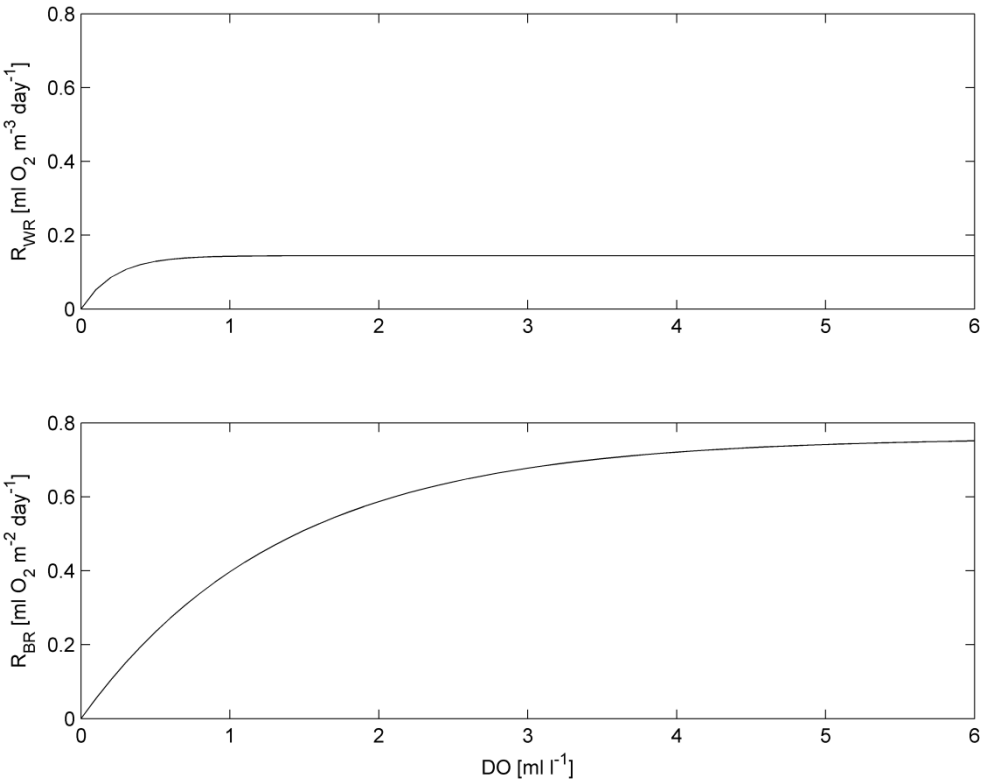

Figure 2.7 The water column respiration (upper panel) and benthic respiration (bottom panel) at 25 °C used in the model.

Water-column respiration was a function of local DO concentration and applied to each bin, which is developed based on the statement that water-column respiration appeared insensitive to DO concentrations when DO concentration > 35 mmol O_2 m^{-3} (Murrell and Lehrter 2011; Sampou and Kemp 1994),

$$R_{WR} = R_{AWR}\left(1 - \exp\left(\frac{-O_2}{5}\right)\right), \tag{9}$$

where R_{AWR} is the cruise averaged water-column respiration rate and given as 6.5 mmol O_2 m^{-3} day^{-1} (Murrell and Lehrter 2011). R_{WR} as a function of DO concentration is shown in the top panel of Figure 2.7.

The bottom boundary condition specifies benthic respiration as a function of bottom temperature and bottom DO concentration. The functional form is given by data collected by Rowe et al. (2002) and modified by Hetland and DiMarco (2008):

$$R_{BR} = 6.0 \times 2^{\frac{T}{10}} \times \left[1 - \exp\left(\frac{-O_2}{30}\right)\right]. \tag{10}$$

The local temperature (T) was set to 25 °C for the simulations. R_{BR} as a function of DO concentration is shown in the bottom panel of Figure 2.5.

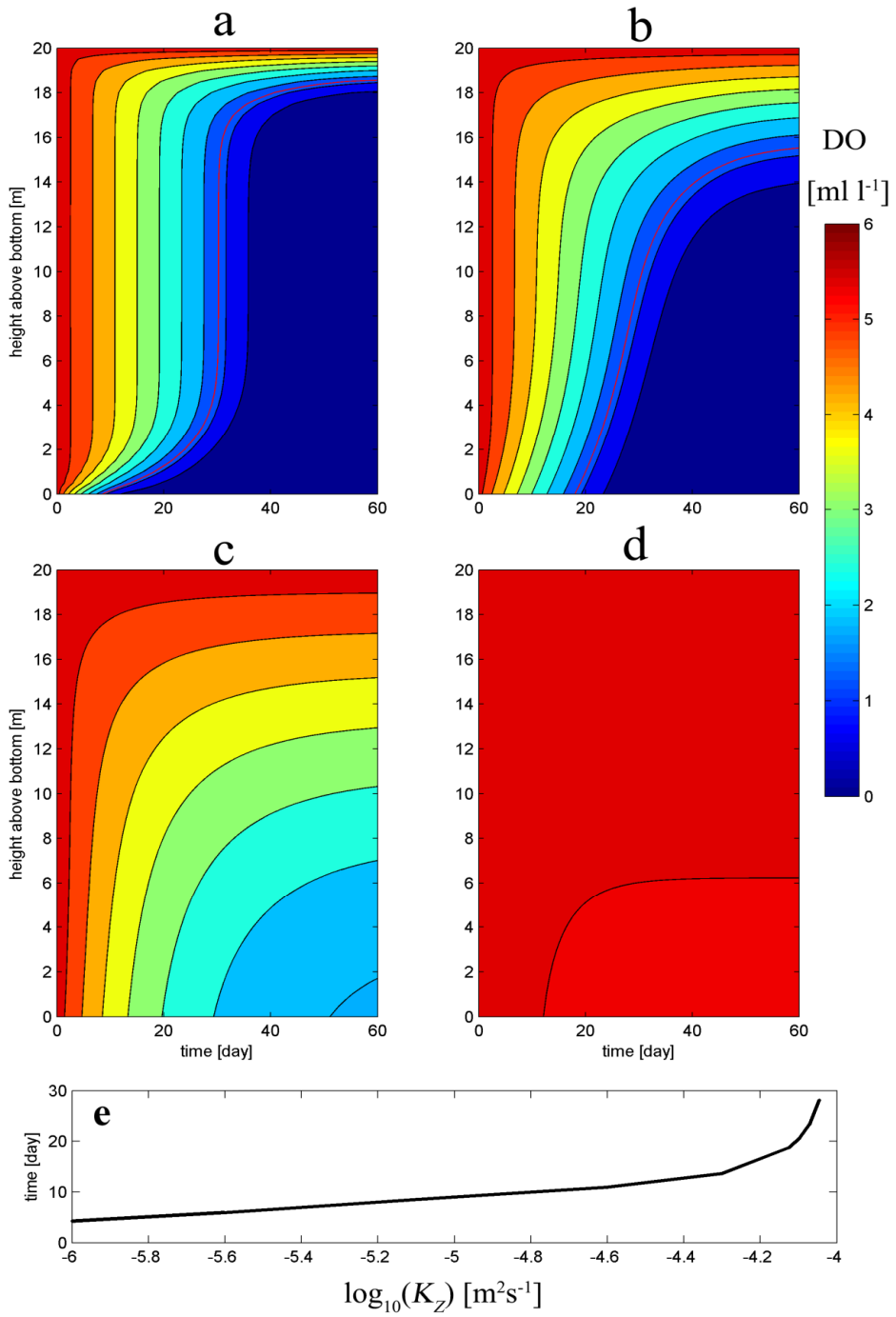

Figure 2.8 Simulated DO profiles changing with time with different K_Z: (a) $K_Z = 1 \times 10^{-6}$ m^2s^{-1}; (b) $K_Z = 1 \times 10^{-5}$ m^2s^{-1}; (c) $K_Z = 1 \times 10^{-4}$ m^2s^{-1}; (d) $K_Z = 1 \times 10^{-3}$ m^2s^{-1}. Hypoxia formation time in bottom layer with different K_Z is shown in (e).

K_Z ranges from 10^{-6} m^2s^{-1} (strongly stratified) to 10^{-3} m^2s^{-1} (mixing) in the ocean. To choose different K_Z for the strongly stratified layer, moderately stratified layer, and mixed layer, I tested different value of K_Z in the model (Figure 2.8e). K_Z was given as a constant value from surface to bottom to simulate the DO changes in the water column. The results show that hypoxia formation time in the bottom layer increases with the increasing of K_Z (Figure 2.8e). Four K_Z values are tested: 1×10^{-6} m^2s^{-1} (Figure 2.8a), 1×10^{-5} m^2s^{-1} (Figure 2.8b), 1×10^{-4} m^2s^{-1} (Figure 2.8c), and 1×10^{-3} m^2s^{-1} (Figure 2.8d). When $K_Z = 1 \times 10^{-6}$ m^2s^{-1}, bottom DO concentrations show the fastest decrease and DO is highly depleted in almost the whole water column (Figure 2.8a). It suggests that the value of $K_Z = 1 \times 10^{-6}$ m^2s^{-1} stands for strongly stratified status. And this value is also the same order as the estimated averaged K_Z along the pycnocline in Chapter IV. When $K_Z = 1 \times 10^{-5}$ m^2s^{-1}, bottom DO concentrations also decrease to zero (Figure 2.8b), but not as fast as the one with $K_Z = 1 \times 10^{-5}$ m^2s^{-1}. It suggests that the value of $K_Z = 1 \times 10^{-5}$ m^2s^{-1} stands for moderately stratified status. When $K_Z = 1 \times 10^{-4}$ m^2s^{-1}, no hypoxia is formed in the bottom and there are slight DO gradients in the water column (Figure 2.8c). It suggests that the value of $K_Z = 1 \times 10^{-4}$ m^2s^{-1} stands for lightly stratified status. When $K_Z = 1 \times 10^{-3}$ m^2s^{-1}, the water column is well mixed (Figure 2.8d). It suggests that the value of $K_Z = 1 \times 10^{-3}$ m^2s^{-1} stands for mixing status. Based on these analysis, I assume that the peak value of K_Z at the main-pycnocline is $K_{p1} = 1 \times 10^{-6}$ m^2s^{-1}; the peak value of K_Z at the secondary-pycnocline is $K_{p2} = 1 \times 10^{-5}$ m^2s^{-1}; the back ground K_Z is $K_b = 1 \times 10^{-6}$ m^2s^{-1}; and the K_Z in the mixed layer is $K_m = 1 \times 10^{-3}$ m^2s^{-1}.

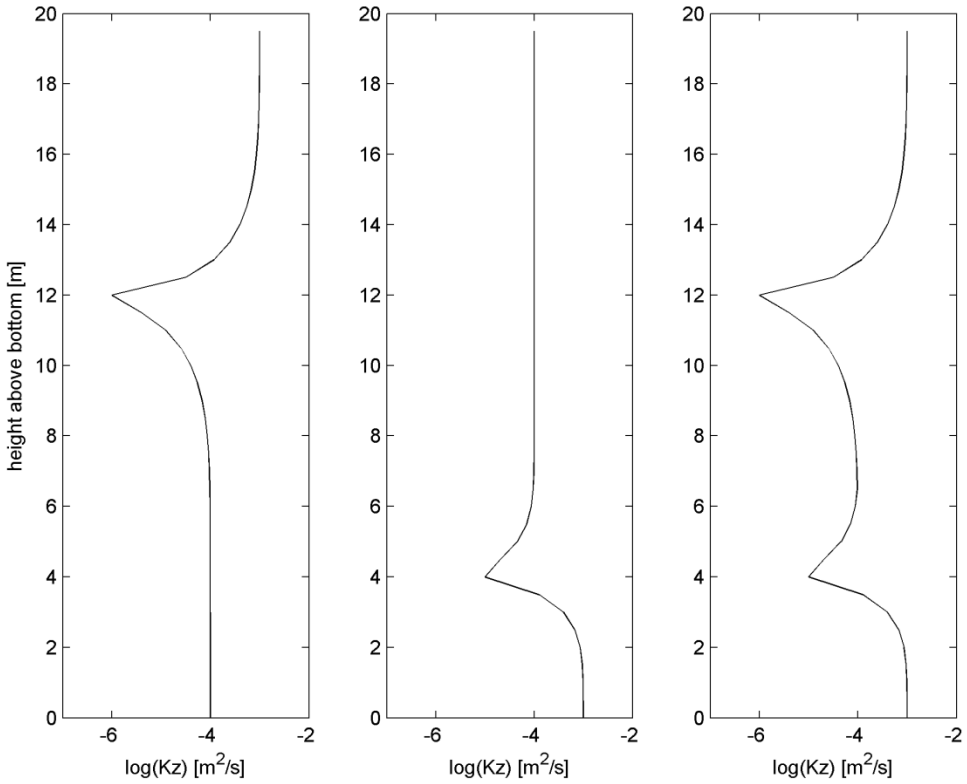

Figure 2.9 The vertical profile of K_Z of the three cases: single main pycnocline, single near-bottom pycnocline and double pycnoclines (from left to right).

A series of cases are designed with different K_Z profiles to study how hypoxia develops under different stratification structures. The parameterization (Bourgault et al. 2012) of the K_Z profile for pycnocline is given as

$$K_Z\ (z) = K_b\ - \left(K_b\ - K_p\ \right)\exp\left[-\frac{(z-H)^2}{d}\right], \tag{11}$$

where $K_b = 1 \times 10^{-4}$ m^2s^{-1} is the background K_Z, K_p is the peak value of the K_Z at the pycnocline, z is the height above bottom, H is the height of the pycnocline above bottom,

d = 4.0 m is the scale thickness of the pycnocline. Three cases are (1) single pycnocline below the surface mixed layer: $K_{p1} = 1 \times 10^{-6}$ m^2s^{-1}, H = 12 m (averaged thickness of the main-pycnocline is 8m, which means the pycnocline is 12 m above the bottom for a 20 m station); (2) single pycnocline above the bottom mixed layer: $K_{p2} = 1 \times 10^{-5}$ m^2s^{-1}, H = 4 m (averaged thickness of the secondary-pycnocline); (3) double-pycnocline, which is a combination of cases (1) and (2). The K_Z in the surface and bottom mixed layer are given as $K_m = 1 \times 10^{-3}$ m^2s^{-1} to stand for mixing status. The vertical profiles of K_Z for these three cases are shown in Figure 2.9.

CHAPTER III

STRATIFICATION STRUCTURE AND VERTICAL DISTRIBUTION OF DO

In this chapter, I analyzed the horizontal and vertical distributions of DO concentrations. Historical CTD data was used to determine stratification structures and vertical distributions of hypoxia, in particular a double-pycnocline structure. I also present the results from the one-dimension mixing model to show how stratification structure controls the formation of hypoxia, especially the effects of bottom mixed layer and double-pycnocline structure.

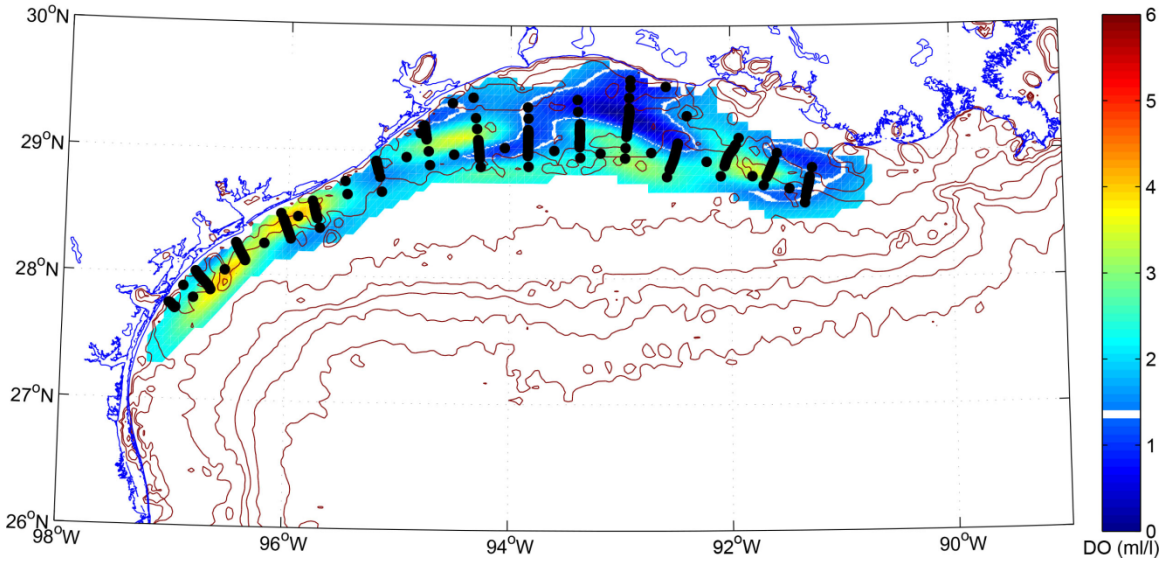

Figure 3.1 Near bottom DO concentration during MS2 cruise, 2-7 August 2010, using optimal interpolation of CTD and "Acrobat" data. Black dots represent the location of CTD casts and bottom measurements from "Acrobat". Hypoxic (DO < 1.4 ml l^{-1}) regions are in deep blue and circled out by white lines (S. F. DiMarco unpublished).

In the summer of the year 2010 and 2011, hypoxia zone was reported to cover 10352 km^2 (Figure 3.1) (roughly 20% of the region visited) and 8772 km^2 (Figure 3.2) (roughly 14% of the region visited), respectively. (Source: S. F. DiMarco, unpublished).

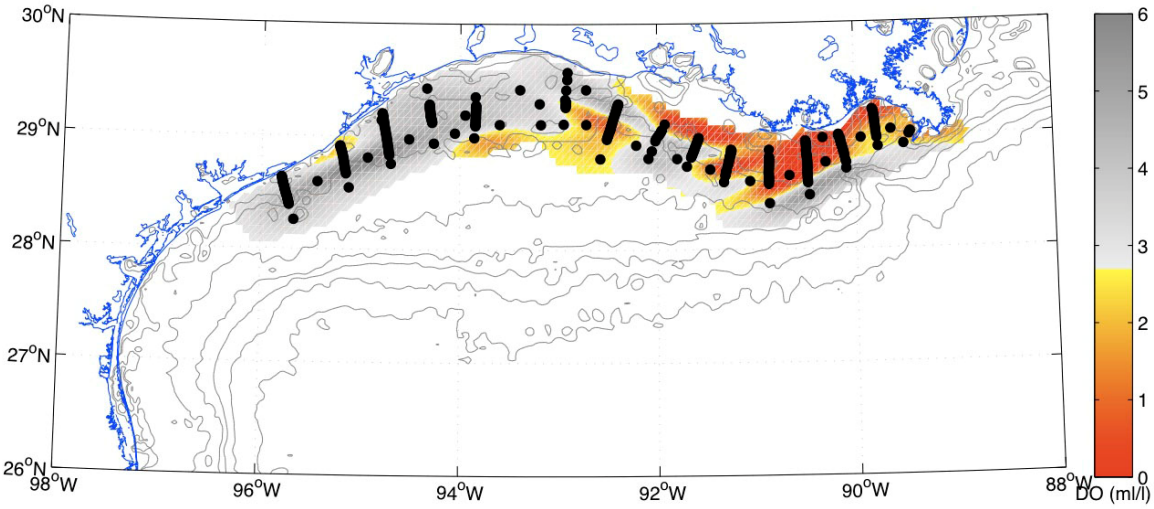

Figure 3.2 DO concentration during MS4 cruise, 8-15 August 2011, using optimal interpolation of CTD data. Black dots represent locations of CTD casts (S. F. DiMarco unpublished).

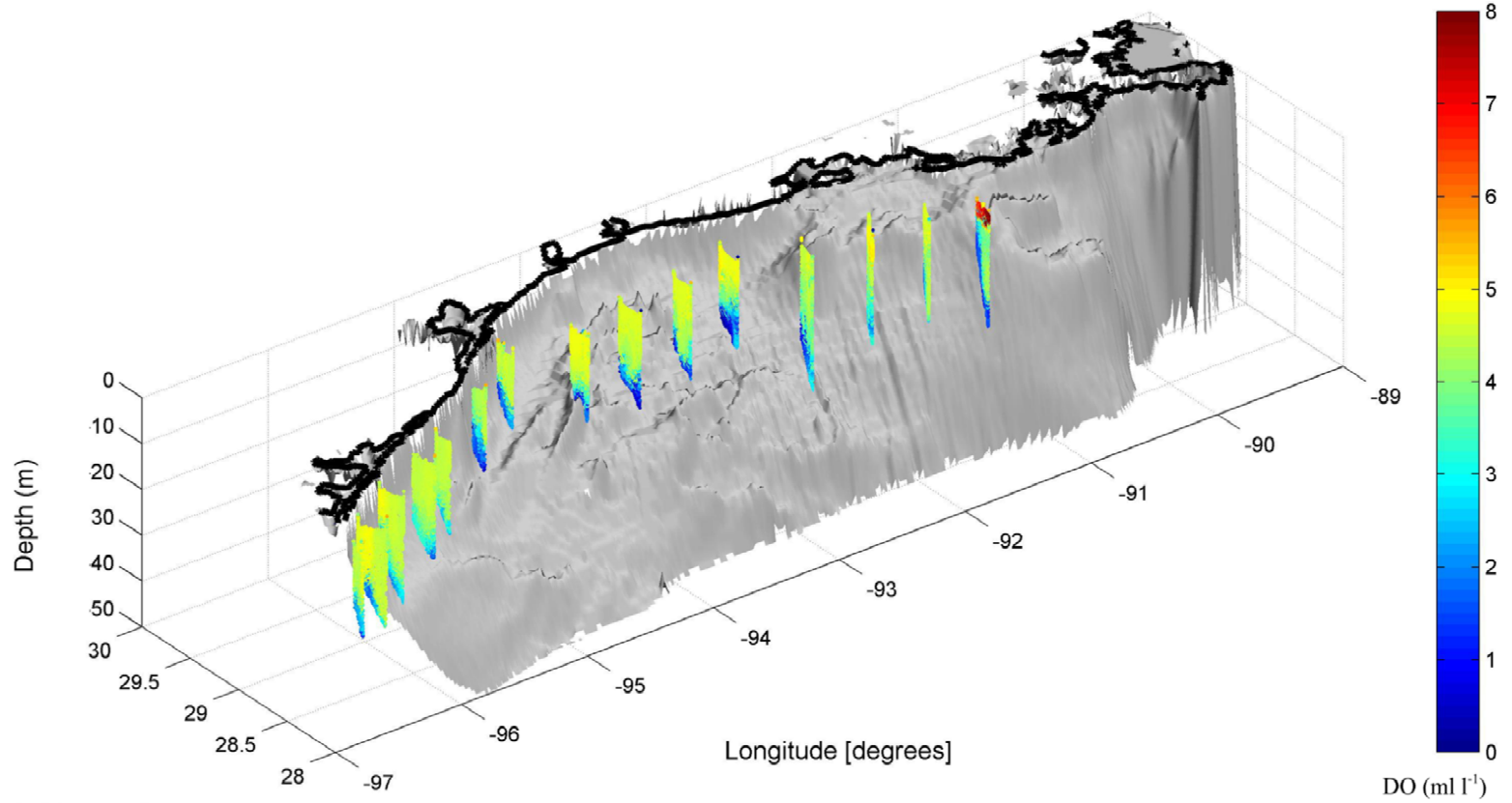

Figure 3.3 Vertical DO (ml l^{-1}) distributions along the "Acrobat" transects on the Texas-Louisiana Shelf during MS2 cruise in August 2010. Coastlines and bathymetry are included.

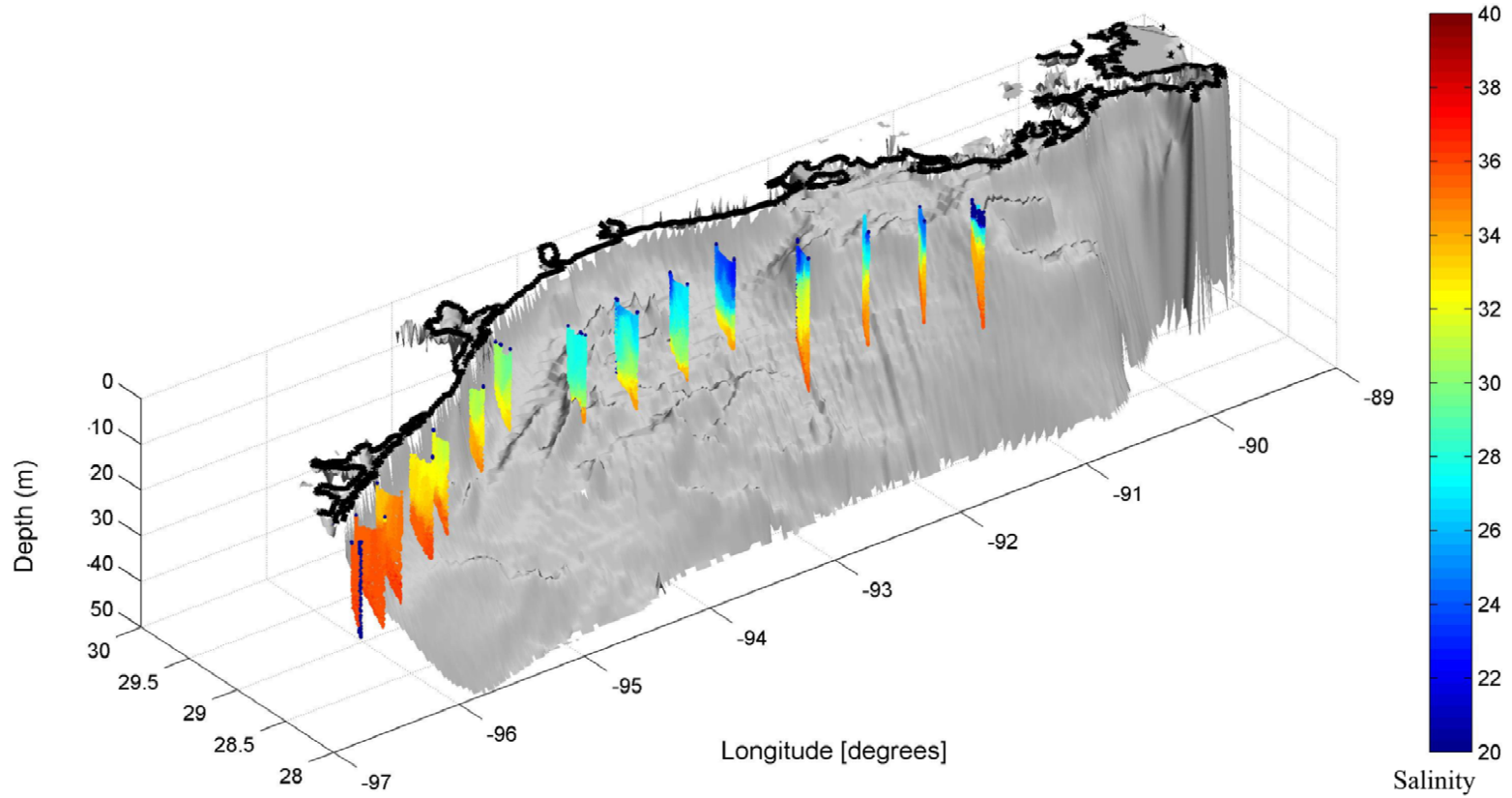

Figure 3.4 Vertical salinity (PSU) distributions along the "Acrobat" transects on the Texas-Louisiana Shelf during MS2 cruise in August 2010. Coastlines and bathymetry are included.

3.1. Results

3.1.1. Horizontal distribution of hypoxia

During the MS2 cruise, 2-7 August 2010, the horizontal distribution of hypoxia formed a patchwork of two separate regions, not a continuous band along the coast. The low DO concentration was found at the bottom of the water-column along the continental shelf between 10 m and 30 m isobaths (Figure 3.3, 3.4). The largest region was offshore south of Lake Charles, LA; the smaller region was south of the Atchafalaya Bay.

The MS4 survey cruise (8-15 August 2011) showed a different horizontal pattern (Figure 3.5). The MS4 cruise extended further east, between the Mississippi River Delta and the Terrebonne Bay. However, the hypoxic area was nearly all in shallow water on the eastern shelf, i.e., south and east of the Atchafalaya Bay (eastern part of the shelf). There was only one station south of San Luis Pass, TX, (29°N, 95°W) with significantly depleted bottom DO in the western shelf area. The shelf waters west of 93°W were found with high salinity (35) and high DO concentrations (> 4ml l^{-1}), indicating that the western shelf was covered by salty oceanic water but not freshwater. The western waters were vertically uniform in temperature, salinity and DO concentration, indicating that the water column there was well mixed (Figure 3.5, 3.6).

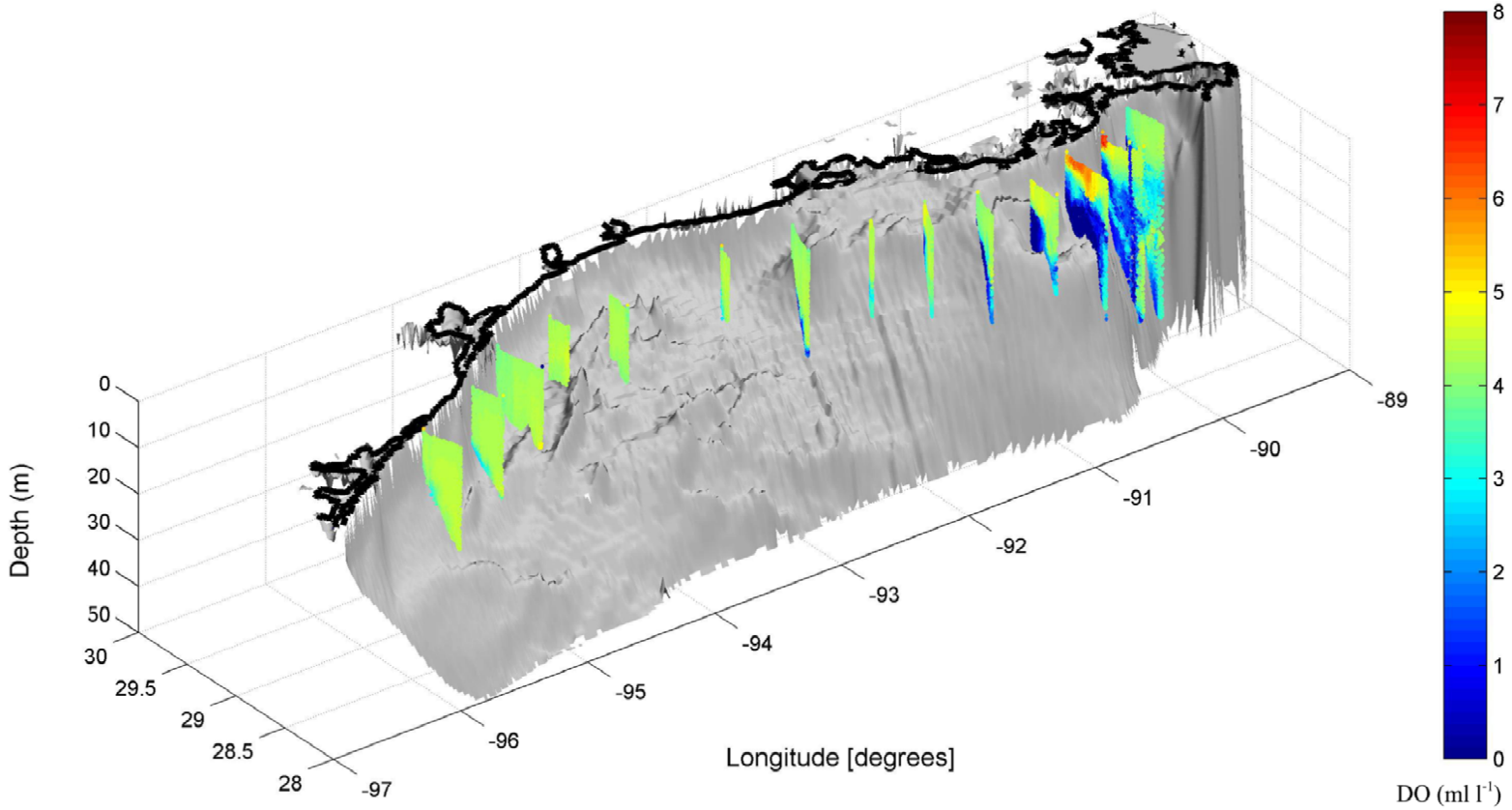

Figure 3.5 Vertical DO (ml l^{-1}) distributions along the "Acrobat" transects on the Texas-Louisiana Shelf during MS4 cruise in August 2011. Coastlines and bathymetry are included.

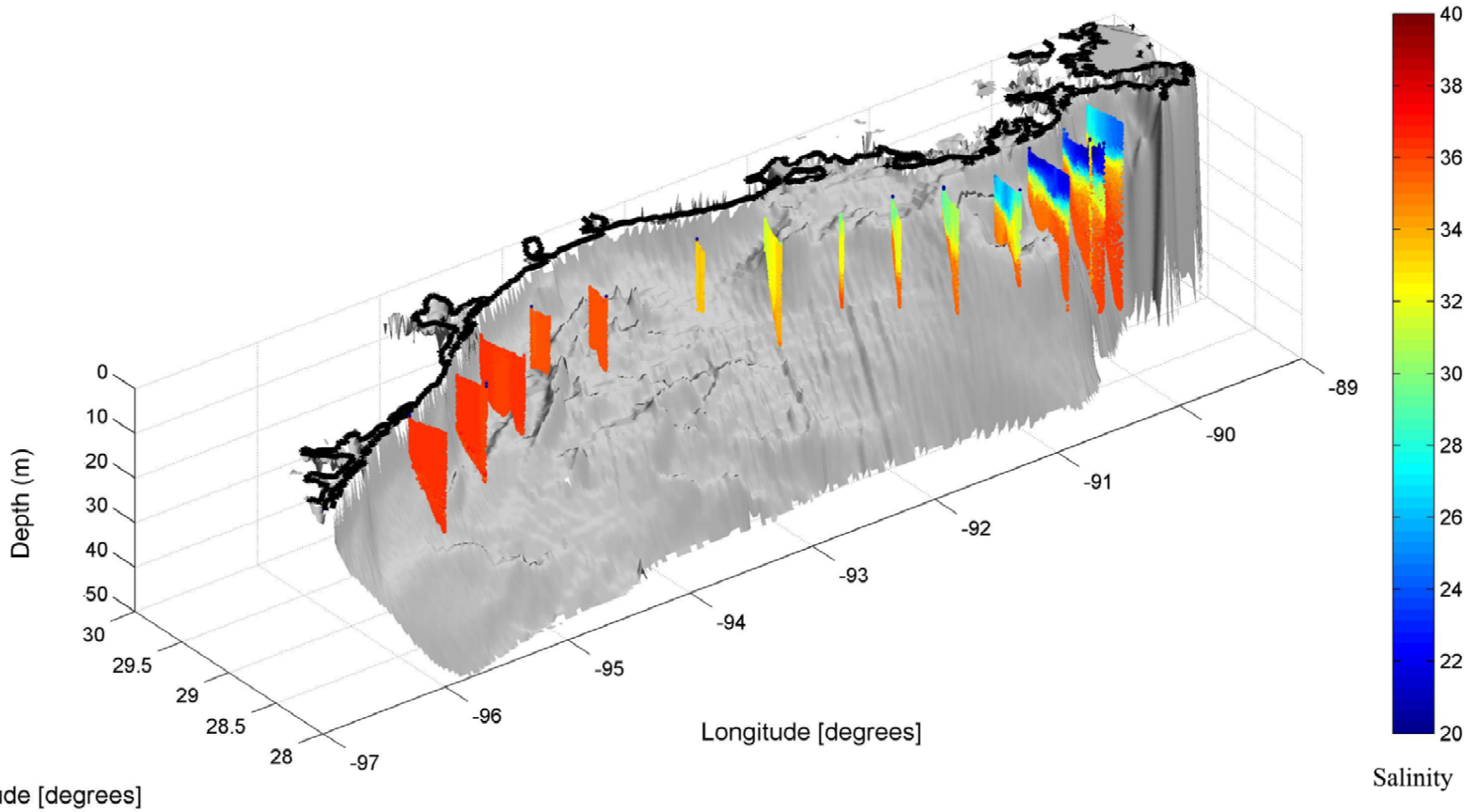

Figure 3.6 Vertical Salinity (PSU) distributions along the "Acrobat" transects on the Texas-Louisiana Shelf during MS4 cruise in August 2011. Coastlines and bathymetry are included.

3.1.2. Vertical distribution of hypoxia from Acrobat transects

Hypoxia was observed along the cross-shelf transects during MS2 and MS4 cruises. Vertical distributions of hypoxia under different stratification structures observed were described in this section.

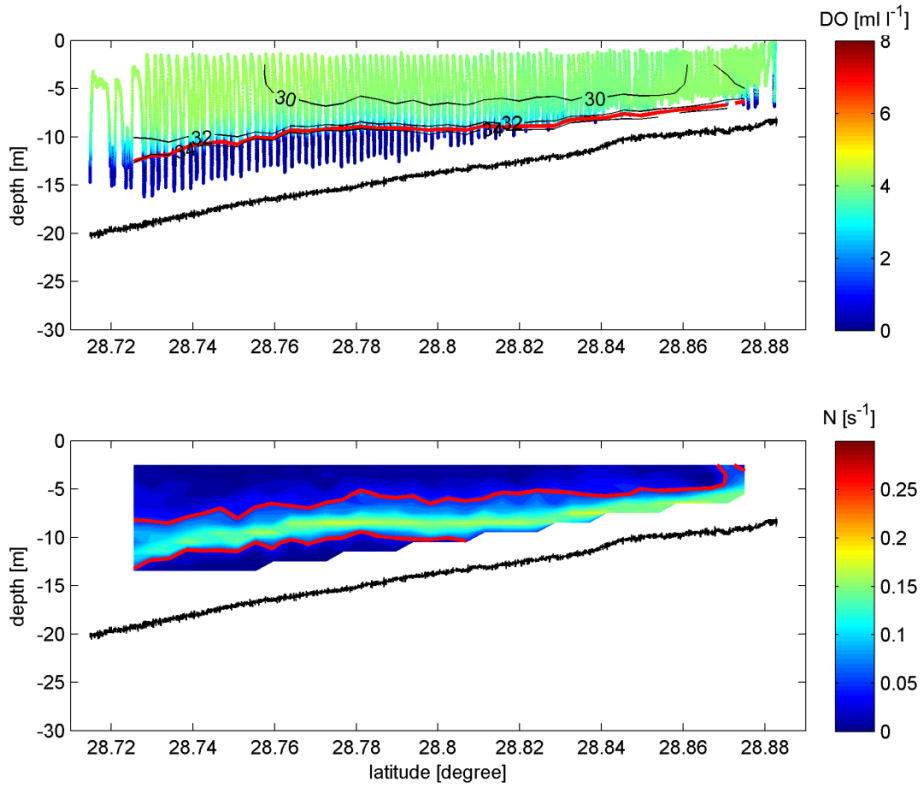

Figure 3.7 Cross-shore transect during the MS2 cruise in August 2010. Top: the color map denotes DO concentration, the red contour lines denote the boundary of the hypoxia and the black contour lines denote salinity. Bottom: contour plot of N for the same section in unit of s^{-1} while the red contour lines denote $N = 0.05\ s^{-1}$. Black lines below the color map show the bottom in both panels.

A transect with single pycnocline is shown in Figure 3.7 at a depth near 15 m during the MS2 cruise, 2-7 August 2010. A single pycnocline is found at 15m with $N \sim 0.1\ s^{-1}$ (Figure 3.7 bottom). In the layer above the pycnocline, salinity is around 24 and DO concentration is around 5 ml l^{-1}. In the layer below the pycnocline, salinity is around 32 and DO concentration is about 1 ml l^{-1}, which is hypoxic. Both the salinity and DO concentration show large vertical gradient at the pycnocline (Figure 3.7 top). 1.4 ml l^{-1} DO isopleth is located at the pycnocline (Figure 3.7 top). Hypoxic water is found below the pycnocline, which covers from the bottom to 15 m depth vertically.

Hypoxic water is also found with a double-pycnocline structure shown in the top of Figure 3.8 at a cross-shelf transect south of Atchafalaya Bay during the MS2 cruise, 2-7 August 2010. A double-pycnocline structure is shown in the bottom panel of Figure 3.8. The main-pycnocline is located at 4 to 10 below the surface, which is formed by the low salinity (about 18) water in the surface (Figure 3.8 top). The secondary-pycnocline was parallel to the bottom bathymetry slope with a thickness about 3 m. The thickness of the thin layer below the secondary-pycnocline varies from 5 m at the offshore end to 3 m at the inshore end of this transect (Figure 3.8 bottom). Although the strength of the main-pycnocline ($N \sim 0.2\ s^{-1}$) is stronger than the secondary-pycnocline ($N \sim 0.1\ s^{-1}$), no hypoxia is found between the main-pycnocline and the secondary-pycnocline. Hypoxia is only observed inside of the thin layer below the secondary-pycnocline.

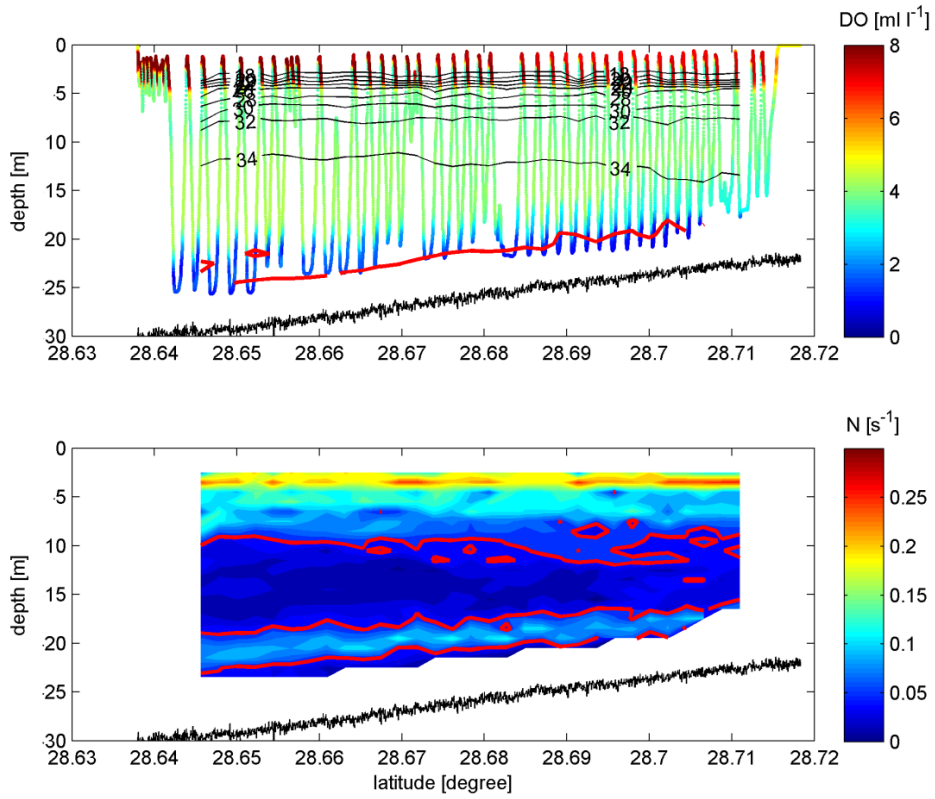

Figure 3.8 Cross-shore transect during MS2 cruise, August 2010. Top: the color map denotes DO concentration, the red contour lines denote the boundary of hypoxia, and the black contour lines denote salinity. Bottom: contour plot of N for the same transect in unit of s^{-1} while the red contour lines denote $N = 0.05$ s^{-1}. Black lines below the color map show the bottom in both panels.

Non-hypoxic water is observed between two hypoxic layers during the MS4 cruise, August 2011. Figure 3.9 shows the vertical DO distribution at a cross-shelf "Acrobat" transect on the eastern part of the shelf. Two hypoxic layers are detected below the pycnocline, which are separated by a high DO layer (DO concentration is about 4 ml l^{-1}). One hypoxic layer is near the bottom with a thickness of 4 to 5 m along

the shelf slope. The other hypoxic layer is 8 to 10 meters above the bottom from offshore to inshore. A high DO layer is located between these two hypoxic layers. All three layers are below the main-pycnocline and the thickness of these layers increases with depth.

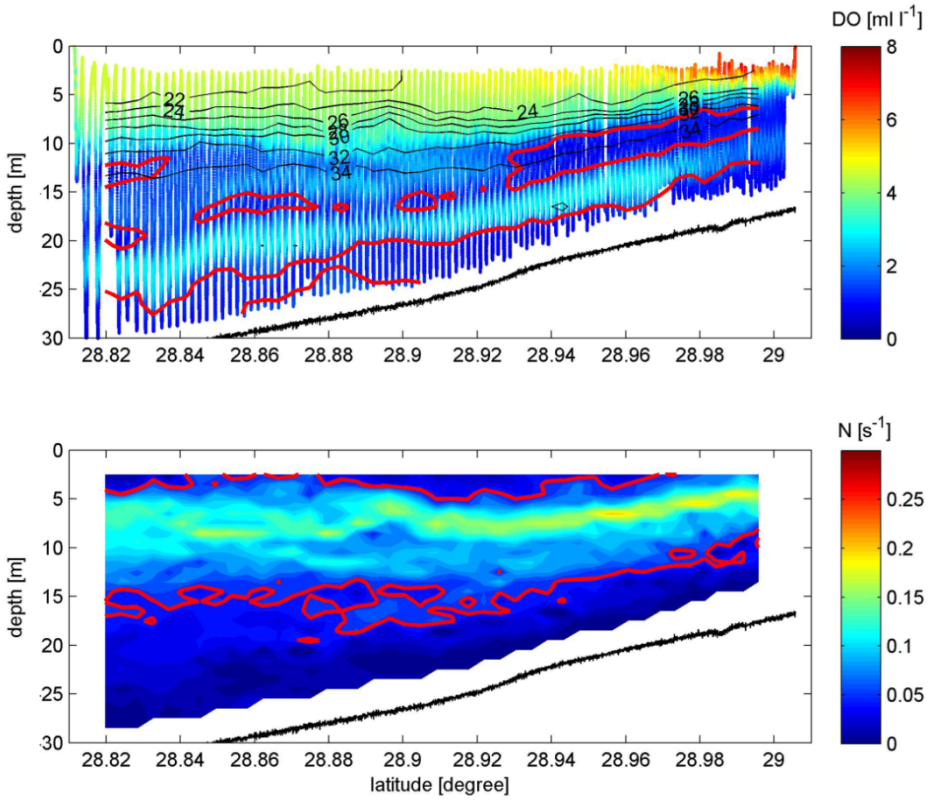

Figure 3.9 Cross-shore transect during the MS4 cruise in August 2011. Top: the color map denotes DO concentration, the red contour lines denote the boundary of the hypoxia, and the black contour lines denote salinity. Bottom: contour plot of *N* for the same section in unit of s^{-1} while the red contour lines denote N = 0.05 s^{-1}. Black lines below the color map show the bottom in both panels.

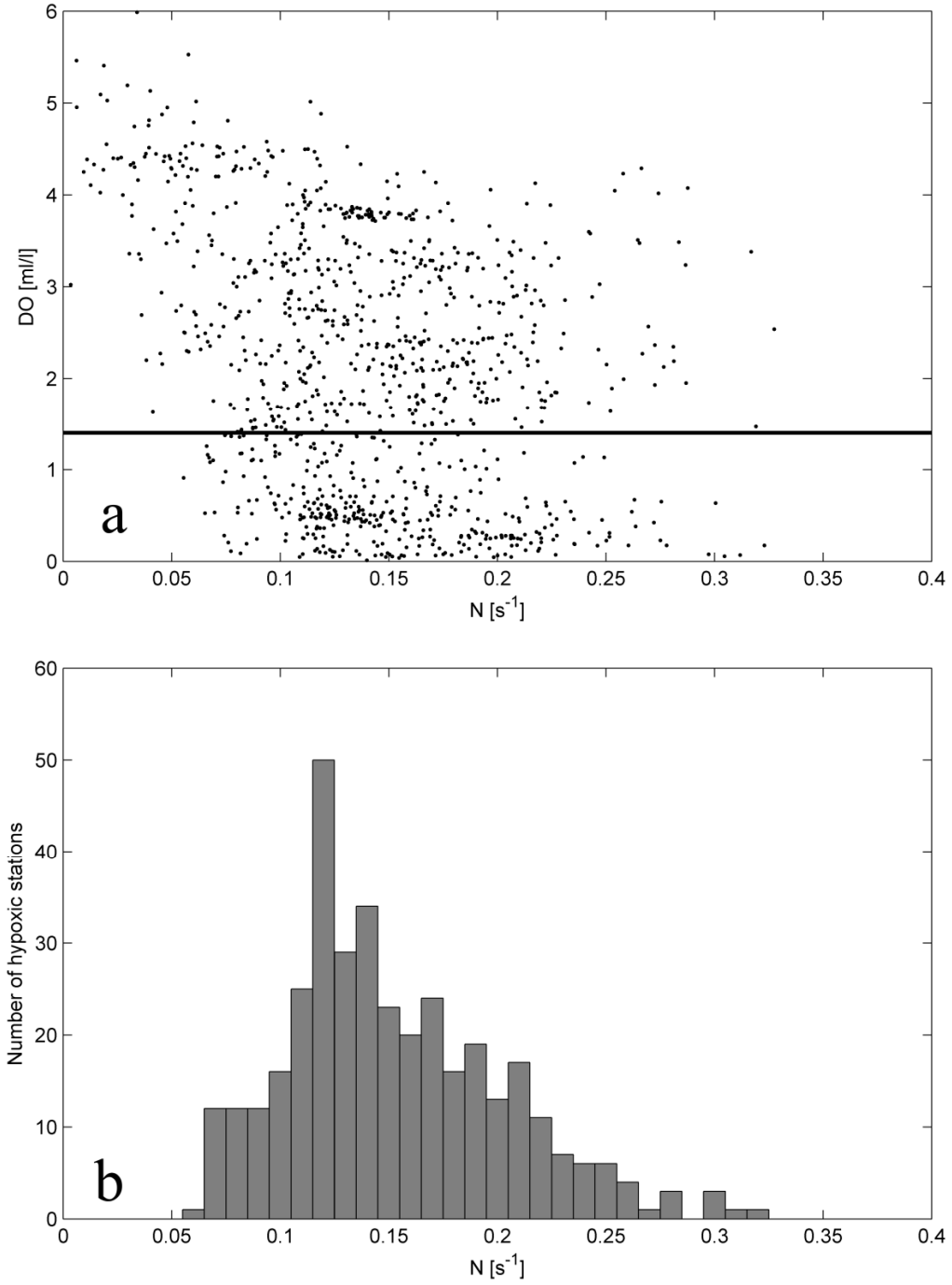

Figure 3.10 Upper panel: near-bottom DO concentration versus N_{max} for all the CTD profiles from MCH cruises between 2003 and 2009. The threshold of 1.4 ml l^{-1} for hypoxia are shown with horizontal solid line. Bottom panel: histogram of the number of hypoxic stations at different N_{max}.

3.1.3. Stratification strength and development of hypoxia

N_{max} (the maxima of N) and near-bottom DO concentrations for each CTD profile from MCH cruises between 2003 and 2009 (1202 CTD profiles in total) are shown in Figure 3.10a. No hypoxic station was observed when $N_{max} < 0.05$ s^{-1}. However, there is only one hypoxic station between $N_{max} = 0.05$ s^{-1} and $N_{max} = 0.06$ s^{-1} (Figure 3.10b). The number of hypoxic stations shows a peak at $N_{max} = 0.12$ s^{-1} and decreases when stratification becomes either stronger (larger N) or weaker (smaller N). Fewer hypoxic stations are expected to be observed with weaker stratification, which is shown in the Figure 3.10b where $N_{max} < 0.12$ s^{-1}. Why does the number of hypoxic stations become fewer as N_{max} increasing when $N_{max} > 0.12$ s^{-1}? The explanation is that fewer stations are found with such a high $N_{max} > 0.12$ s^{-1} in all the CTD profiles. However, hypoxia is expected to have a higher rate to be found in the profiles with larger N_{max}. Most of the hypoxic stations are observed with $N_{max} = 0.1$~0.2 s^{-1}.

A lower limit of N_{max} is considered to provide the stratification environment for hypoxia development. The accumulation line of hypoxic station numbers in percentage along the N_{max} from the MCH cruises between 2003 and 2009 are shown as a solid line in Figure 3.11. The percentage of hypoxic stations increases slowly when N_{max} between 0.05 s^{-1} and 0.1 s^{-1}. The slow increase of hypoxic station numbers is probably caused by the errors in estimation of N due to measurements noise. The lower limit of N_{max} is estimated as the 1% cut-off of the accumulation line to avoid the errors in estimation of N. The estimated lower limit of N_{max} is 0.06 s^{-1}. A series of shelf wide cruises had been made to estimate the hypoxic area size every summer by LUMCON (Louisiana

Universities Marine Consortium). The CTD profiles of these cruises from 1998 to 2007 were also used to estimate the lower limit of $N_{max,}$ shown by dashed line in Figure 3.11. The estimated lower limit of N_{max} is 0.07 s^{-1} for the LUMCON cruises, which is close to the estimate from the MCH cruises.

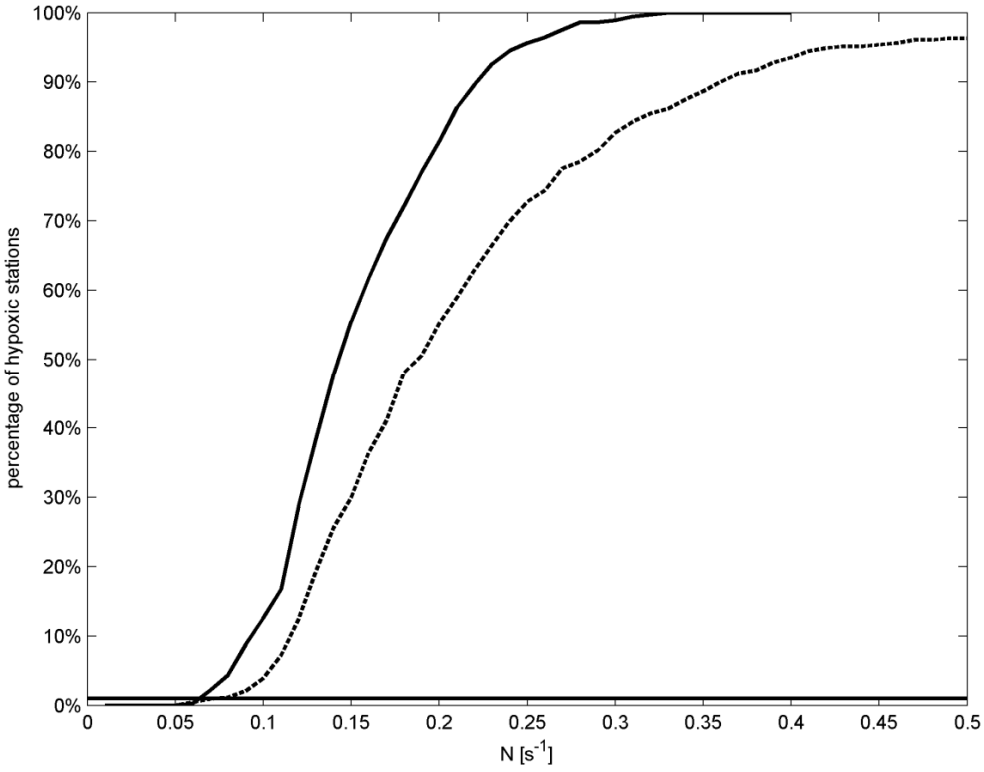

Figure 3.11 Accumulation lines of hypoxic station numbers in percentage along with the N_{max} for CTD profiles from MCH cruises between 2003 and 2009 (solid) and CTD profiles from the cruises made by LUMCON to estimate the hypoxic area size between 1998 and 2007 (dashed). The horizontal solid line denotes the 1% cut-off.

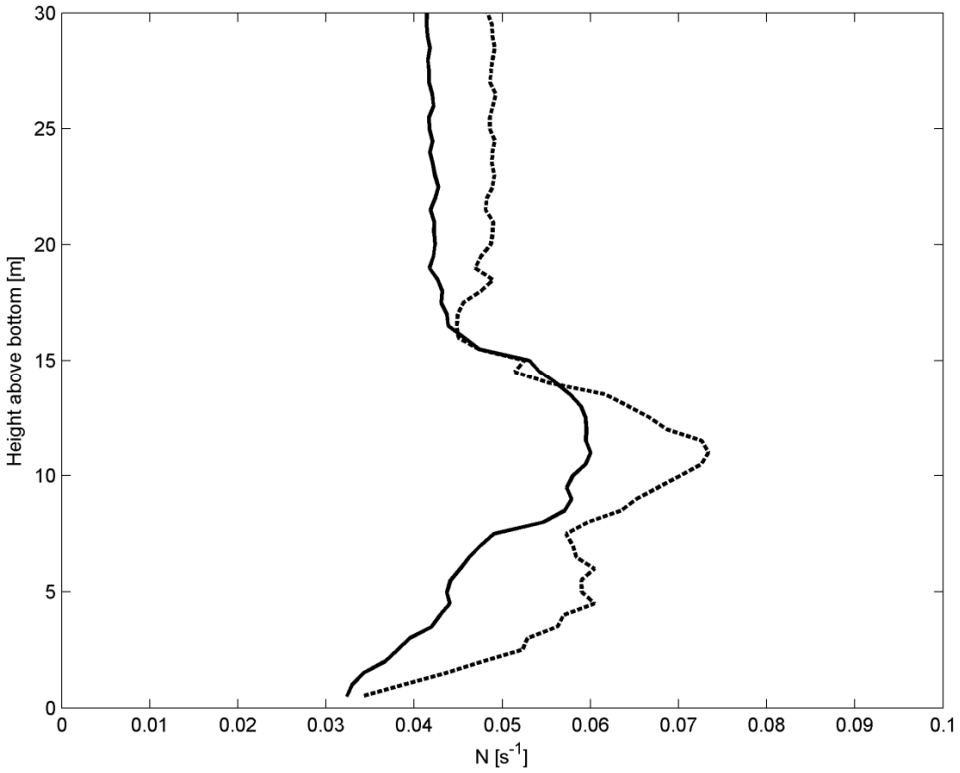

Figure 3.12 Averaged *N* at each height above bottom for all the profiles (solid) and hypoxic profiles (dashed lines).

The averaged *N* at each height above bottom for all the CTD profiles are shown in Figure 3.12 by solid line. The back ground stratification is around $N = 0.04\ s^{-1}$. *N* in the strongly stratified layer from eight to fifteen meters above bottom is around $0.06\ s^{-1}$. The near bottom averaged *N* is even smaller than $0.04\ s^{-1}$. The dashed line in Figure 2.4 shows the averaged *N* at each height above the bottom for all the hypoxic profiles. For most of the depth, the averaged *N* in the hypoxic profiles is larger than average of all the

profiles. The largest averaged *N* differences between the hypoxic profiles and all profiles are about 9~13 m above the bottom, and the second largest differences are about 4~6 m above the bottom. These two layers are just at the locations of the main-pycnocline below the surface mixed layer and the secondary-pycnocline above the bottom mixed layer (Figure 2.2, Figure 2.3). It suggests that the major stratified layers causing hypoxia are probably these two layers.

3.1.4.Observed stratification structure and vertical distribution of hypoxia

Hypoxia is observed in 245 of the 704 CTD profiles (34%) during the MCH cruises between 2003 and 2009 (continuous stations with CTD casts every an hour are considered as one profile). The hypoxic layer thickness is set to zero if only the deepest DO concentration is hypoxic. The histogram of the thicknesses of the hypoxic layers is shown in Figure 3.13. 75% of the hypoxic layers are within 4 m above the bottom. Furthermore, 58% of the hypoxic layers are in or along the bottom mixed layers.

The thicknesses of bottom and surface mixed layers are shown in Figure 3.14. The averaged thickness of bottom mixed layer is 2.8m. 86% of the bottom mixed layers are thinner than 5 m. The averaged thickness of the surface mixed layer is 5.1m. 62% of the surface mixed layers are thinner than 5 m. The stratified layer is between the bottom mixed layer and surface mixed layer. A strong pycnocline was usually observed below the surface mixed layer, and a relatively weak pycnocline was usually observed above the bottom mixed layer. If the water depth of the CTD station, e.g. 10 m, is close to the sum of bottom and surface mixed layers' thicknesses, the stratified layer between them

is thin. Therefore, the relatively weak pycnocline above the bottom mixed layer is merged into the strong pycnocline below the surface mixed layer. If the water depth of the CTD station, e.g. 20 m, is much larger than the sum of bottom and surface mixed layers' thicknesses, the stratified layer between them is thick. A double-pycnocline structure is supposed to be observed (Figure 2.3).

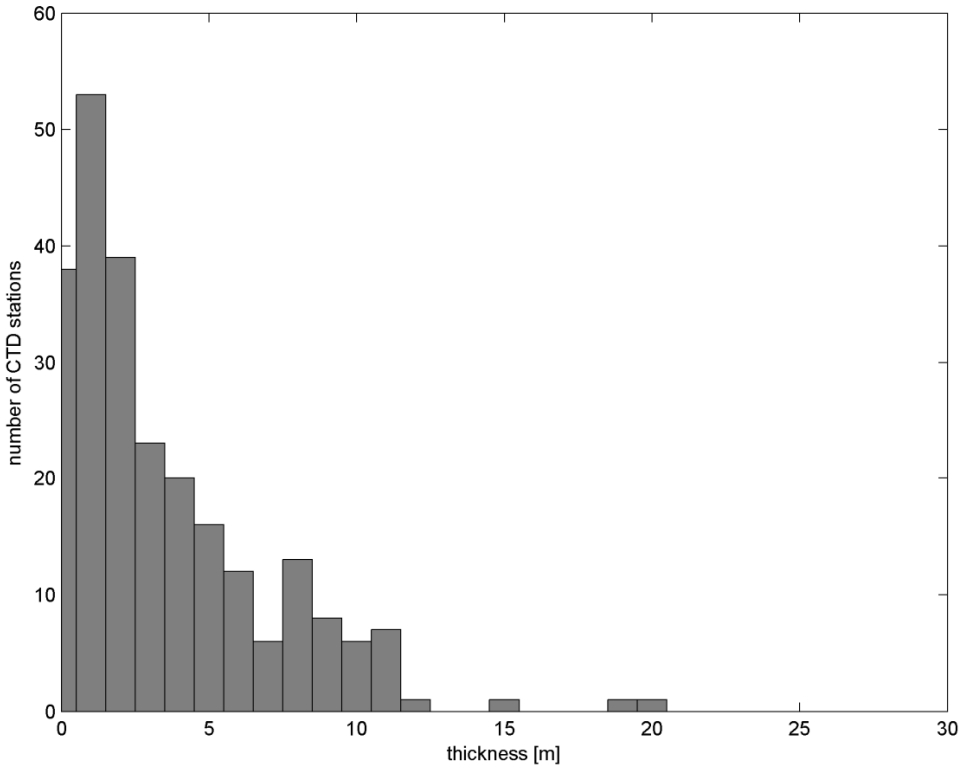

Figure 3.13 Histogram of the thicknesses of the hypoxic layers (or heights of the hypoxic layers above bottom) for all the profiles from the MCH cruises between 2003 and 2009.

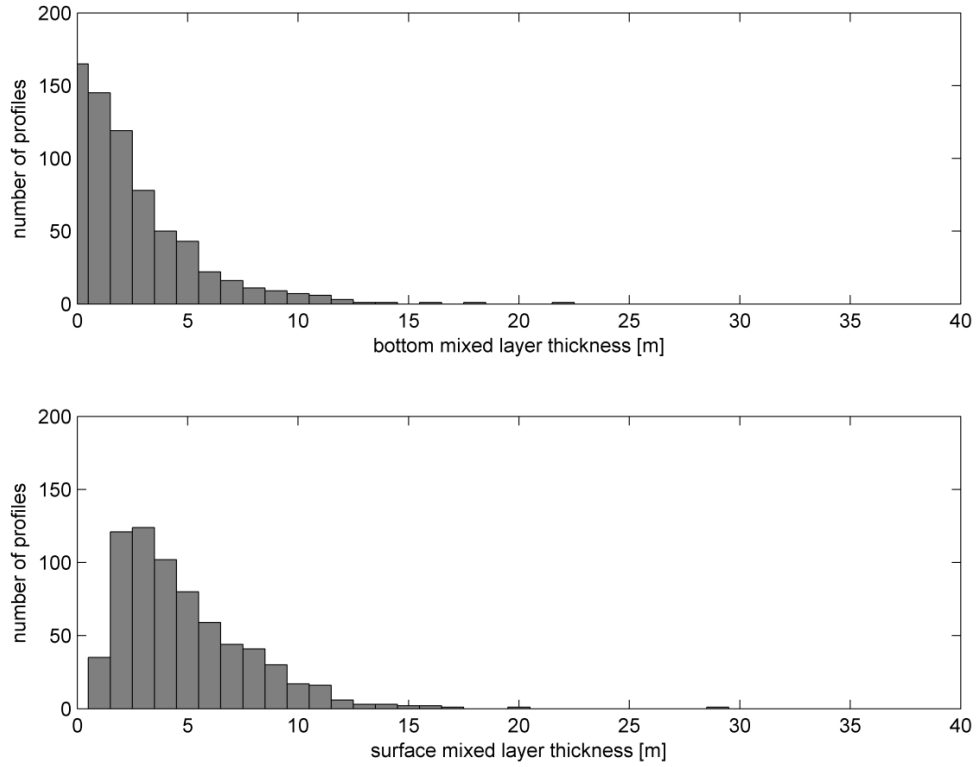

Figure 3.14 Histograms of thicknesses of the bottom (top) and surface mixed layers observed in the CTD profiles from MCH cruises between 2003 and 2009.

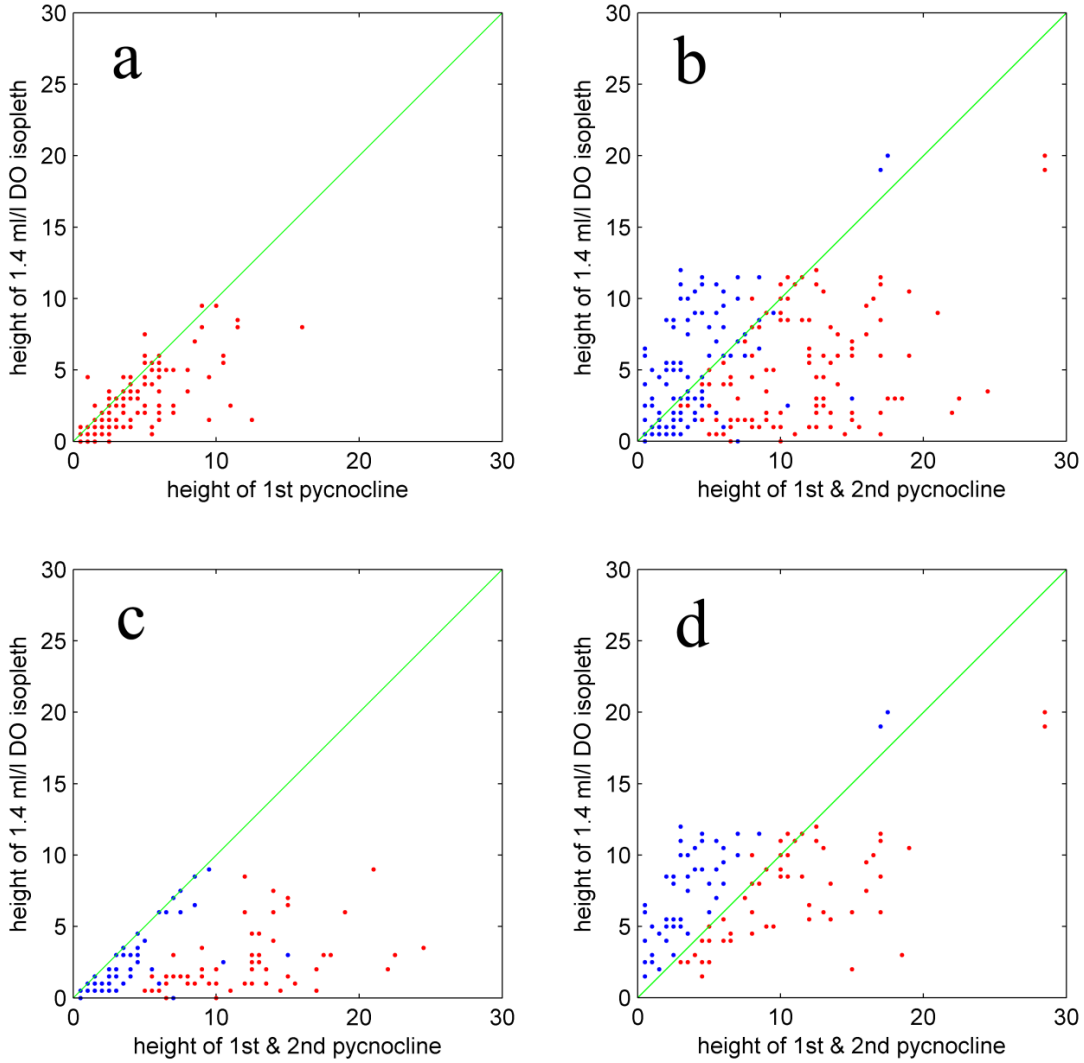

Figure 3.15 Scatter plot of the height of the 1.4 ml l^{-1} DO concentration isopleth above the bottom against the height of the main (red dots) and secondary (blue dots) pycnocline for the CTD profiles from MCH cruises between 2003 and 2009. (a) CTD profiles with single pycnocline (n=132). (b) CTD profiles with double-pycnocline (n=113). (c) CTD profiles with hypoxia below the secondary-pycnocline (n=57). (d) CTD profiles with hypoxia top interface between the main and secondary-pycnoclines (n=56).

Among 245 hypoxic profiles, there are 132 profiles (54%) with single-pycnocline structures and 113 profiles (46%) with double-pycnocline structures. For the profiles with single-pycnocline structure, the height of the pycnocline is closely associated with height of the hypoxic layer (1.4 ml l^{-1} DO isopleth) (Figure 3.15a), in agreement with Wiseman et al. (1997). For the profiles with double-pycnocline structures, most of the hypoxic water is below the main-pycnocline and fills the bottom-layer (Figure 3.15b). The secondary-pycnocline is found several meters above the hypoxic layer in several profiles, which is considered to be caused by the error in estimating the secondary-pycnocline. It suggests that all the water in the bottom-layer is hypoxic once there is hypoxia. However, neither the main-pycnocline nor the secondary-pycnocline is associated with height of the 1.4 ml l^{-1} DO isopleth (Figure 3.15b). Consider two possible double-pycnocline structure cases: (1) the hypoxic layer is in the bottom-layer, below the secondary-pycnocline (57 profiles, Figure 3.15c), and (2) the hypoxic layer extends into the mid-layer, above the secondary-pycnocline but below the main-pycnocline (56 profiles, Figure 3.15d). For case (1), the height of the secondary-pycnocline is associated with height of 1.4 ml l^{-1} DO isopleth (Figure 3.15c), which is also in agreement with Wiseman et al. (1997). For case (2), when hypoxia extends across the secondary-pycnocline, hypoxia develops in the mid-layer and the secondary-pycnocline is no longer the top boundary of hypoxic water, but hypoxia is still below the main-pycnocline (Figure 3.15d).

3.1.5. Modeling hypoxia development under different stratification structures

A one-dimensional DO model was developed to study the development of hypoxia under different stratification structures. Three basic cases are described in Chapter II. The modeling results are shown in this section.

The single mid-depth pycnocline case simulates a situation in the natural environment with a strong pycnocline at a depth of 10 m caused by surface fresh water. Near-bottom DO concentration reaches hypoxic level in 27 days and decreases to zero after about 35 days (Figure 3.16a2, and 3.16a3). The DO concentrations at bottom and mid-layer (7 m above the bottom) decrease linearly from the initial value (5.7 ml l^{-1}) to zero. Meanwhile, DO concentration remains at the saturated value in the surface-layer (Figure 3.16a2). There are strong vertical DO gradients at the pycnocline. DO concentration in the subpycnocline water shows a small vertical gradient, a sign that the subpycnocline water is mixed (Figure 3.16a3). The simulation reaches a steady state when the vertical DO flux from the surface balances the local DO consumption. In this case, hypoxia is confined below the pycnocline and the pycnocline is the upper boundary for hypoxia.

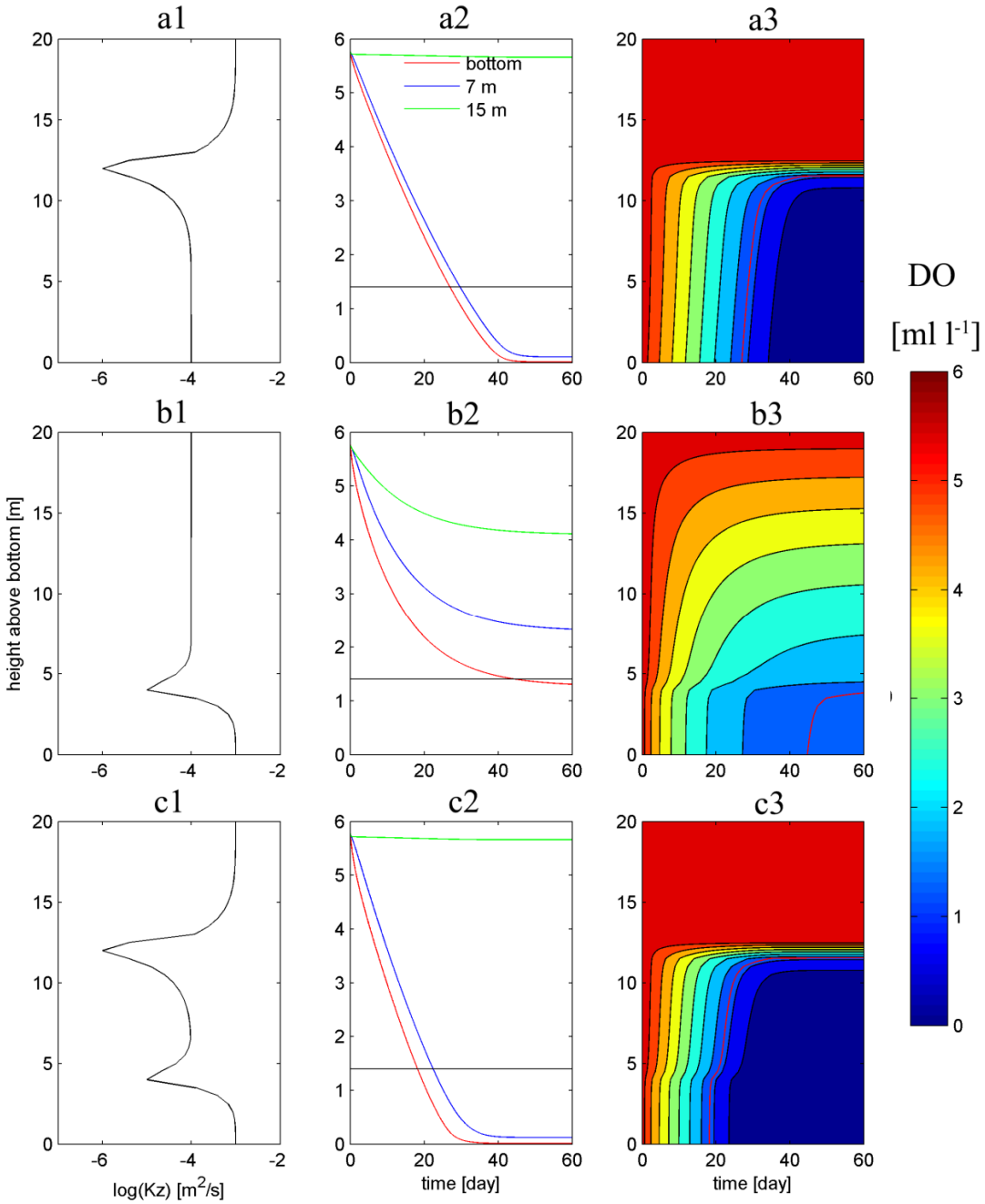

Figure 3.16 Simulation results from the one-dimension DO model. Three cases are shown by rows from top to bottom: single mid-depth pycnocline (a1, a2, a3), single near-bottom pycnocline (b1, b2, b3), and double-pycnocline (c1, c2, c3). Figures in the left, middle and right columns are the K_Z profiles, DO concentration changes with time at bottom, 7 m and 15 m above bottom, and contour plots of DO concentration changes with time for each case.

The single near-bottom pycnocline simulates a situation in the natural environment with a relative weak near-bottom pycnocline, considered to be the top interface of the bottom boundary layer (section 3.3.4). It takes 45 days for the bottom water to become hypoxic (Figure 3.16b2, and 3.16b3). The DO concentrations at bottom and mid-layer (7 m above the bottom) decrease linearly from the initial value in the first 15 days. The rate of decrease slows down and the simulation reaches steady state after 50 days of simulation. Meanwhile, surface DO concentration decreases about 1.6 ml l^{-1} (Figure 3.16b2). When the simulation reaches steady states, the vertical DO gradient is also at the pycnocline, but weaker than the single mid-depth pycnocline case. However, the vertical DO gradient is found above the pycnocline. The 1.4 ml l^{-1} DO isopleth is located 3 m above the bottom, which is also the depth of the near-bottom pycnocline. In this case, hypoxic water is still confined below the single near-bottom pycnocline and this pycnocline is the upper boundary for hypoxia.

The double-pycnocline case simulates the situation when both a fresh water caused mid-depth strong pycnocline and a near-bottom secondary-pycnocline exist. As such, this is a combination of the case (1) and case (2) above. It takes 18 days for the bottom water to reach hypoxia (figure 3.16c2 and 3.16c3). The DO concentration at bottom decreases linearly from the initial value to zero in about 35 days. For the mid-layer, the DO concentration also decreases linearly from the initial value to almost zero in about 40 days, which is about 5 days late than near-bottom DO concentration. Meanwhile, the surface DO concentrations remain at the saturated value (Figure 3.16c2). Hypoxia first develops in the layer below the secondary-pycnocline, then extends across

the secondary-pycnocline, and finally reaches the main-pycnocline 5 days after the bottom water become hypoxic (Figure 3.16c3). In this case, the secondary pycnocline is not the upper boundary of hypoxia. Hypoxia extends across the secondary pycnocline and develops to the main-pycnocline. Finally, the main pycnocline becomes the upper boundary of the pycnocline. Compared to the single-pycnocline cases, the double-pycnocline structure enhance the DO depletion below the secondary-pycnocline and reduce the time for the near-bottom water becoming hypoxic for 9~27 days. However, the secondary-pycnocline can not limit the vertical extension of hypoxia. The strong main-pycnocline is the final upper boundary of hypoxia when the simulation reaches steady state.

Three numerical experiments were designed to test: (A) the effects of the bottom mixed layer on hypoxia formation; (B) the effects of the secondary-pycnocline in controlling vertical distribution of hypoxia; (C) The effects of the water column respiration and benthic respiration; (D) The effects of the thickness of the secondary-pycnocline.

3.1.5.1. Experiment A

In experiment A, Different K_Z are given in the bottom layer to simulate the situations with no bottom mixed layer (case A1, $K_Z = 1 \times 10^{-4}$ m^2s^{-1}), moderately mixed bottom layer (case A2, $K_Z = 5 \times 10^{-4}$ m^2s^{-1}), and well mixed bottom layer (case A3, $K_Z = 1 \times 10^{-3}$ m^2s^{-1}). The simulation results are shown in Figure 3.17 and Table 3.1. The vertical structures of DO concentrations of these three cases during the simulations are

similar to the single pycnocline case shown in Figure 3.16a. When there is no bottom mixed layer, hypoxia is formed in the bottom layer in 27 days (case A1, Table 3.1). However, bottom hypoxia forms fastest (20 days) when the bottom layer is well mixed (case A3, Table 3.1). It takes 23 days for the bottom layer to become hypoxic in case A2 with moderately mixed bottom layer. There is a lag of 4 to 5 days of the mid layer becomes hypoxic after hypoxia forms in the bottom layer. By comparing the formation time of hypoxia in the bottom layer, we find that hypoxia forms faster when the mixing is stronger in the bottom layer. It suggests that the existence of the bottom mixed layer can reduce the time of hypoxia formation. The effects of the bottom mixed layer in hypoxia formation will be discussed in the discussion part later.

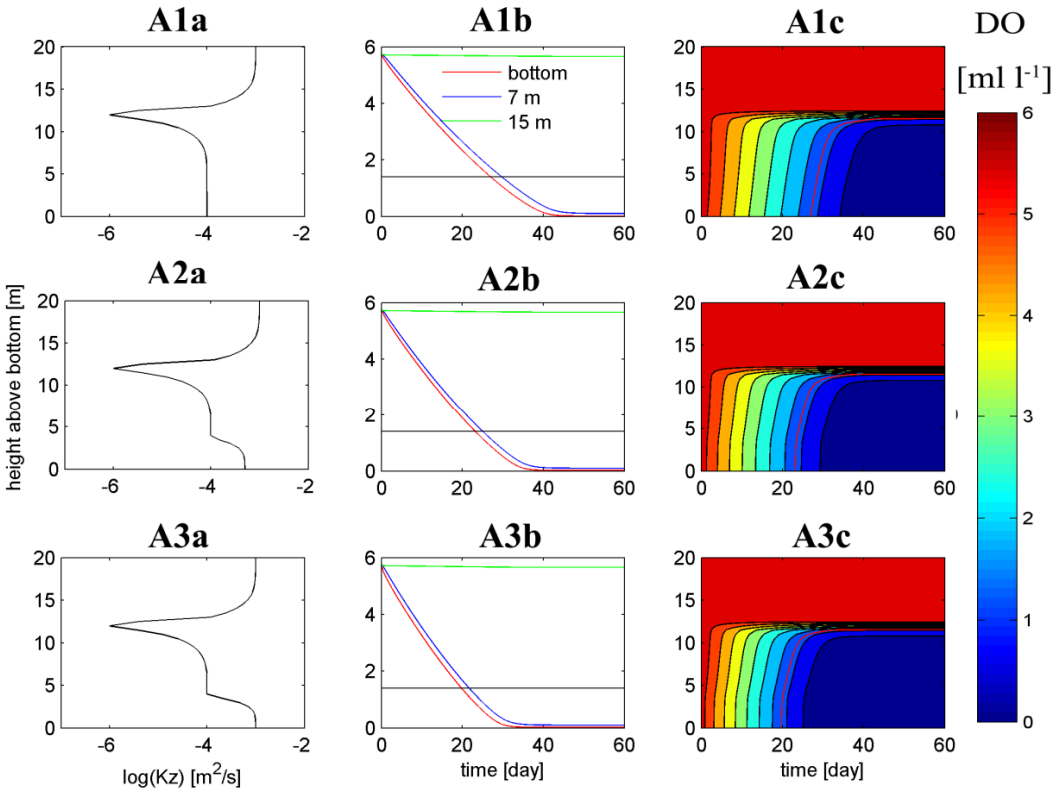

Figure 3.17 Simulation results of experiment A from the one-dimension DO model. Three cases are shown by rows from top to bottom: no bottom mixed layer (A1a, A1b, A1c), moderately mixed bottom layer (A2a, A2b, A2c), and well mixed bottom layer (A3a, A3b, A3c). Figures in the left, middle and right columns are the K_Z profiles, DO concentration changes with time at bottom, 7 m and 15 m above bottom, and contour plots of DO concentration changes with time for each case.

Table 3.1 Simulation results of experiment A. K_Z values in the bottom layer, time of bottom and mid layer becoming hypoxia are listed for each case.

Case	**K_Z in the bottom layer [m^2 s^{-1}]**	**Hypoxia formation time in the bottom layer [day]**	**Hypoxia formation time in the mid layer [day]**
A1	1×10^{-4}	27	32
A2	5×10^{-4}	23	27
A3	1×10^{-3}	20	24

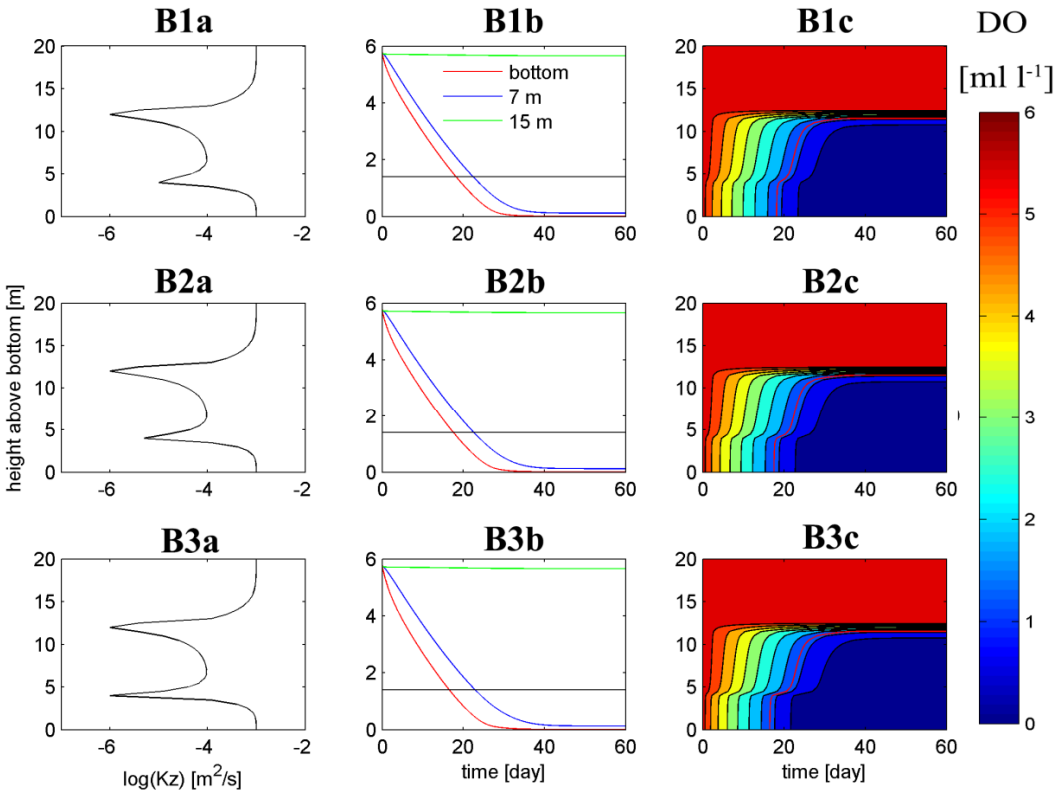

Figure 3.18 Simulation results of experiment B from the one-dimension DO model. Three cases are shown by rows from top to bottom: weak secondary pycnocline (B1a, B1b, B1c), moderately strong secondary pycnocline (B2a, B2b, B2c), and strong secondary pycnocline (B3a, B3b, B3c). Figures in the left, middle and right columns are the K_Z profiles, DO concentration changes with time at bottom, 7 m and 15 m above bottom, and contour plots of DO concentration changes with time for each case.

3.1.5.2. Experiment B

In experiment B, I want to test the effect of the secondary pycnocline above the bottom mixed layer on the formation of hypoxia with a double-pycnocline structure. Three test cases were carried out by giving different values of K_Z for the secondary

pycnocline: case B1, $K_Z = 1 \times 10^{-5}$ m^2s^{-1}; case B2, $K_Z = 5 \times 10^{-5}$ m^2s^{-1}; and case B3, $K_Z = 1 \times 10^{-6}$ m^2s^{-1}. Stratification strength is increasing from case B1 to B3 by giving decreasing K_Z. The simulation results are shown in Figure 3.18 and Table 3.2. The vertical structures of DO concentrations of these three cases during the simulations are similar to the double-pycnocline case shown in Figure 3.16c. As the stratification strength of the secondary pycnocline increasing from $K_Z = 1 \times 10^{-5}$ m^2s^{-1} to $K_Z = 1 \times 10^{-6}$ m^2s^{-1}, the time of the hypoxia formation decreases from 18 days to 16 days. It takes 20 days for the same structure without a secondary pycnocline (case A3) to have hypoxia formed in the bottom layer. There is only slightly increasing in the time of hypoxia formation with increasing stratification strength of the secondary pycnocline. It takes about 24~25 days for the mid layer becoming hypoxia. The lag between the time of mid and bottom layer becoming hypoxia varies from 9 to 6 days with increasing of the stratification strength in the secondary pycnocline. The top boundary of the hypoxic layer stays along the secondary pycnocline for 2 to 5 days. The stronger the secondary pycnocline is, the longer time the top boundary of hypoxic layer stays in the secondary pycnocline. It suggests that the secondary-pycnocline performs as a barrier to limit the vertical extension of hypoxia.

Table 3.2 Simulation results of experiment B. K_Z values at the secondary pycnocline, time of bottom and mid layer becoming hypoxia are listed for each case.

Case	**K_Z of the secondary pycnocline [m^2 s^{-1}]**	**Hypoxia formation time in the bottom layer [day]**	**Hypoxia formation time in the mid layer [day]**
B1	1×10^{-5}	18	24
B2	5×10^{-5}	17	25
B3	1×10^{-6}	16	25

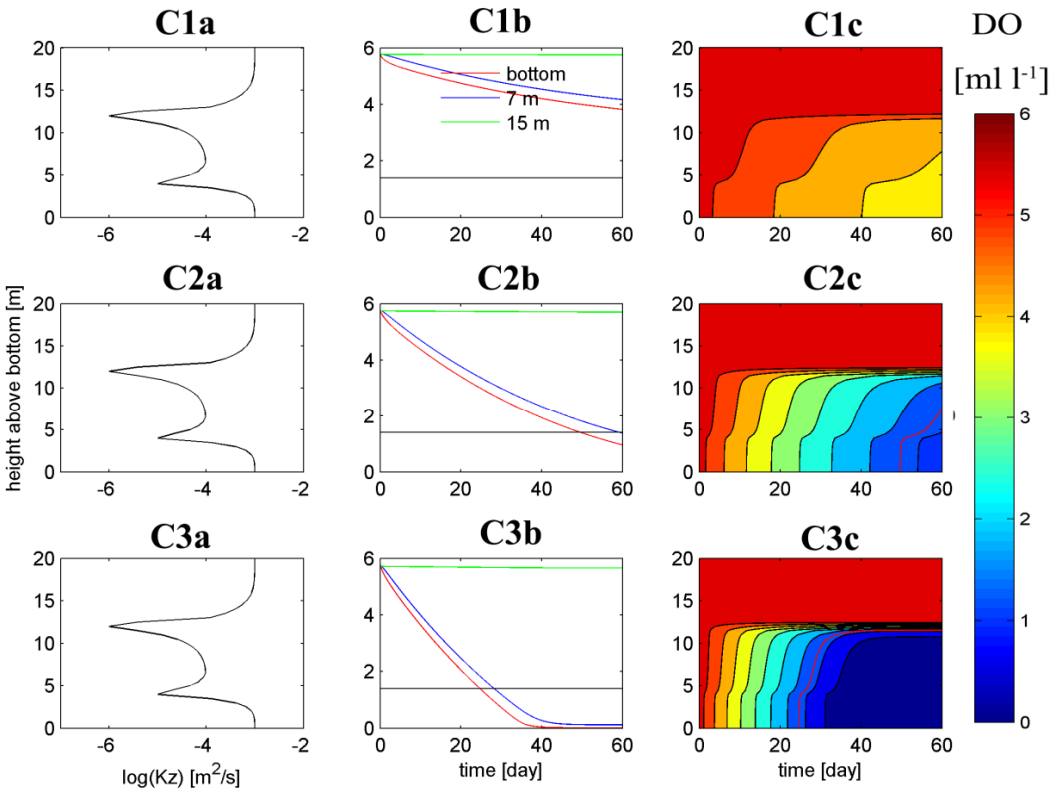

Figure 3.19 Simulation results of experiment C from the one-dimension DO model. Three cases are shown by rows from top to bottom: Benthic respiration only (C1a, C1b, C1c), half water column respiration and half benthic respiration (C2a, C2b, C2c), and water column respiration only (C3a, C3b, C3c). Figures in the left, middle and right columns are the K_Z profiles, DO concentration changes with time at bottom, 7 m and 15 m above bottom, and contour plots of DO concentration changes with time for each case.

Table 3.3 Simulation results of experiment C. Water column respiration and benthic respiration in percentage, time of bottom and mid layer becoming hypoxia are listed for each case.

Case	Water column respiration	Benthic Respiration	Hypoxia formation time in the bottom layer [day]	Hypoxia formation time in the mid layer [day]
C1	0%	100%	No hypoxia	No hypoxia
C2	50%	50%	50	No hypoxia
C3	100%	0%	25	31

3.1.5.3. Experiment C

Experiment C is used to test the relative importance of water column respiration and benthic respiration in a double-pycnocline structure by running the model with benthic respiration only (C1), 50% water column respiration and benthic respiration (C2), water column respiration only (C3). The simulation results are shown in Figure 3.19 and Table 3.3. There is no hypoxia formed in 60 days simulation when only benthic respiration is applied (Figure 3.19C1). The DO consumption rate is not fast enough to decrease the DO concentrations to hypoxic level with only benthic respiration. It suggests that only using benthic respiration to understand the hypoxia formation might not be a good way. When there is only water column respiration applied in the model, it

takes 20 days for the bottom layer to become hypoxic (Figure 3.19C2 and Table 3.3), which is close to the time (18 days) when both water column respiration and benthic respiration are applied. The simulation result of case C3 further suggests that the water column respiration dominants the DO consumption. When water column respiration is reduced by 50% (Figure 3.19C2), it take 31 days for hypoxia to from in the bottom layer. It is 13 days late than the basic case (Figure 3.6c). Reducing the water column respiration can dramatically increase the time of hypoxia formation in the bottom layer. It supports the idea that water column respiration is dominants in this model.

3.1.5.4 Experiment D

Experiment D is used to test how the bottom mix layer thickness affects the formation of hypoxia. The secondary pycnocline is set to 3 m, 4 m, and 5 m above bottom in three test cases, respectively. The simulation results are shown in Figure 3.20 and Table 3.4. As the height of the secondary pycnocline increasing from 3 m to 5 m, hypoxia formation time increases from 15 days to 22 days (Figure 3.20). Comparison of hypoxia formation time of these three cases shows that hypoxia forms faster in a thin bottom mixed layer. The DO decrease rate in the bottom mixed layer is a combination of the DO consumption and DO resupply through the stratified layer. All three cases have the same stratification structure in the stratified layer. It suggests that the DO resupply ability to the bottom mixed layer is the same. Therefore, fast hypoxia formation in a thin bottom mixed layer is caused by enhanced DO consumption rate in the bottom mixed layer. The averaged DO consumption rate in the bottom mixed layer can be expressed as

$R_{WR} + \frac{R_{BR}}{d}$, where d is the thickness of the bottom mixed layer. When d is small, the averaged DO consumption is enhanced and benthic respiration will contribute more to the total respiration. The relative importance of water column respiration and benthic respiration will be discussed later.

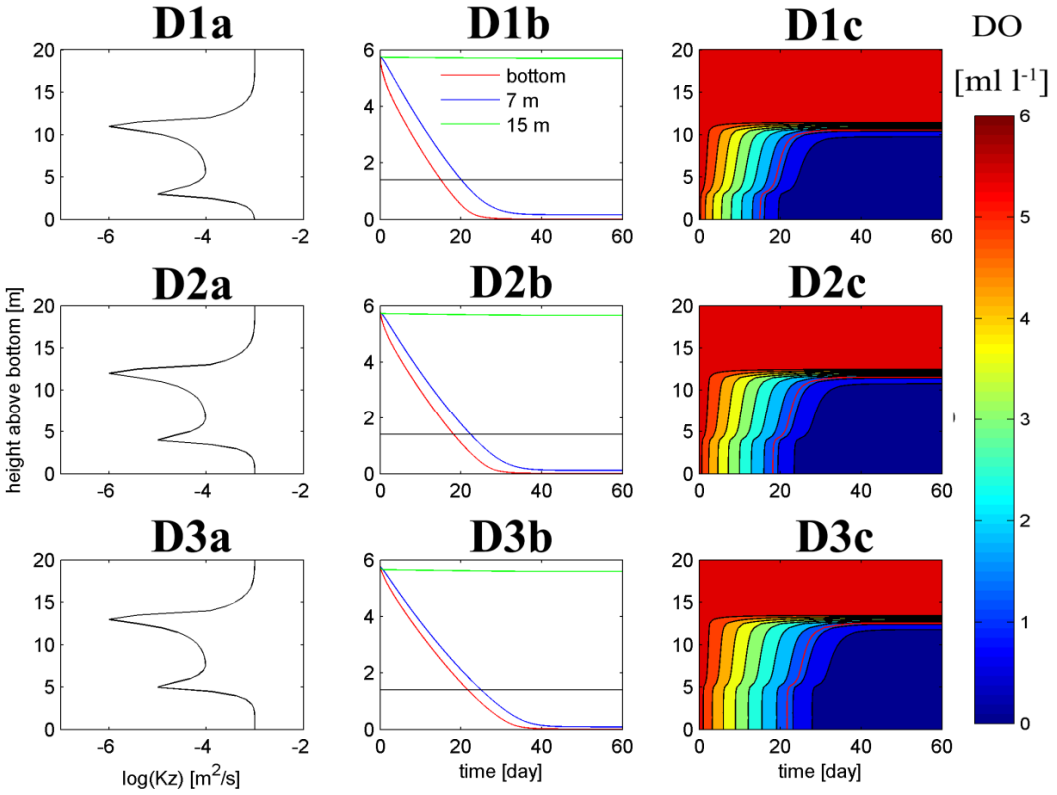

Figure 3.20 Simulation results of experiment D from the one-dimension DO model. Three cases are shown by rows from top to bottom: 3 m bottom mixed layer (D1a, D1b, D1c), 4 m bottom mixed layer (D2a, D2b, D2c), and 5 m bottom mixed layer (D3a, D3b, D3c). Figures in the left, middle and right columns are the K_Z profiles, DO concentration changes with time at bottom, 7 m and 15 m above bottom, and contour plots of DO concentration changes with time for each case.

Table 3.4 Simulation results of experiment D. Height of secondary pycnocline, time of bottom and mid layer becoming hypoxia are listed for each case.

Case	Height of secondary pycnocline [m]	Hypoxia formation time in the bottom layer [day]	Hypoxia formation time in the mid layer [day]
D1	3	15	21
D2	4	18	25
D3	5	22	27

3.2. Discussion

3.2.1. Stratification limit and hypoxia

Using the historical CTD data from 2003 to 2009, a threshold of $N_{max} = 0.06\ s^{-1}$ was determined to represent the lower limit of the stratification strength for existence of hypoxia (Figure 3.11).The development of hypoxia requires a local stratification stronger than this threshold. Belabbassi (2006) showed that hypoxic waters in the Northern Gulf of Mexico were found only in water column with $N_{max} = 0.07\ s^{-1}$ using the LATEX (Louisiana-Texas Shelf Physical Oceanography Program) data for the years 1992 to 1994. However, Belabbassi (2006) defined hypoxia as DO concentration smaller than 2.4 ml l^{-1} to find this threshold, which is 1 ml l^{-1} higher than the value that I used to

define hypoxia in this study. Kiselkova (2008) did the same estimation to find this threshold as $N_{max} = 0.07\ s^{-1}$ using the MCH data for years 2004 and 2005. This threshold is visually identified by finding the value of the smallest N_{max} among all the hypoxic stations in her study. However, there are only two hypoxic stations near this threshold in her figure, which might be caused by noises in the N estimation. Wiseman et al. (1997) defined a near bottom relative weak pycnocline with $N = 0.01\ s^{-1}$ (or a density gradient of 0.01 kg m^{-3} m^{-1}) on the shelf, which was the upper boundary of hypoxia layer. The threshold of stratification defined in this study is 5 times larger than what Wiseman et al. (1997) used. As N larger than $0.01\ s^{-1}$ was found in more than 96% of the total CTD profiles used in this study, $N = 0.01\ s^{-1}$ is too small to be a threshold for the existence of hypoxia. This threshold represents the minimum requirement of the stratification strength to limit the vertical DO resupply and provides the environment for hypoxia development in subpycnocline water. Discovery of this threshold will help research team to find the potential region for hypoxia development on the Texas-Louisiana Shelf.

3.2.2. Stratification structure and vertical distribution of hypoxia

Stratification inhibits vertical DO transport at the pycnocline and provides the precondition for hypoxia development. Therefore, the depth of the main-pycnocline is expected to track the depth of the oxycline. Wiseman et al. (1997) argued that the upper boundary of hypoxic layer was not the main-pycnocline but was the first pycnocline reached from bottom. However, the upper boundary of hypoxia layer is observed between the main-pycnocline and the weak secondary-pycnocline in Figure 3.15b. The

simulation results of the double-pycnocline structure case also support the observations that the secondary-pycnocline does not always track the depth of the hypoxic layer (Figure 3.16c). The development of hypoxia under the double-pycnocline structure simulation, occurred in three stages: (1) hypoxia develops below the secondary pycnocline and fills the bottom layer, which is consistent with the observations shown in Figure 3.16c; (2) hypoxia extends to the mid-layer, but does not reach the main pycnocline, which is consistent with the observations shown in Figure 3.16d; (3) All the water below the main-pycnocline becomes hypoxic and the main-pycnocline is the upper boundary of the hypoxia, which is also consistent with the observation shown in Figure 3.16d. These three stages of hypoxia development under the double-pycnocline structure explain the vertical distribution of hypoxia with a double-pycnocline structure.

There are no high resolution continuous observations of hypoxia development in the presence of a double-pycnocline structure. High temporal and spatial resolution observations are needed to make in the future. However, the model results with double-pycnocline structure support the explanation of vertical distribution of hypoxia in the presence of a double-pycnocline structure.

There was a special vertical distribution of hypoxia in the transect of Acrobat shown in Figure 3.9. There was a thin non-hypoxic layer between two hypoxic layers below the main-pycnocline. The observations (Figure 3.15) and model results (Figure 3.16) of vertical distribution of hypoxia suggest that the subpycnocline should be full of hypoxic water once hypoxia fully developed. Strong vertical DO transport supposes to happen at the interface between the non-hypoxic layer and hypoxic layer, where there is

large vertical DO gradient but no strong stratification as the main-pycnocline. It suggests that this non-hypoxic layer will supply DO to the subpycnocline layer until the vertical DO gradient become zero. A similar vertical distribution of hypoxia was observed by S. DiMarco et al. 2005 (unpublished), who figured out that this non-hypoxic layer was brought into the subpycnocline hypoxic layer by horizontal advection. The further importance of horizontal advection is not clear because of the lack of relevant observations.

3.2.3. Bottom mixed layer and hypoxia

The model experiment A showed that the formation time of hypoxia decreased from 27 to 20 days when there was a bottom mixed layer (Table 3.1). It suggests that the bottom mixed layer can reduce the formation time of hypoxia in the bottom layer. Both case A1 and A3 have the same K_Z structure above the bottom layer, which suggests that the stratified layer have the same effects in resupply DO to the bottom layer. Furthermore, case A1 has a larger K_Z than case A2 in the bottom layer, which means that case A1 has a stronger total stratification than case A2. However, hypoxia was formed 7 days earlier in case A2 than in case A1. The vertical decrease of K_Z at the interface between bottom mixed layer and the stratified layer above it is responsible for that. In Eqn. (9), the vertical changes of DO flux induced DO changes is expressed as $\frac{\partial}{\partial z}(K_z \ \frac{\partial O_2}{\partial z})$. This term can also be written as $\frac{\partial}{\partial z}\left(\mathrm{K_z} \ \frac{\partial \mathrm{O_2}}{\partial z}\right) = \frac{\partial \mathrm{K_z}}{\partial z}\frac{\partial \mathrm{O_2}}{\partial z} + \mathrm{K_z} \ \frac{\partial^2 \mathrm{O_2}}{\partial z^2}$. When there is no bottom mixed layer (Case A1), K_Z is a constant below the main pycnocline,

which means that $\frac{\partial K_z}{\partial z}\frac{\partial O_2}{\partial z} = 0$. The vertical changes of DO flux induced DO changes were controlled by K_z $\frac{\partial^2 O_2}{\partial z^2}$ only. When there is a bottom mixed layer (Case A3), $\frac{\partial K_z}{\partial z}$ is negative at the interface between the bottom mixed layer and the stratified layer above it, where K_Z switched from large value (mixed status) to small value (stratified status). Because $\frac{\partial O_2}{\partial z}$ is positive and large at this interface, $\frac{\partial K_z}{\partial z}\frac{\partial O_2}{\partial z}$ is negative and can increase the DO decrease speed in the bottom layer. K_Z in the bottom mixed layer was decreased to 5×10^{-4} m^2 s^{-1} in case A2, which also decreased $\frac{\partial K_z}{\partial z}$ (Figure 3.17). The hypoxia formation time changed to 27 days, which lay between case A1 and case A2. It supports that the vertical decrease of K_Z at the interface between bottom mixed layer and stratified layer can reduce the hypoxia formation time. Although there was no direct evidence shown in the observations to support this idea, 75% of the hypoxic layers were within 4 m above the bottom and 58% of the hypoxic layers are in or along the bottom mixed layers. It also suggests that the bottom mixed layer is a preferred environment for hypoxia to occur.

3.2.4. Secondary pycnocline

A secondary pycnocline was often observed above the bottom mixed layer and its effect was tested in experiment B (Figure 3.18, Table 3.2). The formation time of hypoxia increased by 2 days when the K_Z became 10 times larger at the secondary pycnocline. It suggests that the existence of the secondary pycnocline only have a minor

effect in help hypoxia formation in the bottom layer. However, the top boundary of the hypoxic layer stayed along the secondary pycnocline from 2 to 5 days for case B1 to B3. The stronger the secondary pycnocline was, the longer time the top boundary of hypoxic layer stays in the secondary pycnocline. It suggests that the secondary-pycnocline performs as a barrier to limit the vertical extension of hypoxia. It is obvious that a stronger secondary pycnocline will inhibit the DO transport go through it, which also means that it will limit the vertical development of hypoxia from bottom layer to the mid layer. In the top part of the secondary pycnocline, K_Z increase with height ($\frac{\partial K_z}{\partial z} > 0$) and $\frac{\partial K_z}{\partial z}\frac{\partial O_2}{\partial z} > 0$. As shown in Eqn. (9), a positive $\frac{\partial K_z}{\partial z}\frac{\partial O_2}{\partial z}$ will help to slow down the DO decreasing speed. It suggests that the vertical K_Z changes at the secondary pycnocline will help limit the vertical extension of hypoxia. Both of these two effects work together, the secondary pycnocline performs as barrier to limit the hypoxia in the bottom layer. However, hypoxia can still extend across this secondary pycnocline when the bottom DO is highly depleted.

3.2.5. Water column respiration and benthic respiration

By calculating the subpycnocline water column respiration and benthic respiration using the parameterization method, I found that the thickness of subpycnocline layer changed the relative importance of water column respiration and benthic respiration. As shown in Figure 3.20, a thin subpycnocline layer (3 m) enhanced the contribution of benthic respiration of the total subpycnocline respiration by limiting

the subpycnocline water volume. The water volume was limited, such that the contribution of water column respiration to the total subpycnocline respiration dropped down and benthic respiration became more important than the water column respiration. For a thick subpycnocline layer (10 m), there was more water below the pycnocline than the thin subpycnocline layer. Water column respiration became more important than benthic respiration. Some studies (Dortch et al. 1994; Quinones-Rivera et al. 2007, 2010) stated that SOC accounted for 75% of the subpycnocline respiration. Murrell and Lehrter (2011) found that water column respiration contribute more than the benthic respiration. However, I argued that the relative importance or the ratio of water column respiration and benthic respiration was decided by the thickness of the subpycnocline layer. Compared with the water column respiration, the DO depletion caused by the benthic respiration was enhanced by the limited potential hypoxic water volume with a near bottom pycnocline. A thin subpycnocline layer can increase the contribution of benthic respiration in the TRV (Figure 3.21).

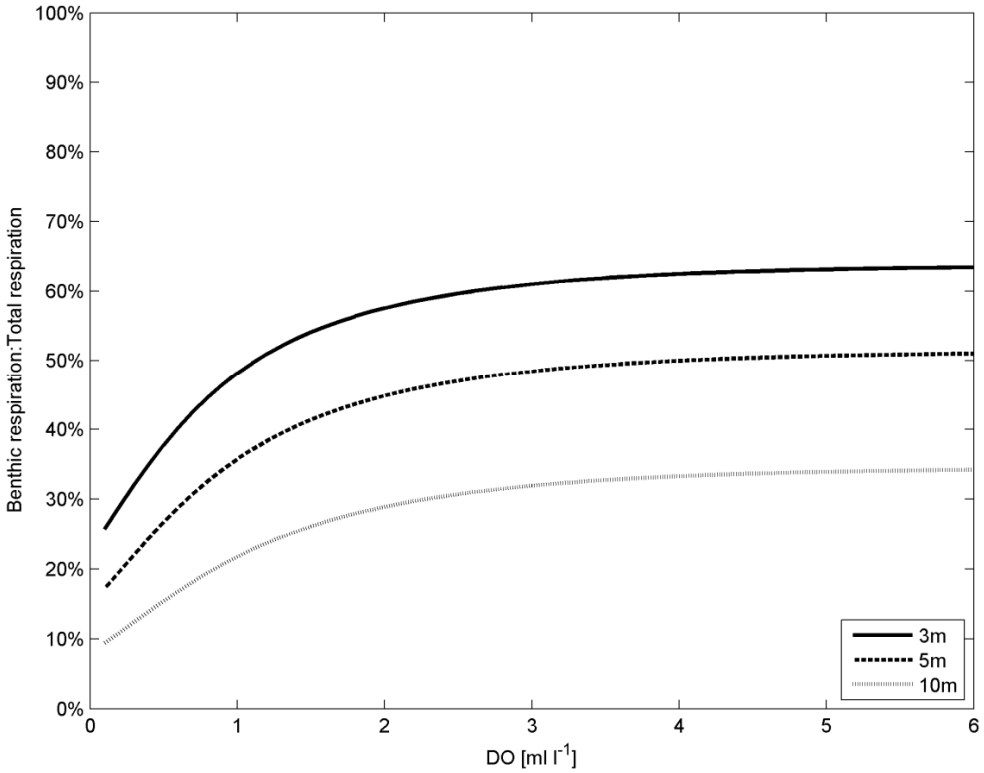

Figure 3.21 Ratio between benthic respiration and total respiration changing with local DO concentrations with a subpycnocline layer of 3 m, 5 m, and 10 m thick.

3.2.6. Mechanisms causing bottom mixed layer

The bottom mixed layer is an important factor for biogeochemical and physical processes on the continental shelf (Bianchi et al. 2010). A number of mechanisms, including winds, tides, density differences, atmospheric pressure gradients, drive the water motion on the shelf. The characteristics of the bottom mixed layer are highly affected by the nonlinear friction process in the boundary layer, and the degrees of complexity dependent upon the types of external forcing present (Grant and Madsen

1986). Moreover, the importance of the various driving mechanisms varies from one continental-shelf region to another (Perlin et al. 2005).

As discussed in section 3.2.3, the bottom mixed layer is a favorable environment for hypoxia formation and development. The secondary-pycnocline that observed in this study was the upper boundary of the bottom mixed layer. The vertical DO transport between the water inside the bottom mixed layer and water above the bottom mixed layer is limited, which favors the development of hypoxia. With the existence of a surface pycnocline, caused by fresh water, the development of hypoxia is also accelerated (Figure 3.16).

The bottom mixed layer on the Texas-Louisiana Shelf is considered to be mainly caused by wind driven current with buoyant coastal plume and near-inertial motions. The tides on the Texas-Louisiana Shelf are found to be small by DiMarco and Reid (1998). Therefore, tidal flow can not be the mechanisms drive the bottom water motions. During the summer time, upwelling favorable wind generates cross-shore motion of water in the surface Ekman layer. This also creates a pressure gradient which drives alongshore flow beneath the surface layer. A consequence of this alongshore flow is a near-bottom Ekman transport opposite in direction to that in the surface layer (Lenz 2004; Perlin et al. 2005), which formed a stable bottom mixed layer. The near-inertial motions on the Texas-Louisiana Shelf which are driven by the passages of atmospheric fronts, hurricanes and tropical storms are thought to be another process to form a bottom mixed layer on the shelf (Nowlin et al. 1998; Nowlin et al. 2005). Inertial oceanic

response is also found significantly enhanced by a near-resonant condition between inertial and diurnal forcing frequencies (Zhang et al. 2009, 2010).

CHAPTER IV

ESTIMATION OF VERTICAL EDDY DIFFUSIVITY AND CROSS-PYCNOCLINE DO FLUX

In this chapter, a series of hourly CTD observations, most acquired at the stations over 24 hours, have been analyzed to study the short-term temporal changes, especially small-scale temporal changes of the vertical distribution of hypoxia. In addition, vertical eddy diffusivity is estimated using the vertical density gradient and vertical shear. The vertical DO flux is calculated based on the estimated vertical eddy diffusivity, surface-bottom DO concentrations and the thickness of pycnocline.

4.1. Results

4.1.1. Temporal changes of the stratification structure and vertical distribution of hypoxia

A series of hourly CTD observations had been made during the MCH project since the year 2005. One special station, located at 29°N, 92°W on the inner shelf of the Louisiana coast, was also the location of the South Marsh mooring. It had been revisited five times at different seasons between 2007 and 2010 (Table 2.3). The observational results are shown in Figures 4.1 to 4.5. To verify day and night, local time is used in the figures.

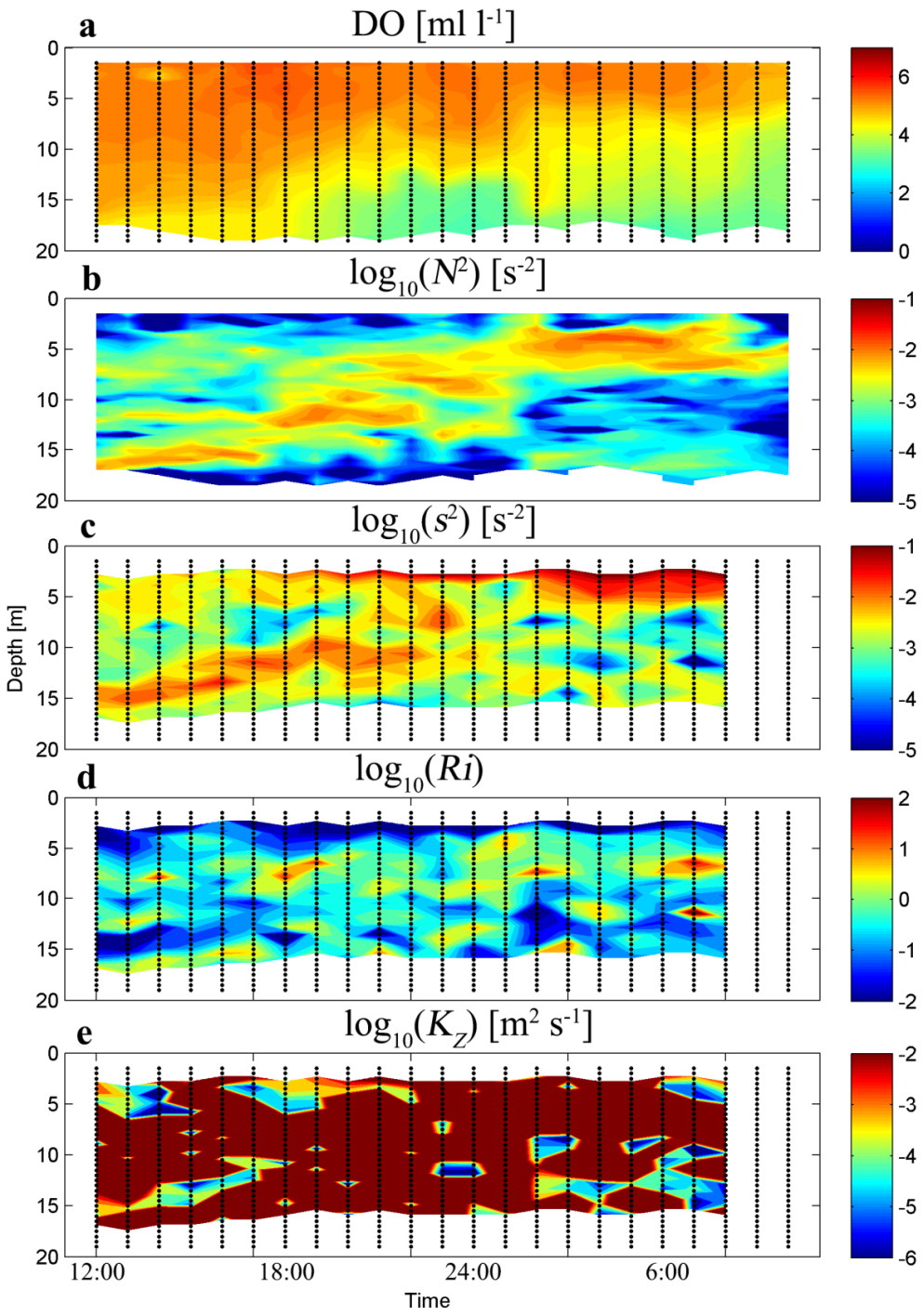

Figure 4.1 Hourly CTD profiles at station CAS1, March 2007. Local DO concentration, $\log_{10}(N^2)$, $\log_{10}(s^2)$ and $\log_{10}(K_Z)$ are shown in each panel from top to bottom. The black contour lines circle out hypoxia (DO concentration < 1.4 ml l^{-1}). Black dots denote the measurement position of CTD casts.

CAS1 station was made in March 2007. There was a weak pycnocline caused by vertical salinity differences which started near bottom at 12:00 and went up to a depth of 5 m at 6:00 (Figure 4.1b). Strong shear was also observed along the pycnocline (Figure 4.1c). It suggests that there might be a weak front moving across the station during the observations. Low DO water was observed in the bottom layer below the weak pycnocline. The low DO water extended from bottom (12:00) to 5 m below the surface (6:00), which is consistent with the temporal changes of the position of the pycnocline. The observation at this station showed the conditions usually observed in spring with weak stratification and low DO water in the layer below the pycnocline. The stratification was not strong enough to inhibit the DO resupply and the DO consumption was limited by lack of organic matters. Both of these two conditions were not strong enough to form hypoxia in the spring time. It also suggests that the stratification structure is not stable but can change as fast as hours.

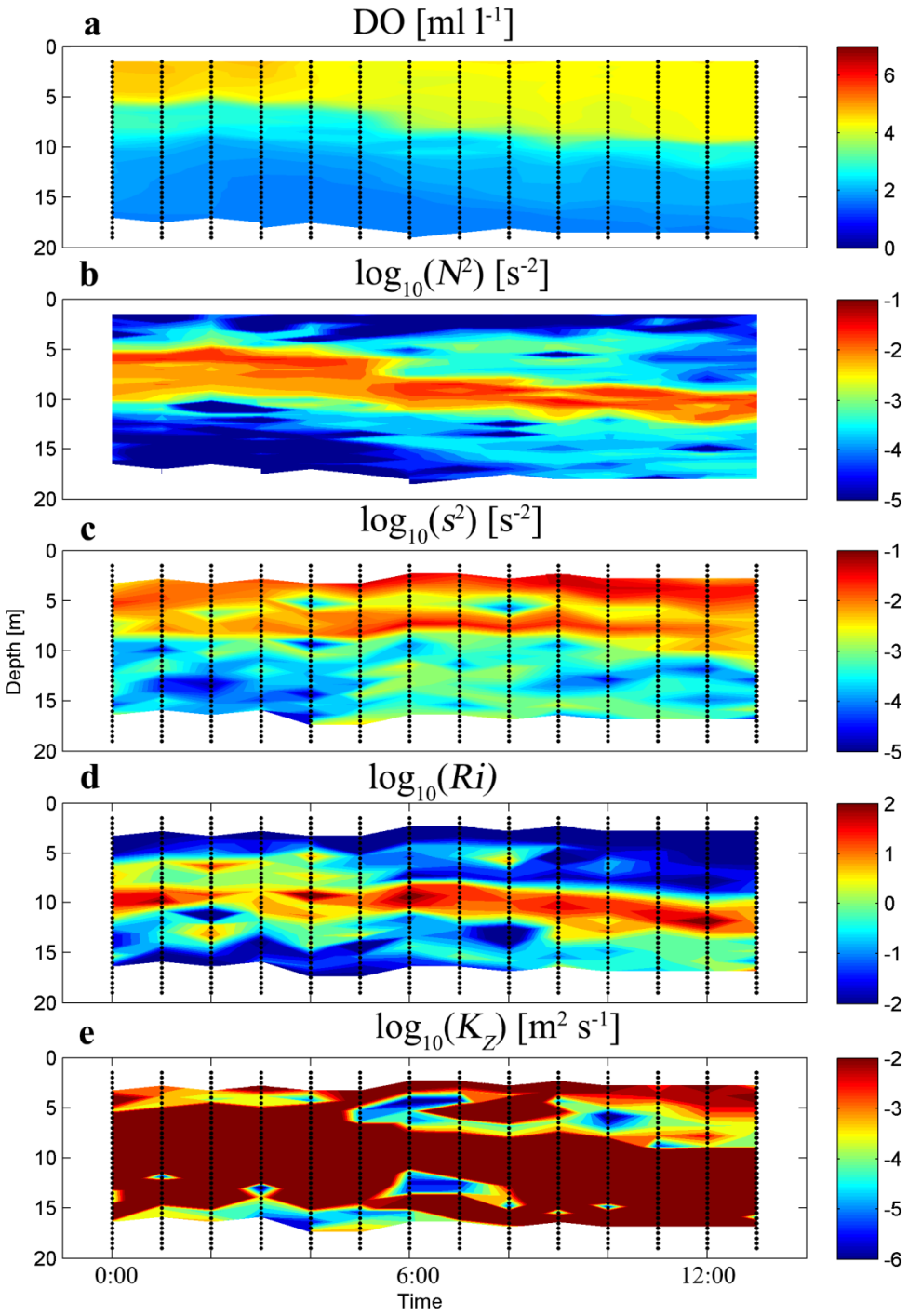

Figure 4.2 Hourly CTD profiles at station CAS2, July 2007. Local DO concentration, $\log_{10}(N^2)$, $\log_{10}(s^2)$ and $\log_{10}(K_Z)$ are shown in each panel from top to bottom. The black contour lines circle out hypoxia (DO concentration < 1.4 ml l^{-1}). Black dots denote the measurement position of CTD casts.

Station CAS2 was occupied in July with fresh water (S~30) at surface. A 5 m thick pycnocline with N around 0.1 s^{-1} was found at a depth between 5m and 10m (Figure 4.2b). The pycnocline was also found to go deeper from 6 m to 12 m during the observations. Strong shear was observed above the pycnocline (Figure 4.2c). Subpycnocline DO was depleted to a low level, about 2.5 ml l^{-1} (vs. 5 ml l^{-1} in the surface), but was not hypoxic. Little mixing was expected to be happen at the pycnocline with a Ri much larger than one. Vertical DO transport to subpycnocline layer was inhibited with such a strong mid-depth pycnocline. Although there was no respiration rate measurement for the subpycnocline layer at this station, this strong pycnocline provided the precondition for hypoxia formation.

A distinct hypoxic water type was found near the bottom with a thickness about 2 m at the CAS3 station (Figure 4.3a). Although there was no strong pycnocline, the water column was slightly stratified (Figure 4.3b). Near-bottom DO concentration showed variations as small as hours. Hypoxia (showed by the 1.4 ml l^{-1} DO isopleth in Figure 4.3a) was observed around 10:00, 18:00, 23:00, and 6:00 in the next day. It suggests that the bottom DO concentration also showed temporal variations. However, the causes for these small scale temporal changes are not clear.

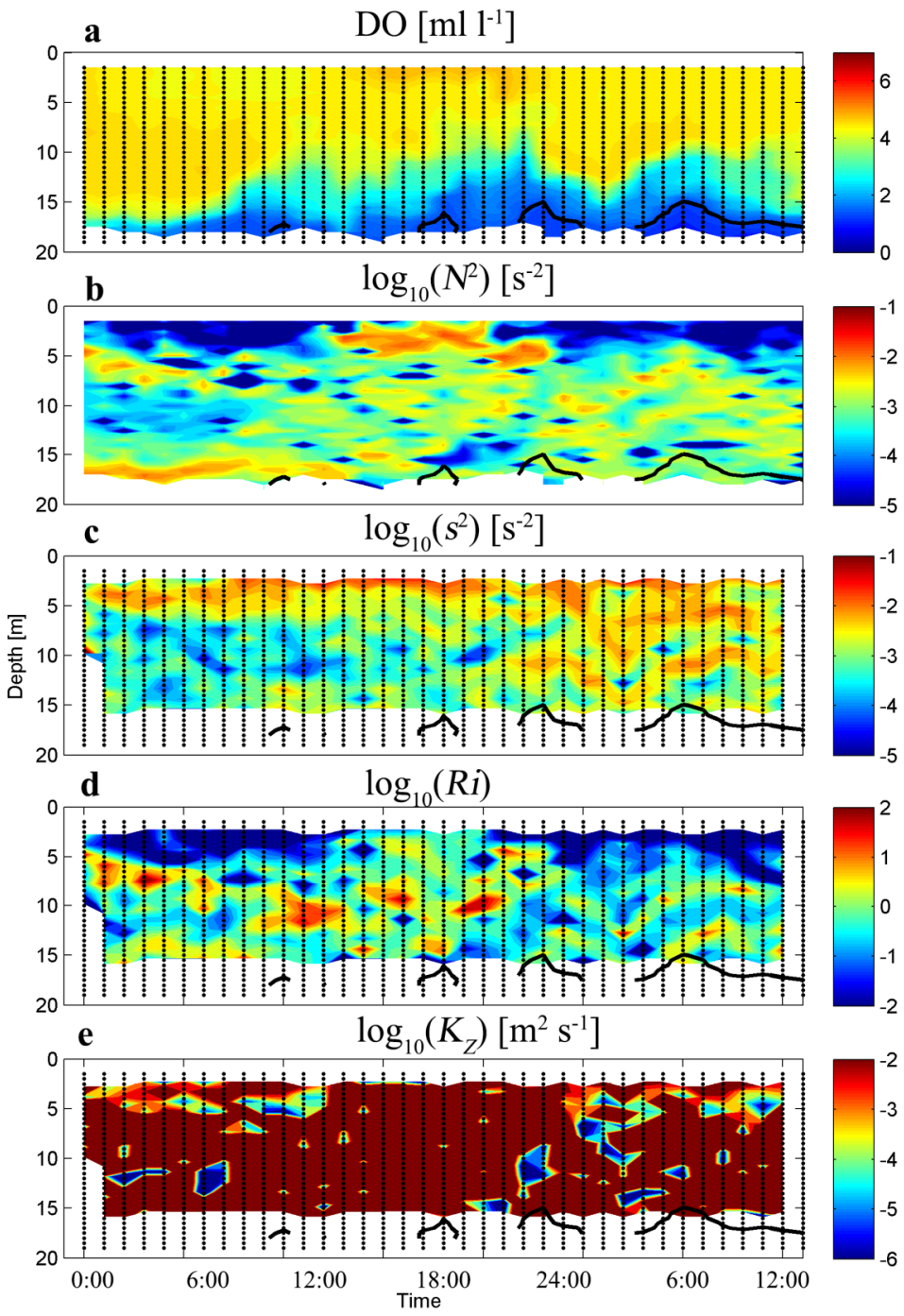

Figure 4.3 Hourly CTD profiles at station CAS3, September 2007. Local DO concentration, $\log_{10}(N^2)$, $\log_{10}(s^2)$ and $\log_{10}(K_Z)$ are shown in each panel from top to bottom. The black contour lines circle out hypoxia (DO concentration < 1.4 ml l^{-1}). Black dots denote the measurement position of CTD casts.

There was a thick hypoxic layer (~12 m) below the pycnocline at the station CAS4 in July 2008 (Figure 4.4a). The pycnocline with $N \sim 0.2\ s^{-1}$ was located at a depth of about 7 m and divided the water column into two layers (Figure 4.4b). A thin layer about 2 m thick with relative high DO concentration, around 2.5 ml l^{-1}, was observed inside hypoxic water at a depth of 10 m, which existed from 0:00 to 12:00 and 18:00 to next day 1:00. The salinity and temperature of the water in this non-hypoxic layer were the same as the salinity and temperature of the surrounded hypoxic water. A similar vertical distribution was discussed in Chapter III, Figure 3.9. This special vertical distribution of hypoxia results from horizontal advections. This non-hypoxic layer first appeared when this station started and last for about 12 hours and then disappeared for about 6 hours. It showed up again around 18:00 at the same depth and with almost the same thickness and stayed there until the end of this station. These temporal changes suggest that the horizontal advections below the pycnocline caused variation in vertical distribution of hypoxia are complex and the time scale of these changes is as small as hours.

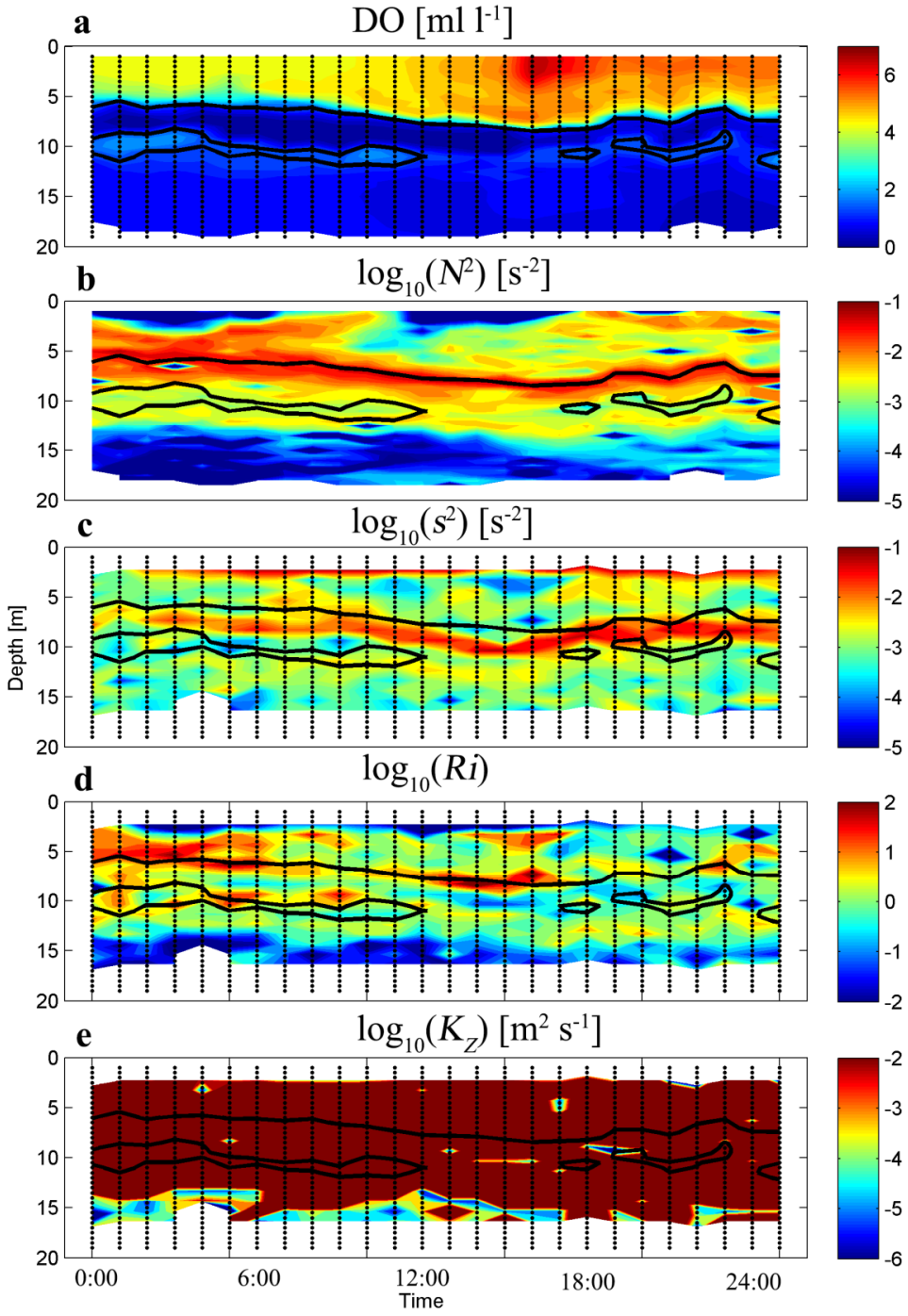

Figure 4.4 Hourly CTD profiles at station CAS4, July 2008. Local DO concentration, $\log_{10}(N^2)$, $\log_{10}(s^2)$ and $\log_{10}(K_Z)$ are shown in each panel from top to bottom. The black contour lines circle out hypoxia (DO concentration < 1.4 ml l^{-1}). Black dots denote the measurement position of CTD casts.

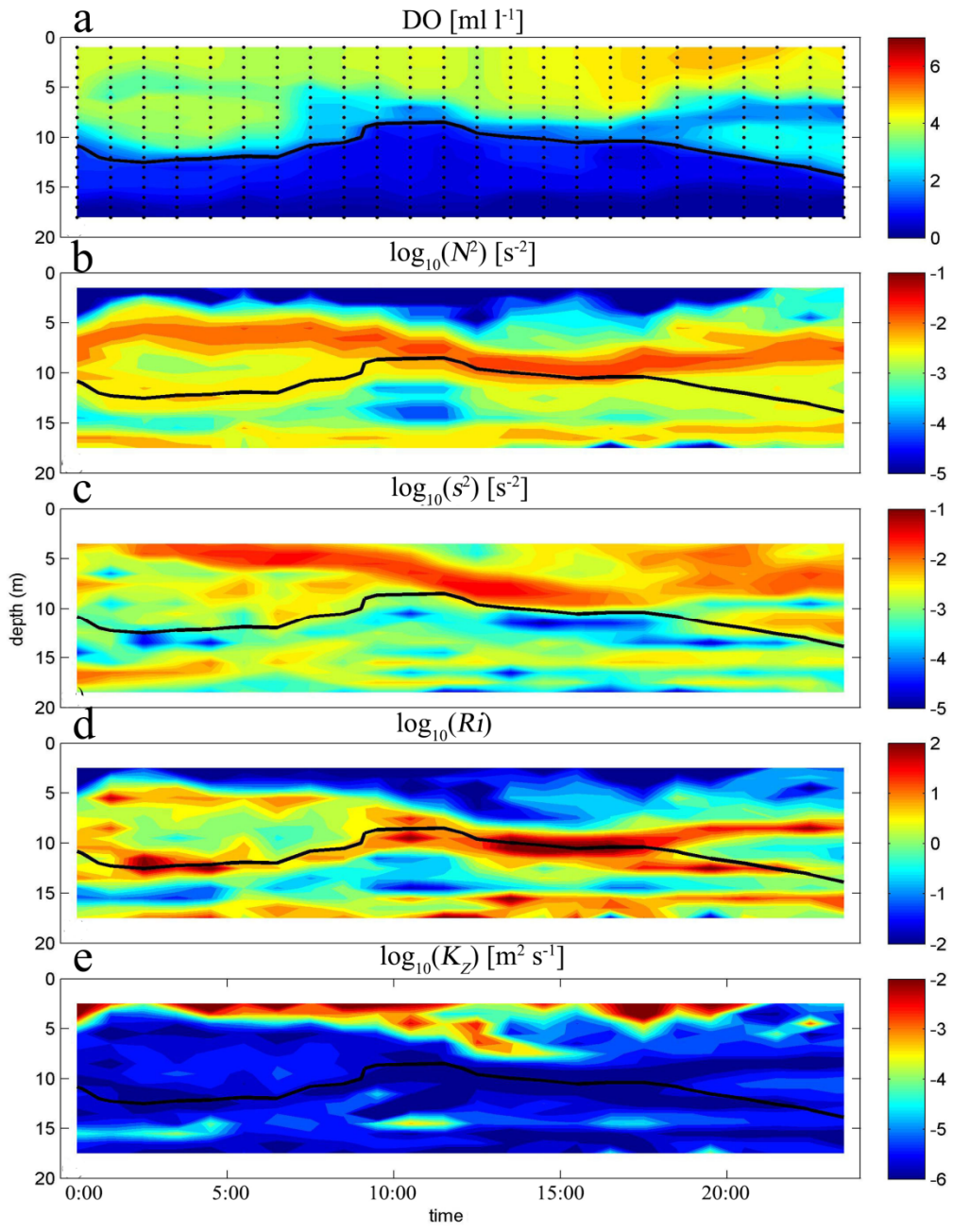

Figure 4.5 Hourly CTD profiles at station CAS5, August 2010. Local DO concentration, $\log_{10}(N^2)$, $\log_{10}(s^2)$ and $\log_{10}(K_Z)$ are shown in each panel from top to bottom. The black contour lines circle out hypoxia (DO concentration < 1.4 ml l^{-1}). Black dots denote the measurement position of CTD casts.

4.1.2. Estimation of K_Z

K_Z was estimated at these five stations. A 600-kHz RDCP was used to measure the velocity profiles at stations CAS1, CAS2, CAS3, and CAS4 (Figure 4.1e, Figure 4.2e, Figure 4.3e, and Figure 4.4e). The velocity profiles measured by RDCP had a cell size of 2 m and 50% vertical overlap of each cell. It leaded to an inaccurate estimation of vertical shear. K_Z were overestimated when using RDCP measured velocity profile and not consistent with the stratified/mixing status. In Figure 4.2d, *Ri* was much larger than 1 at the pycnocline, which suggests a stratified condition. However, the estimated K_Z at the same location showed strong mixing (Figure 4.2e). ADCP measured velocity profile had a vertical resolution of 1 m and better accuracy to provide better estimation of K_Z.

K_Z at station CAS5 in August 2010 (Figure 4.5e) is calculated based on the methods described in Chapter II, using observed vertical shear (Figure 4.5c) calculated from ADCP profile and N^2 (Figure 4.5b) calculated from CTD profile. The time averaged diapycnal diffusivity along the pycnocline is 3×10^{-6} m^2 s^{-1}. From Figure 4.5b, we see that the pycnocline at 8 m separates the water column into two layers. The time averaged vertical eddy diffusivity in the bottom layer is 2×10^{-5} m^2 s^{-1}, which is an order of magnitude larger than the diapycnal diffusivity (Figure 4.5e). There was strong mixing at the top of the surface layer with a K_Z of 5-10 $\times 10^{-3}$ m^2 s^{-1}. The average K_Z in the surface layer is 3×10^{-4} m^2 s^{-1}, about an order of magnitude larger than that in the bottom layer.

The Richardson number is calculated from observed vertical velocity shear and density gradient (Figure 4.5d). Along the pycnocline, Richardson number is greater than

0.25, indicating a highly stratified water-column. In the surface layer, the Richardson number is much smaller than 0.25, implying mixing in the surface layer. Strong vertical shear is found in the surface layer above pycnocline, leading to the small Richardson number ($Ri < 0.1$) in the surface layer. The Richardson number in the bottom layer shows stronger mixing than the pycnocline, but much weaker mixing than the surface layer.

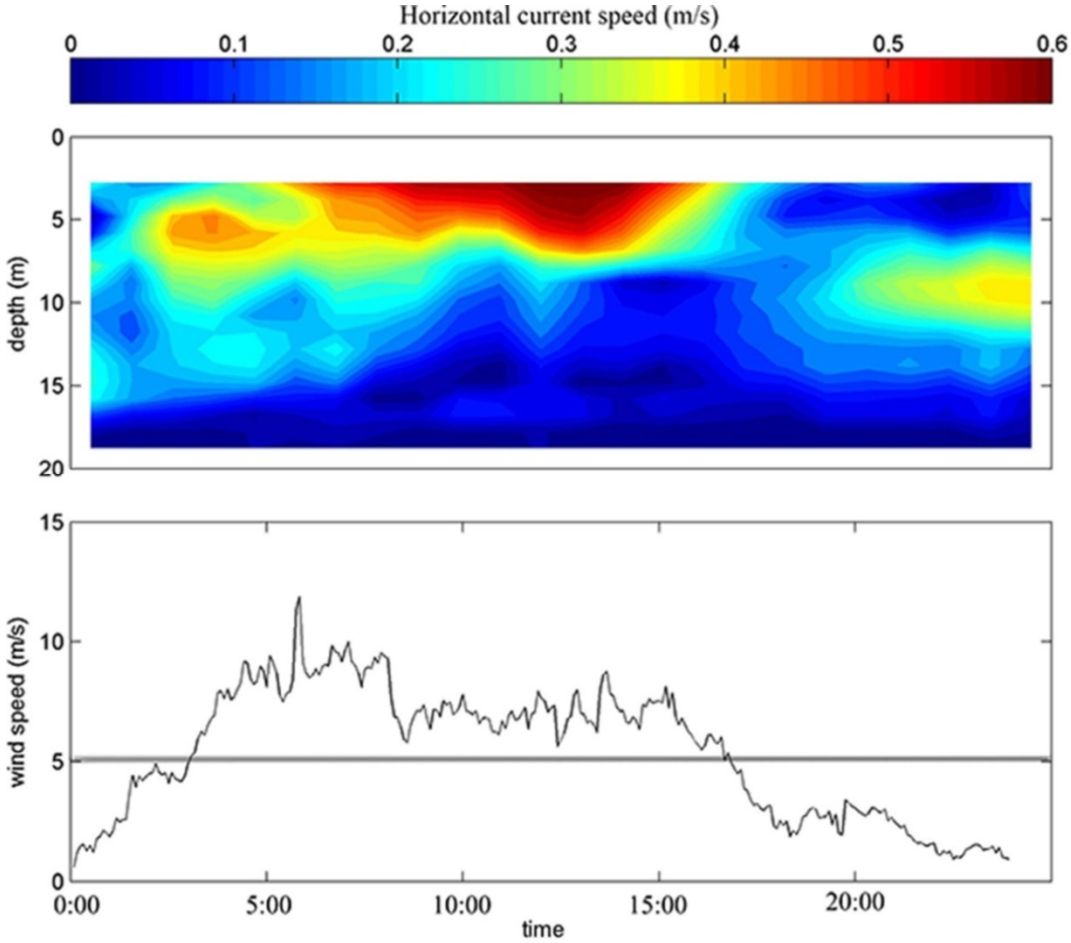

Figure 4.6 Magnitude of horizontal current (top) and wind speed (bottom) at station CAS5.

There was wind induced mixing at station CAS5 in August 2010. Strong wind (wind speed > 5 m s^{-1}) started at about 5:00 and stopped around 15:00, with a peak wind speed of 11.5 m s^{-1} (Figure 4.6 bottom). A horizontal flow, as strong as 0.5 m s^{-1}, 3 m below surface, was induced by the wind (Figure 4.6 top). During the 10 hours the wind lasted, this wind-induced horizontal flow became stronger and deeper, with a peak speed of 0.62 m s^{-1} and went as deep as 8 m below the surface. The speed of the wind-induced flow decreased after the wind speed became smaller than 5 m s^{-1} at 18:00. The surface flow speed decreased to 0 at 20:00. The Richardson number (Ri < 0.1) was small inside of the flow region, indicating mixing there (Figure 4.5d). The pycnocline moved downward to 10 m below the surface after the wind event (Figure 4.5b). However, this wind event was not strong enough to mix the whole water column and break the stratification. The pycnocline was still the upper boundary of the hypoxia during the observation. The hypoxic layer became thinner as the pycnocline moving downward forced by the wind-induced surface flow. However, the effect of horizontal advections induced by this wind events was still no clear, because there was not enough data about the water property distribution around this station.

4.1.3. Vertical DO flux through pycnocline

Vertical DO flux through the pycnocline was calculated using the diapycnal eddy diffusivity (averaged K_Z at the pycnocline) at station CAS5 using Fick's Law,

$$F = K_z \frac{\Delta O_2}{\Delta z}, \tag{12}$$

where F is the vertical DO flux through the pycnocline, ΔDO is the DO difference between the surface and bottom layer, Δz is the thickness of the pycnocline (Rowe 2001; Justic et al. 2002). At station CAS5, the time averaged DO difference between the surface and bottom layer and the pycnocline thickness are 3.0 ml l^{-1} and 5 m, respectively. By substituting these parameters into Eqn. (13), the calculated vertical DO flux through pycnocline is 156.8 ml m^{-2} d^{-1}.

4.2. Discussion

4.2.1. Temporal changes of DO concentration

The near-bottom DO concentration can change within hours (Figure 4.3a). An annual shelf-wide cruise has been carried out to map the area extent of hypoxia by measuring bottom DO concentration using CTD during each summer since 1985 (Rabalais et al. 2001, 2002). The estimated hypoxia size is taken as a critical value to qualify the severity of hypoxia on the shelf. However, these cruises lasted for about a week to cover the whole shelf. As our results suggest that bottom DO concentrations vary in hours (Figure 4.3a), a high resolution of sampling, both spatial and temporal, is needed to identify the boundary of hypoxia region and give a better estimation of hypoxia areal size.

Horizontal advection can change the vertical distribution of hypoxia. A typical example is shown in Figure 4.4, non-hypoxic water mass is between two hypoxic layers below the subpycnocline layer. As discussed in section 3.2.1, horizontal advection is

responsible for this special vertical distribution of hypoxia. This non-hypoxic layer is observed between the two hypoxic layers for the first 12 hours, disappear in the next 6 hours and stay between the hypoxic layers again in the last 6 hours of the 24 h continuous station CAS4. Horizontal advection appears to be responsible for these temporal changes.

Wind-induced surface flow is another way to change the vertical distribution of hypoxia (Figure 4.5). The pycnocline is moved downward by the wind-induced surface flow and advections (Figure 4.5). The upper boundary of the hypoxia, which is also the pycnocline, is moved downward too, leading to thinner hypoxic layer below the pycnocline. However, if the wind speed is large enough or the duration of the wind event is long enough, we can expect that the whole water column will become well mixed and hypoxia will no longer exist. A study about intermittent ventilation in the hypoxic zone of western Long Island Sound (O'Donnell et al. 2008) suggested that increased vertical mixing is crucial to understand the duration and extent of hypoxia.

4.2.2. Diapycnal diffusivity and vertical DO flux through pycnocline

Diapycnal eddy diffusivity is calculated using the observations in the hypoxic zone on the Texas-Louisiana Shelf. The estimated time-averaged diapycnal diffusivity is 3×10^{-6} m^2 s^{-1} along the pycnocline, comparable to observed open-ocean thermocline values which ranges from 5×10^{-6} m^2 s^{-1} to 3×10^{-5} m^2 s^{-1} (Gregg 1998; Polzin et al. 1995), and close to the averaged diapycnal diffusivity, 5×10^{-6} m^2 s^{-1} to 20×10^{-6} m^2 s^{-1}, in stratified water on the outer New England Shelf in the later summer (Mackinnon and

Gregg 2002). Rowe (2001) presented a DO budget using a constant diapycnal diffusivity of 1×10^{-6} m^2 s^{-1}, the same order of magnitude as our estimation at the pycnocline, to calculate the DO flux through the pycnocline. In this study, diapycnal diffusivity is calculated in strong stratified water with hypoxic water below the pycnocline. This estimation will help determine the DO flux through the pycnocline at hypoxic condition and quantify the effect of the pycnocline on the development of hypoxia.

Averaged cross-pycnocline DO flux is calculated in a two-layer stratified water column with subpycnocline hypoxia in this study. The estimated value is 156.8 ml m^{-2} d^{-1}. The cross-pycnocline DO flux is the resupply of DO to the subpycnocline layer. To understand the relative importance of subpycnocline DO consumption and DO resupply to the lower layer, I calculated the time averaged sediment oxygen consumption at the same station using bottom temperature and DO concentration (Rowe 2001). The estimated sediment oxygen consumption rate is 246.4 ml m^{-2} d^{-1}, which is 1.6 times larger than the DO flux through the pycnocline.

Dortch et al. (1994) used electron transport system (ETS) activity to estimate the water-column respiration rate in the water column. Their mean value for the C-line stations was 103.0 ml m^{-2} d^{-1}, which was an integration of the water column below the pycnocline, or approximately 10 m. The total respiration rate below the pycnocline is the sum of the sediment oxygen consumption and water column respiration, 349.4 ml m^{-2} d^{-1}. Cross-pycnocline DO flux resupplies 45% of the DO consumption below the pycnocline, which is crucial for the DO budget in the subpynocline layer. However, Murrell and Lehrter (2011) measured a total below-pycnocline respiration as large as

1456.0 ml m^{-2} d^{-1}. If we compare the cross-pycnocline DO flux to this value, the DO resupply from surface layer to the bottom layer was only 11% to the consumption.

As the diapycnal diffusivity varies with the stratification conditions and the DO gradient along the pycnocline keeps on changing when bottom DO is depleting, the cross-pycnocline DO flux varies with different locations and time. Long time series with measurements of DO flux will help understand DO budget during the development of hypoxia. This study shows that cross-pycnocline DO flux could resupply as much as 45% DO consumption in the subpycnocline layer. This estimation is also expected to help improve the numerical model studies in determining the vertical eddy diffusivity. However, no field study using microstructures to measure the turbulent dissipation rates of salinity or temperature fluctuations has been reported for the Texas-Louisiana Shelf. An investigation of the diapycnal diffusivity using field measurements is still needed for further study.

CHAPTER V

INTERMITTENT VENTILATION IN THE HYPOXIC ZONE ON TEXAS-LOUISIANA SHELF

It is already known that stratification is the precondition for hypoxia formation. However, O'Donnell (2008) found that ventilation events can resupply DO to the bottom layer in the hypoxic zone in west long island using mooring observations. Rabalais et al. (2001, 2002b) suggested that hypoxia persisted until fall when the stratification broke down by enhanced mixing. In this chapter, I use the year-long mooring data to study the intermittent ventilation events that resupply DO to the bottom layer in the hypoxic zone on the Texas-Louisiana Shelf and also the mechanisms that lead to these ventilation events.

5.1. Results

5.1.1. Observation results from the raw time series

Figure 5.1a shows the time evolution of the observations of DO concentration at the sensor levels of the South Marsh mooring from May to November in the year 2010. The decline of the near-bottom DO concentration is evident in the records. There were several DO decline events from May to November, such as 20 April to 11 May, 24 May to 28 June, 14 July to 25 July, 2 August to 20 August, 27 August to 2 September and 9 October to 25 October during the stratification times, which were marked by grey bands in Figure 5.1. The longest near-bottom water hypoxia was found in June during summer

time. Near-bottom DO concentration began to decrease at late-May and decreased to hypoxic level in early-June. Finally, the DO concentration reached zero in mid-June and kept anoxia until the end of June. During the DO concentration decline event between 24 May and 20 June (27 days), near-bottom DO concentration showed a decline from ~4.5 to ~0 ml l^{-1} implying a rate of DO removal of approximately 0.16 ml l^{-1} d^{-1}. The mid-depth DO record showed a similar trend as the near-bottom DO concentration changes, but was higher in the DO concentrations than the near-bottom DO concentrations. Near-surface record showed less decline events in DO concentration than the near-bottom record, but exhibited more high frequency (with a period smaller than 40 hours) variance. At all three levels, the DO concentrations remained significantly below the saturated concentration throughout the time.

The surface water had a low salinity, about 30, from May to September (Figure 5.1 b). Near-bottom salinity was around 35, indicating offshore derived oceanic water. Mid-depth salinity was 32 to 33, between the surface and bottom salinity. Figure 5.1b shows that the high-frequency (with a period smaller than 40 hours) variability in salinity was larger at the surface than at the mid-depth, while the near-bottom salinity record showed minor variance except when the whole water-column mixing up. Significant bottom-surface salinity differences ($\Delta S > 3$) were found in four major periods: 20 April to 11 May, 24 May to 31 June, 14 July to 4 September, and 9 October to 25 October, which covered all the DO decline events.

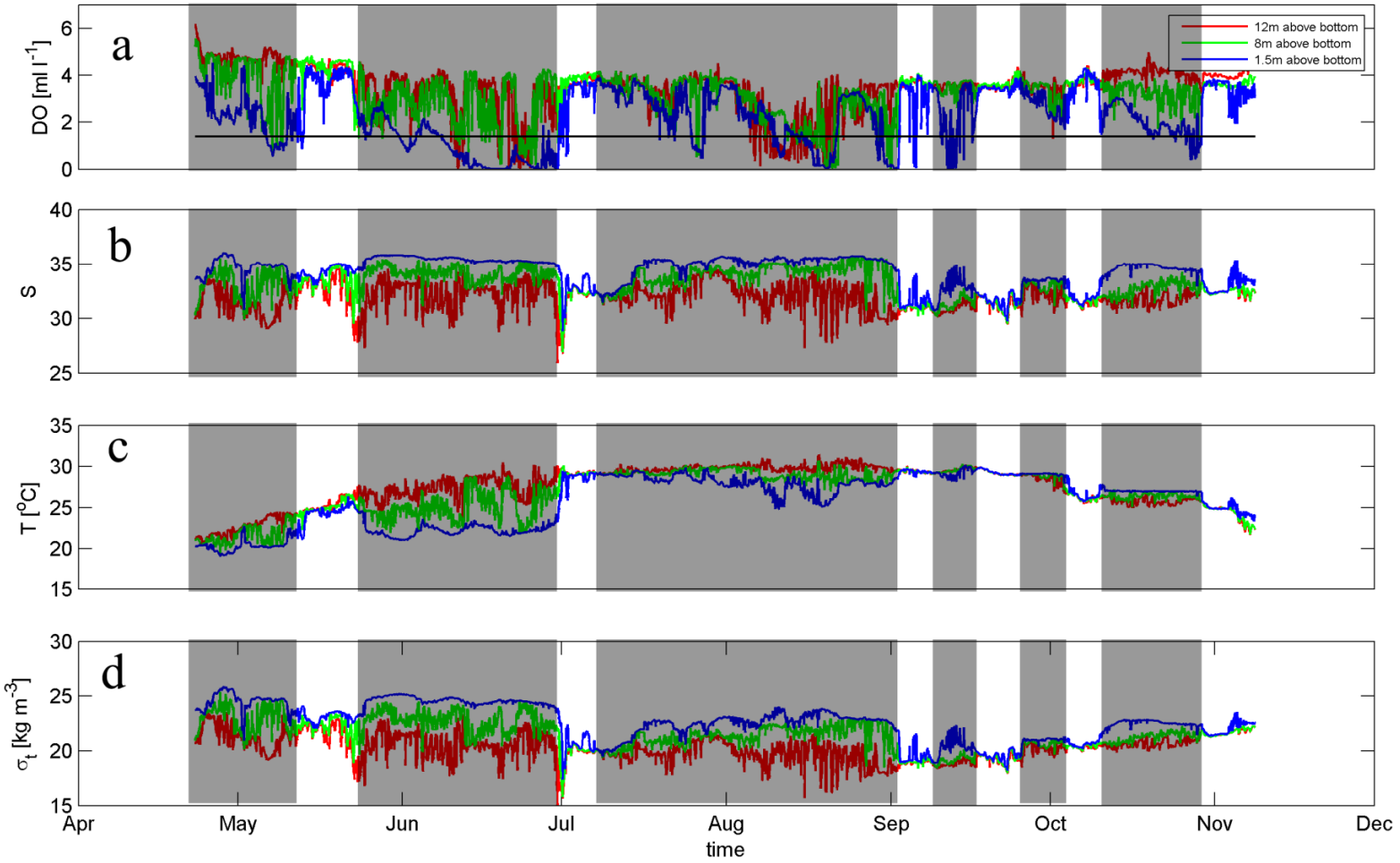

Figure 5.1 Observations at South Marsh mooring in the year 2010: (a) DO concentration (ml l^{-1}); (b) salinity; (c) temperature (°C); (d) density, σ_t. The curves marked by blue, green and red show the data at 1.5 m, 8 m and 12 m above the bottom. Grey bands are the stratification times.

Figure 5.1c presents the temperature records at three different depths. Surface temperature record shows a seasonal circle associated with changes of solar insolation (Etter et al. 2004). The surface temperature increased from ~20 °C at mid-April and reached a peak of ~30 °C in August as the sun light radiation decreased during the summer time. After August, surface temperature dropped to ~25 °C in November with the decrease of sun light radiation. Near-bottom temperature was lower than the surface temperature during the summer time, because the surface water warms up faster than the bottom water. After September, near-bottom temperature was higher than the surface temperature, because the surface water cooled down faster than the bottom water. This seasonal cycle turned out to increase the stratification (vertical density differences) from May to August and decrease the stratification after September. However, near-bottom temperature record showed small amplitudes in high-frequency variation.

The density records are shown in Figure 5.1d. The density is controlled by both salinity and temperature. Stratification times were marked by gray bands in Figure 5.1d using the surface-bottom density differences. During the stratification time, bottom DO concentrations decreased by the imbalance between DO consumption and DO resupply (Figure 5.1a).

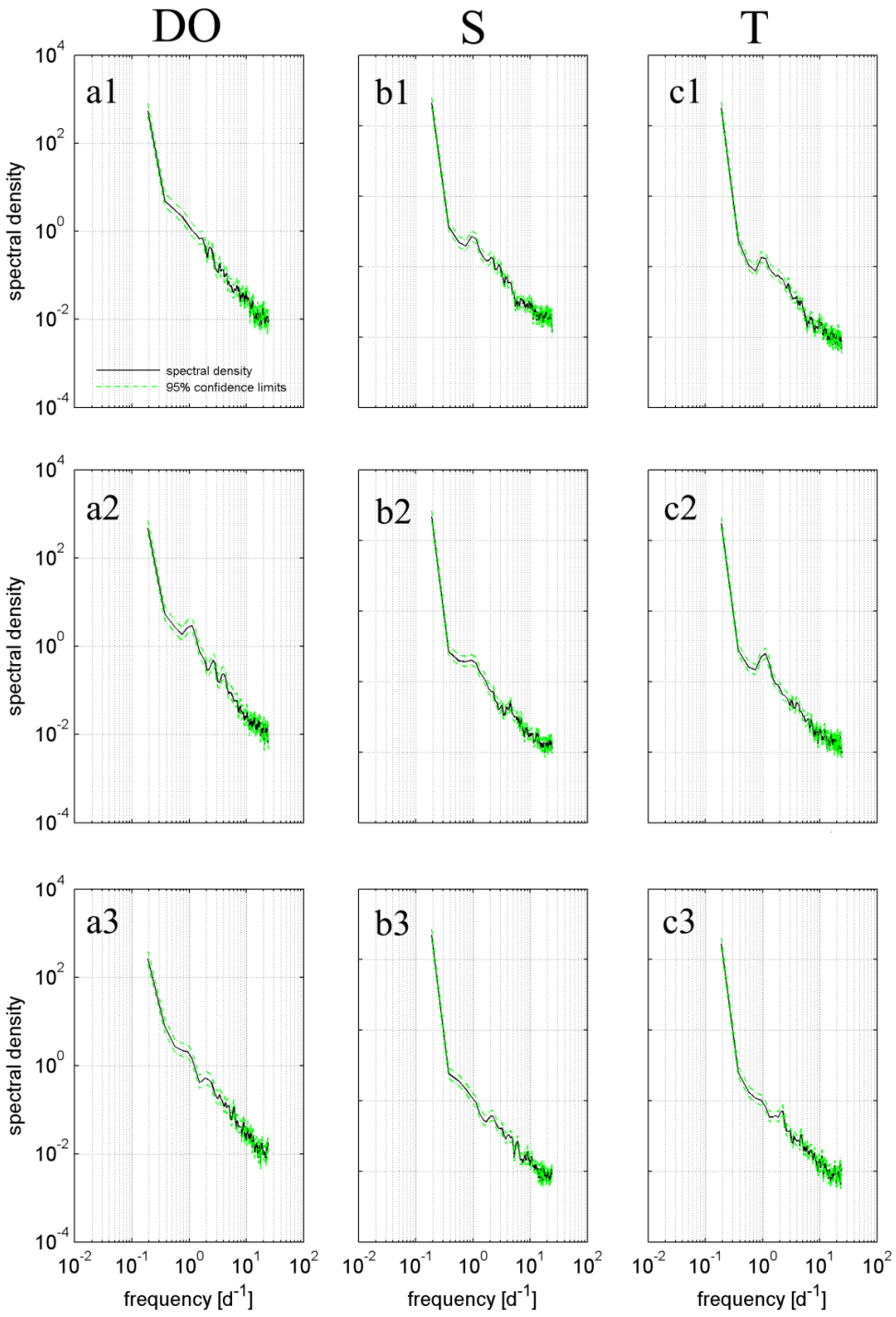

Figure 5.2 Spectra of the raw DO (a1, a2, and a3), salinity (b1, b2 and b3) and temperature (c1, c2 and c3) time series at each depth (surface, mid, and bottom) at South Marsh Mooring. Green dash lines show the 95% confidence level.

The spectra of the raw data of DO concentration, salinity and temperature profiles at each depth are shown in Figure 5.2. For the spectra of DO concentration, there was no significant peaks in the surface record (Figure 5.2 a1), peaks of one day and half a day period were found in the mid and bottom record (Figure 5.2 a2 and a3). For the spectra of salinity, peak of one day period was shown in the surface and mid record (Figure 5.2 b1 and b2), but not in the bottom record. In the bottom record of salinity (Figure 5.2 b3), only a peak of half a day period was found which was different from the record in surface and mid. For spectra of temperature, peak of one day period was shown in the surface and mid record (Figure 5.2 c1 and c2), but not shown in the bottom record. Same as the spectra of the bottom salinity, only a peak of half a day period was found. Both O1 and M2 tidal currents were observed at this location by Reid and DiMarco (1998). Tidal currents caused front motion might lead to these one day and half a day variations. Diurnal changes of sunlight radiations and photosynthesis can also contribute to the diurnal changes of temperature and DO concentrations.

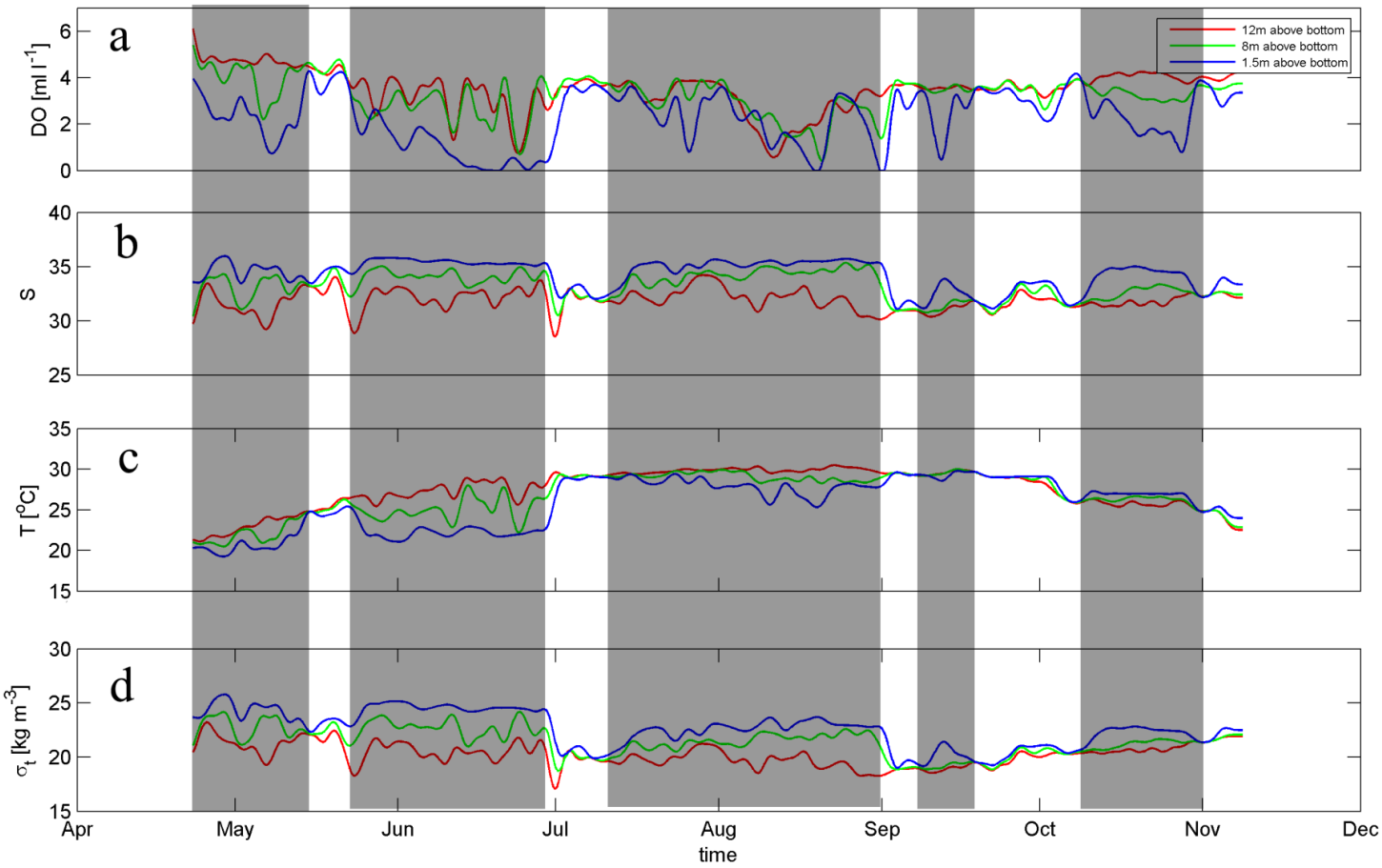

Figure 5.3 Low-pass filtered Observations at South-Marsh mooring in the year 2010: (a) DO concentration (ml l^{-1}); (b) salinity; (c) temperature (°C); (d) density, σ_t. The curves marked by blue, green and red show the data at 1.5 m, 8 m and 12 m above the bottom. Grey bands shows the time with stratification.

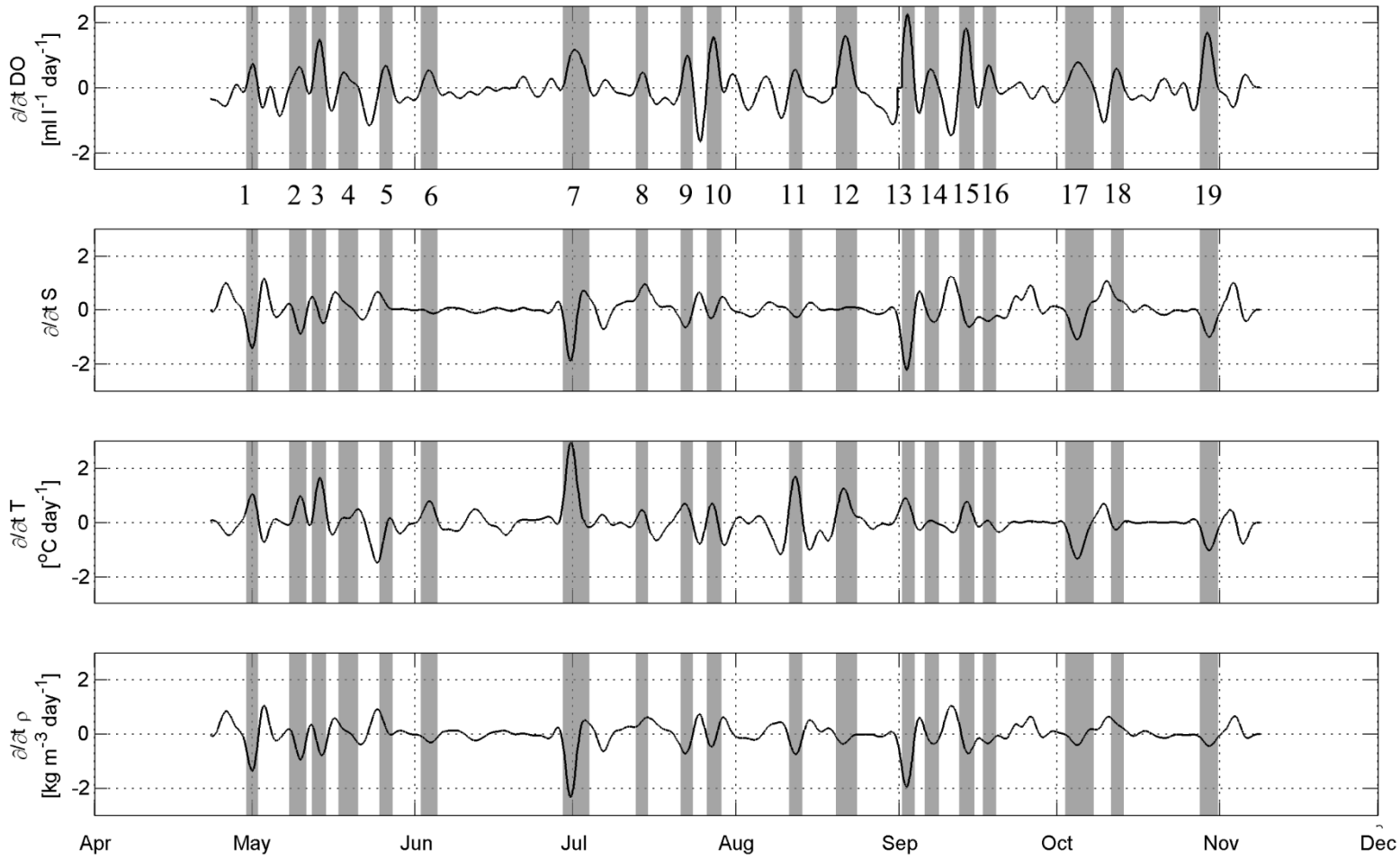

Figure 5.4 (a) The rate of change of the low-pass filtered bottom DO concentration (ml l^{-1} d^{-1}); (b) The rate of change of low-pass filtered bottom salinity; (c) The rate of change of low-pass filtered bottom temperature; (d) Low-pass filtered bottom density (kg m^{-3}). Grey bands show the ventilation-intervals.

5.1.2. Intermittent ventilation in the hypoxic zone

Intermittent ventilation of subpycnocline water is observed to turn the hypoxic water into non-hypoxic water in Figure 5.1, especially at the end of the DO decline events or the right end of the grey bands on the figure. To clarify the variability and investigate the mechanisms that are responsible for the ventilation events, I computed the low-frequency variation at different depths applying a fifth-order Butterworth filter (Roberts and Roberts 1978) with a cutoff period of 40 hours (Figure 5.3). By comparing Figure 5.3b, 5.3c and 5.3d, salinity was found to dominant the density changes and temperature only played a secondary role in control the density. The low-passed filtered DO records (Figure 5.3a) showed that the bottom DO decline events only found with existence of stratification or vertical density differences (grey bands in Figure 5.3d). It was agreed with the previous studies that stratification was the precondition for hypoxia development (Wiseman et al, 1997; Rabalais et al. 2002)

The time derivative of the low-passed filtered DO records (DO concentration changes with time) was calculated for each depth (Figure 5.4a). Positive values indicated increasing DO, or the ventilation of the subpycnocline waters. Times of increasing DO ($\frac{\partial}{\partial t} O_2 > 0$) that exceed 24 hours in duration were high-lighted by gray bands to assist the association of ventilation events and changes in other variables and were defined as the ventilation-intervals. There are 19 ventilation intervals in the DO records with a time period of 1~3 days. During the ventilation-intervals, the near-bottom DO concentration increased up to ~3.4 ml l^{-1} and switched from hypoxic to non-hypoxic over a short time

about 1~3 days, which was much faster than the time for hypoxia to develop (about 2 weeks). The mechanisms that leaded to these ventilation events will be discussed later.

The intervals between the ventilation-intervals, where $\frac{\partial}{\partial t} O_2 < 0$, are defined to be the respiration-intervals with a time period of 3~15 days. An interesting phenomenon during the respiration-intervals was that several respiration-intervals showed a rapid decline in DO concentration, as fast as ~-1.1 ml l^{-1} d^{-1}, following ventilation-intervals, especially the one suffering severe hypoxia or anoxia, e.g., the respiration-intervals between ventilation-intervals 9 and 10 (Figure 5.4a and 5.5a). During this respiration-interval, the DO decline rate reaches a peak of ~-1.8 ml l^{-1} d^{-1}. The causes for this fast DO depletion will be discussed later.

During the ventilation-intervals, the average and standard deviation rate of near-bottom DO concentration increase was 0.48 ± 0.45 ml l^{-1} d^{-1} at South Marsh Mooring. The largest DO increasing rate during ventilation-intervals was ~2.2 ml l^{-1} d^{-1} at ventilation-interval 13 and raised the near-bottom DO concentration from 0 to 3.4 ml l^{-1} in two days. The averaged and standard deviation of the near-bottom DO concentration decrease during the respiration-intervals is -0.36 ± 0.30 ml l^{-1} d^{-1}.The magnitude of the mean DO increase rate during ventilation-intervals exceeded that of the respiration-intervals. However, the duration of ventilation-intervals (1~3 days) was much shorter than that of the respiration intervals (3~15days).

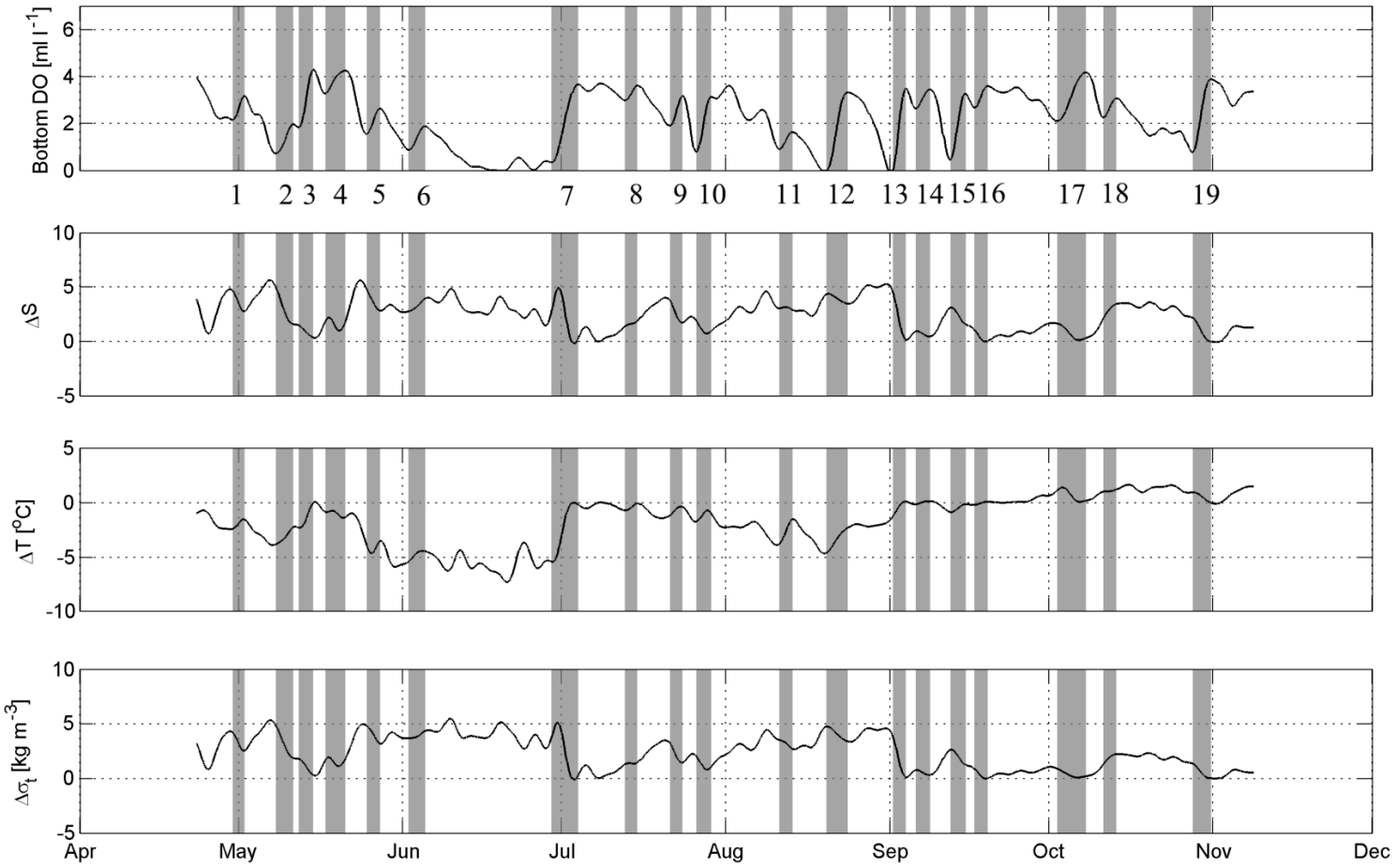

Figure 5.5 (a) Low-pass filtered bottom DO concentration (ml l^{-1}); (b) low-pass filtered bottom-surface salinity difference; (c) low-pass filtered bottom-surface temperature difference; (d) low-pass filtered bottom-surface density difference (kg m^{-3}). Grey bands show the ventilation-intervals.

Table 5.1 Correlations between the time-series of DO & AOU and other different parameters at the South Marsh Mooring. All the P values for the correlation is much smaller than 0.0001. Each calculated correlation coefficient is significant.

Correlation	S	T	σ_t	ΔS	ΔT	$\Delta \sigma_t$	wind speed
DO	0.56	0.39	0.56	0.56	0.67	0.69	0.21
AOU	0.58	0.54	0.66	0.57	0.72	0.72	0.19

5.1.3. Mixing induced intermittent ventilation

Vertical mixing through the pycnocline would lead to ventilation of the near-bottom waters and increase the near-bottom DO concentrations. The surface water is warm and fresh, while the bottom water is cool and salty (Figure 5.3 b and c). Vertical mixing can mix the surface water with bottom water and lead to temperature increase and salinity decrease in the bottom layer. Therefore, a negative sign of the time derivative of near-bottom salinity and a positive sign of the time derivative of near-bottom temperature present mixing events. However, because the surface water temperature is lower than the bottom water after mid-September, a negative sign of the time derivative of near-bottom salinity and a negative sign of the time derivative of near-bottom temperature present mixing events for the time period from mid-September to November. The signature sign of the time derivatives of salinity and temperature during ventilation intervals allows us to identify mixing events.

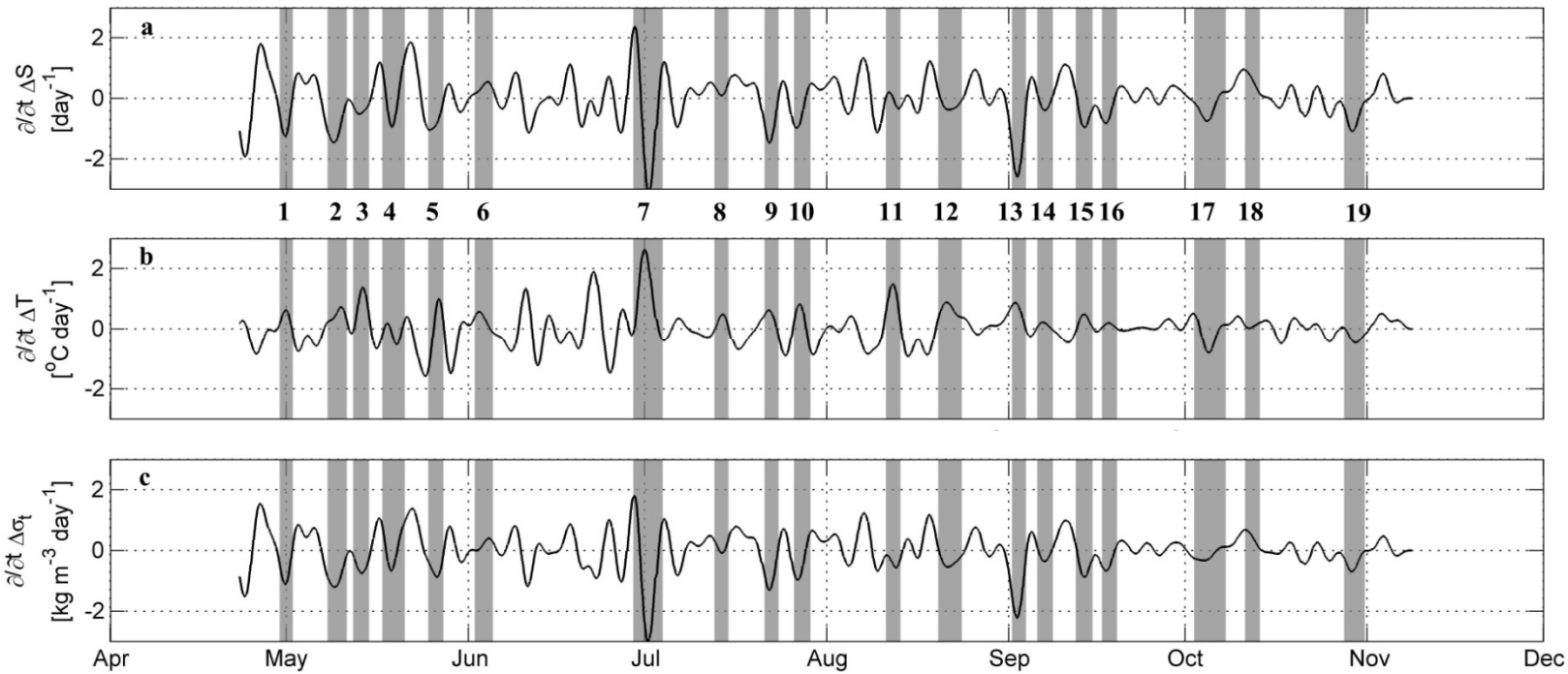

Figure 5.6 (a) The rate of change of low-pass filtered bottom-surface salinity difference; (b) the rate of change of low-pass filtered bottom-surface temperature difference; (c) the rate of change of low-pass filtered bottom-surface density difference (kg m^{-3}). Grey bands show the ventilation-intervals.

Figure 5.4a shows the observations of the time derivative of the DO concentration 1.5 m above the bottom superimposed on numbered gray bands that identify 19 ventilation intervals during which DO concentration was increasing for more than 24 hours. The corresponding time derivatives of near-bottom temperature and salinity were shown in Figure 5.4b and 5.4c. To remove the high frequency noise, all theses time series have been filtered by a low-pass filter shown in Figure 5.5. 11 mixing events have been identified among 19 ventilation-intervals during which vertical mixing lead to the ventilation-intervals. All these ventilation-intervals are found with increasing temperature and decreasing salinity at the near-bottom sensor during the ventilation intervals and caused by vertical mixing events. The mixing events leaded ventilation-intervals are the ventilation-intervals: 1, 2, 3, 7, 9, 10, 11, 13, 14, 15, 17, and 19.

Figure 5.6c shows the evolution of the time derivative of the low-pass filtered density difference between the bottom and surface sensors. It is obvious that almost all of the ventilation intervals, the gray bands, are closely associated with the decreasing stratification as expected when mixing is happening. The evolution of the time derivative of the low-pass filtered salinity and temperature difference between the bottom and the surface sensors are shown in Figure 5.6a and Figure 5.6b. The curve of the salinity differences shows a better correlation with density differences than the temperature differences. It suggests that stratification was dominated by surface-bottom salinity differences.

The correlations between near-bottom DO concentration/AOU (apparent oxygen utilization, defined as the difference between the measured DO concentration and its

equilibrium saturation concentration in water with the same physical and chemical properties) and different water properties and vertical water properties differences have been calculated (Table 5.1). Near-bottom DO concentration showed a significant correlation with near-bottom salinity and density with a correlation coefficients (r) of 0.56, which was larger than the correlation coefficients with near-bottom temperature (0.39). However, larger correlation between the near-bottom DO concentration and vertical salinity, temperature and density differences was found (0.56, 0.67, and 0.69, respectively). Because the vertical differences of these variables can better reflect the vertical stability of the water column. Among all these variables, the near-bottom density (r = 0.56) and vertical density difference (r = 0.69) had larger correlation coefficients than others, because both salinity and temperature changed the water-column stability by changing the density. When AOU was applied, all the calculated correlations were improved, especially the correlations associated with temperature. Because AOU better quantify how much DO was used up in the subpycnocline water.

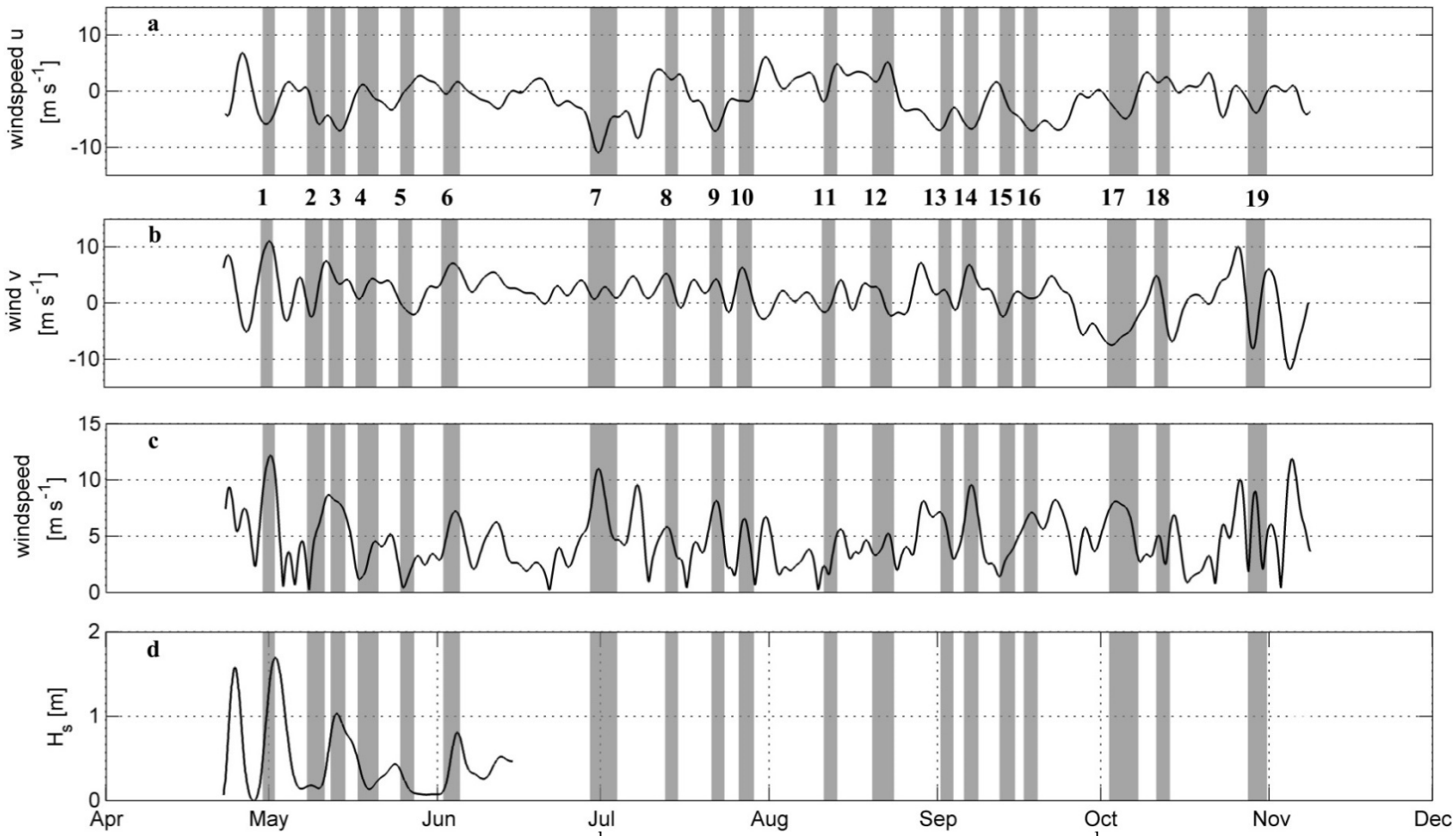

Figure 5.7 (a) u component of the wind speed (m s^{-1}); (b) v component of the wind speed (m s^{-1}); (c) Magnitude of the wind speed (m s^{-1}); (d) significant wave height (m) at the South Marsh mooring. Grey bands show the ventilation-intervals.

5.1.4. Wind induced mixing

The magnitude of the low-pass filtered wind speed from NCAR at the mooring location was shown in Figure 5.7c. Comparing the gray band with wind speed, ventilation intervals 1, 2, 3, 7, 9, 10, 11, 14, 17, 19 were observed with large wind speed. The correlation between the wind speed and the bottom DO concentration was also calculated with results shown in Table 5.1. The correlation coefficient ($r = 0.21$) was low, but passes the p-test. The explanation is that the ventilation events are only associated with large wind events, while wind contributes little to DO variance when wind speed is small. Furthermore, if the water column is already mixed up or non-hypoxic conditions, wind events induced vertical mixing will not change the near-bottom DO concentration, salinity and temperature.

Local wind events enhanced vertical mixing by vertical shears and lead to ventilation events. The significant wave height was consistent with the wind events and suggested that the mixing events were induced by the local wind events (Figure 5.7d). By comparing the along-shore and cross-shore components of the wind (Figure 5.7a and 5.7b) with the mixing events, I found that the mixing events were only decided by the magnitude of the wind speed, the direction of the winds had nothing to do with the local mixing.

5.2. Discussions

5.2.1. DO budget

The averaged and standard deviation of the near-bottom DO concentration changes during the respiration-intervals was -0.36 ± 0.30 ml l^{-1} d^{-1} in this study. This DO decline rate was comparable to -0.44 ± 0.2 ml l^{-1} d^{-1}, which was calculated from the near-bottom DO concentrations from the mooring at C6 (20 m total depth) between the year 1991 and 1997 (Rabalais et al. 1997). I calculated the time averaged benthic respiration at the South Mash Mooring using bottom temperature and DO concentration (Rowe 2001). The estimated benthic respiration was averaged 246.4 ml m^{-2} d^{-1}. Dortch et al. (1994) used electron transport system (ETS) activity to estimate WR in the water column, after calibration by comparison with other methods. Their mean for the C-line stations was 103.0 ml m^{-2} d^{-1}, which was an integration of the water column below the pycnocline, or approximately 10 m. Then the total respiration below the pycnocline is the sum of the benthic respiration and water column respiration, 349.4 ml m^{-2} d^{-1}. The cross-pycnocline DO flux from Chapter IV is 156.8 ml m^{-2} d^{-1}. Combining these terms together, a mean DO decline rate of -192.6 ml m^{-2} d^{-1} is expected. Assuming that the subpycnocline layer was 10 m thick, the decline rate is -0.02 ml l^{-1} d^{-1}, which is too small to compare to the mooring observations (-16.3 ± 13.6 mmol m^{-3} d^{-1}). However, Murrell et al. (2011) measured a total below-pycnocline respiration of 1456 ml m^{-2} d^{-1}, which lead to a decline rate of 0.13 ml l^{-1} d^{-1} with the same assumption. This decline rate is closer to the mooring observed rate.

5.2.2. Fast DO depletion after ventilation-intervals

As noticed in the respiration-intervals, a rapid decline in DO, as fast as ~-1.1 ml l^{-1} d^{-1}, was found following ventilation-intervals, especially the one suffering severe hypoxia or anoxia, e.g., the respiration-intervals between ventilation-intervals 9 and 10 marked in Figure 5.4a and Figure 5.5a. The DO decline rate could reach a peak of ~-1.8 ml l^{-1} d^{-1}, which was much faster than the regular DO depletion rate in the subpycnocline water observed in the previous studies.

Millerway et al. (1994) did several experiments to explore how sediments responded to oxygenation after a period of hypoxia. They replaced the overlying water in sediment cores with re-oxygenated bottom water sample. They found that benthic respiration rates increased from 141.1 ml m^{-2} d^{-1} to 710.0 ml m^{-2} d^{-1} when overlying water was re-oxygenated. Murrell et al. (2011) also did similar experiments and reached a similar conclusion. This response was consistent with the expected accumulation of anaerobic metabolites (e.g., Fe^{2+}, HS^{-}) during hypoxia, which become chemically re-oxidized as oxygen availability is increased. This theory helps to explain the extreme high DO depletion rate after the ventilation-intervals.

5.2.3. Ventilation mechanisms

Most of the ventilation-intervals observed at the mooring location had characteristics associated with increased vertical mixing, which contributed 58% of the total ventilation intervals. Although I can not separate the advection and other associated

events out based on this data set, it suggested that mixing events dominated the ventilation-intervals at the South Marsh mooring.

Horizontal advection is another way to make these ventilation intervals by transport high DO water into low DO water (discussed in Chapter III and Chapter IV). As I have only one mooring to measure the DO concentration, I can not obtain the horizontal gradient of DO concentrations. I can not distinguish the horizontal advections caused ventilation-intervals out. A horizontal DO gradient is necessary for the horizontal advections to transport DO and change the local DO concentrations. Therefore, horizontal advections are still considered to be a way to make horizontal DO transport below the pycnocline. More research is needed to study the horizontal transport of DO in the future, especially at the horizontal boundary of the hypoxic zone.

There are a lot of ways to make transport of DO and lead to the oscillation of $\frac{\partial}{\partial t} O_2$. Several previous studies have already showed that these fluctuations could be the result of increased mixing or decreased stratification associated with the spring-neap tidal cycle (Simpson et al. 1990), the modulation of the subtidal currents by wind and sea level changes (Wong 1990), wind fluctuations (Scully et al. 2005, 2010), or horizontal advections (O'Donnell et al. 2008).

In this chapter, the evolution of the bottom DO concentration was presented to show intermittent ventilation events in the hypoxic zone with time period of 1~3 days. 58% of ventilation events are caused by mixing events. Local large wind events are proved to be responsible for the enhanced vertical mixing.

CHAPTER VI

CONCLUSIONS

Seasonal hypoxia has been observed in the northern Gulf of Mexico science 1985. Eutrophication due to nutrient loading has traditionally been regarded as the most important element controlling hypoxia on the Texas-Louisiana Shelf. Water column stability and wind forcing also play important roles in controlling hypoxia formation and spatial distribution. In this study, both field observations and model tools are used to investigate the relationship between hypoxia and stratification, and the physical processes that affect the formation, duration and break down of hypoxia on Texas-Louisiana Shelf. Specific conclusions are as follows:

1. A threshold of N=0.06 s^{-1} was defined to represent the lower limit of the stratification strength for existence of hypoxia using the historical CTD data between 2003 and 2009. Vertical stratification controlled the vertical distribution of low DO water. 75% of the hypoxic layers were within 4 m above the bottom. 58% of the hypoxic layers were in or along the bottom mixed layers. When there was only one pycnocline, this pycnocline was the upper boundary of the hypoxic layer. However, with a double-pycnocline structure, hypoxic layers were either limited by the secondary-pycnocline or between the main-pycnocline and the secondary-pycnocline.

2. A double-pycnocline structure was proved to reduce hypoxia formation time by a one-dimension DO model with parameterized DO consumption (Figure 3.16). Comparison among the three cases showed that double-pycnocline structure can reduce 9 to 15 days for the near-bottom water to become hypoxic. The model results also

showed that hypoxia can develop across the secondary-pycnocline and the main-pycnocline is the final upper boundary of hypoxia.

3. Bottom mixed layer was approved to accelerate hypoxia formation speed using the one-dimensional DO model (Figure 3.17). The vertical changes of K_Z at the interface between the bottom mixed layer and stratified layer was responsible for that. Model experiments also showed that the secondary pycnocline could work as barrier to inhibit the vertical extension of hypoxia (Figure 3.18).

4. The vertical distribution of near-bottom hypoxic water changes in hours. As our results suggest that bottom DO concentrations vary at a temporal scale of hours, a high resolution of sampling, both spatial and temporal, is needed to identify the boundary of hypoxia region and give a better estimate of hypoxia areal size.

5. Diapycnal diffusivity was calculated using observations in the hypoxic zone on the Texas-Louisiana Shelf. The estimated time-averaged diapycnal diffusivity is 3×10^{-6} m^2 s^{-1} along the pycnocline. Averaged cross-pycnocline DO flux is calculated in a two-layer stratified water column with subpycnocline hypoxia in this study. The estimated value is 156.8 ml l^{-1} d^{-1}. Cross-pycnocline DO flux could resupply as much as 45% DO consumption in the subpycnocline layer. More investigation of the vertical eddy diffusivity and cross pycnocline DO flux is necessary for a full understanding of the DO budget and hypoxia development in the subpycnocline layer on the Texas-Louisiana Shelf.

6. The observations of DO, salinity and temperature at the South Marsh Mooring described in this study provided highly resolved observations of short timescale

fluctuations in the DO concentrations in the seasonal hypoxic waters on Louisiana Shelf. The most significant feature of the observations presented in this study was the intermittent ventilation of the subpycnocline waters. There were 19 ventilation events in the DO records with a time period of 1~3 days.

7. Analysis of the time series of DO, salinity and temperature at different levels of the mooring demonstrated that most of the ventilation-intervals were associated with increased vertical mixing, which contributed 58% of the total ventilation intervals. It suggests that mixing events dominate the ventilation-intervals at the South Marsh mooring.

8. Local large wind events were responsible for the enhanced vertical mixing. Comparison of the time derivative of the low-frequency part of the near-bottom DO concentration to observations of the wind and significant wave height suggested that the rate of mixing was modulated by the magnitude of the wind only, and the direction of the wind played a minor role.

REFERENCES

Belabbassi, L. 2006. "Examination of the relationship of river water to occurrences of bottom water with reduced oxygen concentration in the northern Gulf of Mexico." PhD diss., Texas A&M University.

Bendtsen, J., K. E. Gustafsson, J. Soderkvist, and J. L. S. Hansen. 2009. "Ventilation of bottom water in the North Sea-Baltic Sea transition zone." *Journal of Marine Systems* 75 (1-2):138-149. doi: 10.1016/j.jmarsys.2008.08.006.

Bianchi, T. S., S. F. DiMarco, J. H. Cowan, R. D. Hetland, P. Chapman, J. W. Day, and M. A. Allison. 2010. "The science of hypoxia in the Northern Gulf of Mexico: A review." *Science of the Total Environment* 408 (7):1471-1484. doi: 10.1016/j.scitotenv.2009.11.047.

Boesch, D. F., and N. N. Rabalais. 1991. "Effects of hypoxia on continental-shelf benthos - comparisons between the new-york bight and the Northern Gulf of Mexico." *Modern and Ancient Continental Shelf Anoxia*:27-34.

Bourgault, D., F. Cyr, P. S. Galbraith, and E. Pelletier. 2012. "Relative importance of pelagic and sediment respiration in causing hypoxia in a deep estuary." *Journal of Geophysical Research-Oceans* 117:13. doi: 10.1029/2012jc007902.

Breitburg, D. 2002. "Effects of hypoxia, and the balance between hypoxia and enrichment, on coastal fishes and fisheries." *Estuaries* 25 (4B):767-781. doi: 10.1007/bf02804904.

Breitburg, D. L., D. W. Hondorp, L. A. Davias, and R. J. Diaz. 2009. "Hypoxia, Nitrogen, and Fisheries: Integrating Effects Across Local and Global Landscapes." *Annual Review of Marine Science* 1:329-349. doi: 10.1146/annurev.marine.010908.163754.

Caddy, J. F. 1993. "Toward a comparative evaluation of human impacts on fishery ecosystems of enclosed and semi-enclosed seas." *Reviews in Fisheries Science* 1 (1):57-95.

Carpenter, J. H. 1965. "The Chesapeake Bay Institute technique for the Winkler dissolved oxygen method." *Limnol Oceanogr* 10 ((1)):141-143.

Chen, C. S., R. O. Reid, and W. D. Nowlin. 1996. "Near-inertial oscillations over the Texas Louisiana shelf." *Journal of Geophysical Research-Oceans* 101 (C2):3509-3524. doi: 10.1029/95jc03395.

Cho, K. W., R. O. Reid, and W. D. Nowlin. 1998. "Objectively mapped stream function fields on the Texas-Louisiana shelf based on 32 months of moored current meter data." *Journal of Geophysical Research-Oceans* 103 (C5):10377-10390. doi: 10.1029/98jc00099.

Cochrane, J. D., and F. J. Kelly. 1986. "Low-frequency circulation on the Texas-Louisiana continental-shelf." *Journal of Geophysical Research-Oceans* 91 (C9):645-659. doi: 10.1029/JC091iC09p10645.

Conley, D. J., H. W. Paerl, R. W. Howarth, D. F. Boesch, S. P. Seitzinger, K. E. Havens, C. Lancelot, and G. E. Likens. 2009. "ECOLOGY Controlling Eutrophication: Nitrogen and Phosphorus." *Science* 323 (5917):1014-1015. doi: 10.1126/science.1167755.

Cooper, S. R. 1995. "Chesapeake bay watershed historicalal land-use - impact on water-quality and diatom communities." *Ecological Applications* 5 (3):703-723. doi: 10.2307/1941979.

Dale, V. H. 2010. Hypoxia in the Northern Gulf of Mexico. New York: Springer.

Diaz, R. J. 2001. "Overview of hypoxia around the world." *Journal of Environmental Quality* 30 (2):275-281.

Diaz, R. J., R. J. Neubauer, L. C. Schaffner, L. Pihl, and S. P. Baden. 1992. "Continuous monitoring of dissolved-oxygen in an estuary experiencing periodic hypoxia and the effect of hypoxia on macrobenthos and fish." *Science of the Total Environment, Supplement 1992: Marine Coastal Eutrophication*:1055-1068.

Diaz, R. J., and R. Rosenberg. 1995. "Marine benthic hypoxia: A review of its ecological effects and the behavioural responses of benthic macrofauna." *Oceanography and Marine Biology - an Annual Review, Vol 33* 33:245-303.

Diaz, R. J., and R. Rosenberg. 2008. "Spreading dead zones and consequences for marine ecosystems." *Science* 321 (5891):926-929. doi: 10.1126/science.1156401.

DiMarco, S. F., P. Chapman, N. Walker, and R. D. Hetland. 2010. "Does local topography control hypoxia on the eastern Texas-Louisiana shelf?" *Journal of Marine Systems* 80 (1-2):25-35. doi: 10.1016/j.jmarsys.2009.08.005.

DiMarco, S. F., and R. O. Reid. 1998. "Characterization of the principal tidal current constituents on the Texas-Louisiana shelf." *Journal of Geophysical Research-Oceans* 103 (C2):3093-3109. doi: 10.1029/97jc03289.

DiMarco, S. F., J. Strauss, N. May, R. L. Mullins-Perry, E. L. Grossman, and D. Shormann. 2012. "Texas Coastal Hypoxia Linked to Brazos River Discharge as Revealed by Oxygen Isotopes." *Aquatic Geochemistry* 18 (2):159-181. doi: 10.1007/s10498-011-9156-x.

Dinnel, S. P., and W. J. Wiseman. 1986. "Fresh-water on the Louisiana and Texas shelf." *Continental Shelf Research* 6 (6):765-784. doi: 10.1016/0278-4343(86)90036-1.

Dortch, Q., N. N. Rabalais, R. E. Turner, and G. T. Rowe. 1994. "Respiration rates and hypoxia on the Louisiana shelf." *Estuaries* 17 (4):862-872. doi: 10.2307/1352754.

Eilola, K., H. E. M. Meier, and E. Almroth. 2009. "On the dynamics of oxygen, phosphorus and cyanobacteria in the Baltic Sea; A model study." *Journal of Marine Systems* 75 (1-2):163-184. doi: 10.1016/j.jmarsys.2008.08.009.

Etter, P. C., M. K. Howard, and J. D. Cochrane. 2004. "Heat and freshwater budgets of the Texas-Louisiana shelf." *Journal of Geophysical Research-Oceans* 109 (C2):23. doi: C0202410.1029/2003jc001820.

Feng, Y., S. F. DiMarco, and G. A. Jackson. 2012. "Relative role of wind forcing and riverine nutrient input on the extent of hypoxia in the northern Gulf of Mexico." *Geophysical Research Letters* 39:5. doi: 10.1029/2012gl051192.

Forrest, D. R., R. D. Hetland, and S. F. DiMarco. 2011. "Multivariable statistical regression models of the areal extent of hypoxia over the Texas-Louisiana continental shelf." *Environmental Research Letters* 6 (4). doi: 04500210.1088/1748-9326/6/4/045002.

Fuenzalida, R., W. Schneider, J. Garces-Vargas, L. Bravo, and C. Lange. 2009. "Vertical and horizontal extension of the oxygen minimum zone in the eastern South Pacific Ocean." *Deep-Sea Research Part Ii-Topical Studies in Oceanography* 56 (16):1027-1038. doi: 10.1016/j.dsr2.2008.11.001.

Gaston, G. R., P. A. Rutledge, and M. L. Walther. 1985. "The effects of hypoxia and brine on recolonization by macrobenthos off cameron, Louisiana (USA)." *Contributions in Marine Science* 28:79-93.

Grant, W. D., and O. S. Madsen. 1986. "The continental-shelf bottom boundary-layer." *Annual Review of Fluid Mechanics* 18:265-305. doi: 10.1146/annurev.fluid.18.1.265.

Grantham, B. A., F. Chan, K. J. Nielsen, D. S. Fox, J. A. Barth, A. Huyer, J. Lubchenco, and B. A. Menge. 2004. "Upwelling-driven nearshore hypoxia signals ecosystem

and oceanographic changes in the northeast Pacific." *Nature* 429 (6993):749-754. doi: 10.1038/nature02605.

Greene, R. M., J. C. Lehrter, and J. D. Hagy. 2009. "Multiple regression models for hindcasting and forecasting midsummer hypoxia in the Gulf of Mexico." *Ecological Applications* 19 (5):1161-1175. doi: 10.1890/08-0035.1.

Harper, D. E., L. D. McKinney, R. R. Salzer, and R. J. Case. 1981. "The occurrence of hypoxia bottom water off the upper Texas coast and its effects on the benthic biota." *Contrib. Mar. Sci.* 24:53-79.

Helly, J. J., and L. A. Levin. 2004. "Global distribution of naturally occurring marine hypoxia on continental margins." *Deep-Sea Research Part I-Oceanographic Research Papers* 51 (9):1159-1168. doi: 10.1016/j.dsr.2004.03.009.

Hetland, R. D., and S. F. DiMarco. 2008. "How does the character of oxygen demand control the structure of hypoxia on the Texas-Louisiana continental shelf?" *Journal of Marine Systems* 70 (1-2):49-62. doi: 10.1016/j.jmarsys.2007.03.002.

Howard, L. N. 1961. "Note on a paper of miles,john,w." *Journal of Fluid Mechanics* 10 (4):509-512. doi: 10.1017/s0022112061000317.

Justic, D., N. N. Rabalais, and R. E. Turner. 1996. "Effects of climate change on hypoxia in coastal waters: A doubled CO2 scenario for the northern Gulf of Mexico." *Limnology and Oceanography* 41 (5):992-1003.

Justic, D., N. N. Rabalais, and R. E. Turner. 2002. "Modeling the impacts of decadal changes in riverine nutrient fluxes on coastal eutrophication near the Mississippi River Delta." *Ecological Modelling* 152 (1):33-46. doi: 10.1016/s0304-3800(01)00472-0.

Justic, D., N. N. Rabalais, R. E. Turner, and W. J. Wiseman. 1993. "Seasonal coupling between riverborne nutrients, net productivity and hypoxia." *Marine Pollution Bulletin* 26 (4):184-189. doi: 10.1016/0025-326x(93)90620-y.

Kamykowski, D., and S. J. Zentara. 1990. "Hypoxia in the world ocean as recorded in the historicalal data set." *Deep-Sea Research Part a-Oceanographic Research Papers* 37 (12):1861-1874. doi: 10.1016/0198-0149(90)90082-7.

Karstensen, J., L. Stramma, and M. Visbeck. 2008. "Oxygen minimum zones in the eastern tropical Atlantic and Pacific oceans." *Progress in Oceanography* 77 (4):331-350. doi: 10.1016/j.pocean.2007.05.009.

Kiselkova, V., "Effects of instabilities in the buoyancy-driven flow on the bottom oxygen: applications to the Louisiana Shelf." PhD diss., Texas A&M University, 2008.

Kunze, E., M. G. Briscoe, and A. J. Williams. 1990. "Interpreting shear and strain fine-structure from a neutrally buoyant float." *Journal of Geophysical Research-Oceans* 95 (C10):18111-18125. doi: 10.1029/JC095iC10p18111.

Kunze, E., A. J. Williams, and M. G. Briscoe. 1990. "Observations of shear and vertical stability from a neutrally buoyant float." *Journal of Geophysical Research-Oceans* 95 (C10):18127-18142. doi: 10.1029/JC095iC10p18127.

Kuo, A. Y., and B. J. Neilson. 1987. "Hypoxia and salinity in virginia estuaries." *Estuaries* 10 (4):277-283. doi: 10.2307/1351884.

Lapointe, B. E., and W. R. Matzie. 1996. "Effects of stormwater nutrient discharges on eutrophication processes in nearshore waters of the Florida Keys." *Estuaries* 19 (2B):422-435. doi: 10.2307/1352460.

Leben, R. R. 2005. Altimeter-derived Loop Current metrics. In Circulation in the Gulf of Mexico: Observations and Models. AGU Geophysical Monograph Series 161: 181–201. Washington, D. C.: AGU.

Legovic, T., D. Petricioli, and V. Zutic. 1991. "Hypoxia in a pristine stratified estuary (krka, adriatic sea)." *Marine Chemistry* 32 (2-4):347-359. doi: 10.1016/0304-4203(91)90048-2.

Lentz, S. 2004. "The response of buoyant coastal plumes to upwelling-favorable winds." *Journal of Physical Oceanography* 34 (11):2458-2469. doi: 10.1175/jpo2647.1.

Lipton, D., and R. Hicks. 2003. "The cost of stress: Low dissolved oxygen and economic benefits of recreational striped bass (Morone saxatilis) fishing in the Patuxent River." *Estuaries* 26 (2A):310-315. doi: 10.1007/bf02695969.

MacKinnon, J. A., and M. C. Gregg. 2003. "Mixing on the late-summer New England shelf - Solibores, shear, and stratification." *Journal of Physical Oceanography* 33 (7):1476-1492.

McInnes, A. S., and A. Quigg. 2010. "Near-Annual Fish Kills in Small Embayments: Casual vs. Causal Factors." *Journal of Coastal Research* 26 (5):957-966. doi: 10.2112/jcoastres-d-10-00006.1.

Miles, J. W. 1961. "On the stability of heterogeneous shear flows." *Journal of Fluid Mechanics* 10 (4):496-508. doi: 10.1017/s0022112061000305.

Millerway, T., G. S. Boland, G. T. Rowe, and R. R. Twilley. 1994. "Sediment oxygen-consumption and benthic nutrient fluxes on the Louisiana continental-shelf - a methodological comparison." *Estuaries* 17 (4):809-815. doi: 10.2307/1352749.

Milliman, J. D., and R. H. Meade. 1983. "World-wide delivery of river sediment to the oceans." *Journal of Geology* 91 (1):1-21.

Mullins, R. L., S. F. DiMarco, J. Walpert, N. L. Guinasso, and Ieee. 2009. "Real-time Environmental Monitoring from a Wind Farm Platform in the Texas Hypoxia Zone." In *Oceans 2009, Vols 1-3*, 2477-2486.

Mullins, R. L., S. F. DiMarco, J. Walpert, and N. L. Guinasso, Jr. 2011. "Interdisciplinary Ocean Observing on the Texas Coast." *Marine Technology Society Journal* 45 (1):98-111.

Murrell, M. C., and J. C. Lehrter. 2011. "Sediment and Lower Water Column Oxygen Consumption in the Seasonally Hypoxic Region of the Louisiana Continental Shelf." *Estuaries and Coasts* 34 (5):912-924. doi: 10.1007/s12237-010-9351-9.

Nowlin Jr. W. D., A. E. Jochens, R. O. Reid, and S. F. DiMarco. 1998. Texas-Louisiana shelf circulation and transport processes study: synthesis report. Volume I: technical report. OCS study MMS 98-0035, U.S. Dept. of the interior, Minerals Management Service, Gulf of Mexico OCS region, New Orleans, LA.

Nowlin Jr. W. D., A. E. Jochens, S. F. DiMarco, R. O. Reid, and M. K. Howard. 2001. Deep water physical oceanography reanalysis and synthesis of historicalal data: synthesis report. OCS study MMS 2001-064, U.S. Dept. of the interior, Minerals Management Service, Gulf of Mexico OCS region, New Orleans, LA.

Nowlin Jr. W. D., A. E. Jochens, S. F. DiMarco, R. O. Reid, and M. K. Howard. 2005. Low-frequency circulation over the Texas-Louisiana continental shelf. Circulation in the Gulf of Mexico: observations and models, vol. 161. AGU Geophys Monogr Ser:219-40.

O'Donnell, J., H. G. Dam, W. F. Bohlen, W. Fitzgerald, P. S. Gay, A. E. Houk, D. C. Cohen, and M. M. Howard-Strobel. 2008. "Intermittent ventilation in the hypoxic zone of western Long Island Sound during the summer of 2004." *Journal of Geophysical Research-Oceans* 113 (C9). doi: C0902510.1029/2007jc004716.

Osborn, T. R. 1980. "Estimates of the local-rate of vertical diffusion from dissipation measurements." *Journal of Physical Oceanography* 10 (1):83-89. doi: 10.1175/1520-0485(1980)010<0083:eotlro>2.0.co;2.

Osterman, L. E., R. Z. Poore, P. W. Swarzenski, and R. E. Turner. 2005. "Reconstructing a 180 yr record of natural and anthropogenic induced low-oxygen conditions from Louisiana continental shelf sediments." *Geology* 33 (4):329-332. doi: 10.1130/g21341.1.

Paulmier, A., and D. Ruiz-Pino. 2009. "Oxygen minimum zones (OMZs) in the modern ocean." *Progress in Oceanography* 80 (3-4):113-128. doi: 10.1016/j.pocean.2008.08.001.

Pena, M. A., S. Katsev, T. Oguz, and D. Gilbert. 2010. "Modeling dissolved oxygen dynamics and hypoxia." *Biogeosciences* 7 (3):933-957.

Perlin, A., J. N. Moum, and J. M. Klymak. 2005. "Response of the bottom boundary layer over a sloping shelf to variations in alongshore wind." *Journal of Geophysical Research-Oceans* 110 (C10). doi: 10.1029/2004jc002500.

Peters, H., M. C. Gregg, and J. M. Toole. 1988. "On the parameterization of equatorial turbulence." *Journal of Geophysical Research-Oceans* 93 (C2):1199-1218. doi: 10.1029/JC093iC02p01199.

Pokryfki, L., and R. E. Randall. 1987. "Nearshore hypoxia in the bottom water of the northwestern Gulf of Mexico from 1981 to 1984." *Marine Environmental Research* 22 (1):75-90. doi: 10.1016/0141-1136(87)90081-x.

Quinones-Rivera, Z. J., B. Wissel, N. N. Rabalais, and D. Justic. 2010. "Effects of biological and physical factors on seasonal oxygen dynamics in a stratified, eutrophic coastal ecosystem." *Limnology and Oceanography* 55 (1):289-304. doi: 10.4319/lo.2010.55.1.0289.

Quinones-Rivera, Z. J., B. Wissel, D. Justic, and B. Fry. 2007. "Partitioning oxygen sources and sinks in a stratified, eutrophic coastal ecosystem using stable oxygen isotopes." *Marine Ecology Progress Series* 342:69-83. doi: 10.3354/meps342069.

Rabalais, N. N., R. E. Turner, Q. Dortch, D. Justic, V. J. Bierman, and W. J. Wiseman. 2002a. "Nutrient-enhanced productivity in the northern Gulf of Mexico: past, present and future." *Hydrobiologia* 475 (1):39-63. doi: 10.1023/a:1020388503274.

Rabalais, N. N., R. E. Turner, D. Justic, Q. Dortch, W. J. Wiseman, and B. K. Sen Gupta. 1999. Characterization of hypoxia: topic 1 report for the integrated assessment on hypoxia in the Gulf of Mexico. NOAA coastal ocean program decision analysis series, vol. 15. MD: Silver Spring.

Rabalais, N. N., R. E. Turner, and D. Scavia. 2002b. "Beyond science into policy: Gulf of Mexico hypoxia and the Mississippi River." *Bioscience* 52 (2):129-142. doi: 10.1641/0006-3568(2002)052[0129:bsipgo]2.0.co;2.

Rabalais, N. N., R. E. Turner, B. K. Sen Gupta, D. F. Boesch, P. Chapman, and M. C. Murrell. 2007. "Hypoxia in the northern Gulf of Mexico: Does the science support the plan to reduce, mitigate, and control hypoxia?" *Estuaries and Coasts* 30 (5):753-772.

Rabalais, N. N., R. E. Turner, and W. J. Wiseman. 2001. "Hypoxia in the Gulf of Mexico." *Journal of Environmental Quality* 30 (2):320-329.

Renaud, M. L. 1986. "Hypoxia in Louisiana coastal waters during 1983 - implications for fisheries." *Fishery Bulletin* 84 (1):19-26.

Roberts, J., and T. D. Roberts. 1978. "Use of butterworth low-pass filter for oceanographic data." *Journal of Geophysical Research-Oceans and Atmospheres* 83 (NC11):5510-5514. doi: 10.1029/JC083iC11p05510.

Rowe, G. T. 2001. "Seasonal hypoxia in the bottom water off the Mississippi River delta." *Journal of Environmental Quality* 30 (2):281-290.

Rowe, G. T., M. E. C. Kaegi, J. W. Morse, G. S. Boland, and E. G. E. Briones. 2002. "Sediment community metabolism associated with continental shelf hypoxia, Northern Gulf of Mexico." *Estuaries* 25 (6A):1097-1106. doi: 10.1007/bf02692207.

Scavia, D., D. Justic, and V. J. Bierman. 2004. "Reducing hypoxia in the Gulf of Mexico: Advice from three models." *Estuaries* 27 (3):419-425. doi: 10.1007/bf02803534.

Scavia, D., N. N. Rabalais, R. E. Turner, D. Justic, and W. J. Wiseman. 2003. "Predicting the response of Gulf of Mexico hypoxia to variations in Mississippi River nitrogen load." *Limnology and Oceanography* 48 (3):951-956.

Scully, M. E. 2010a. "The Importance of Climate Variability to Wind-Driven Modulation of Hypoxia in Chesapeake Bay." *Journal of Physical Oceanography* 40 (6):1435-1440. doi: 10.1175/2010jpo4321.1.

Scully, M. E. 2010b. "Wind Modulation of Dissolved Oxygen in Chesapeake Bay." *Estuaries and Coasts* 33 (5):1164-1175. doi: 10.1007/s12237-010-9319-9.

Scully, M. E., C. Friedrichs, and J. Brubaker. 2005. "Control of estuarine stratification and mixing by wind-induced straining of the estuarine density field." *Estuaries* 28 (3):321-326. doi: 10.1007/bf02693915.

Simpson, J. H., J. Brown, J. Matthews, and G. Allen. 1990. "Tidal straining, density currents, and stirring in the control of estuarine stratification." *Estuaries* 13 (2):125-132. doi: 10.2307/1351581.

Solis, R. S., and G. L. Powell. 1999. Hydrography, mixing characterisctics, and residense times of Gulf of Mexico estuaries. Biochemistry of Gulf of Mexico estuaries, 29-61. New York: John Wiley and Sons.

Sturges, W., and R. Leben. 2000. "Frequency of ring separations from the loop current in the Gulf of Mexico: A revised estimate." *Journal of Physical Oceanography* 30 (7):1814-1819. doi: 10.1175/1520-0485(2000)030<1814:forsft>2.0.co;2.

Thronson, A., and A. Quigg. 2008. "Fifty-five years of fish kills in coastal Texas." *Estuaries and Coasts* 31 (4):802-813. doi: 10.1007/s12237-008-9056-5.

Turner, R. E., and N. N. Rabalais. 1994. "Coastal eutrophication near the mississippi river delta." *Nature* 368 (6472):619-621. doi: 10.1038/368619a0.

Turner, R. E., N. N. Rabalais, and D. Justic. 2006. "Predicting summer hypoxia in the northern Gulf of Mexico: Riverine N, P, and Si loading." *Marine Pollution Bulletin* 52 (2):139-148. doi: 10.1016/j.marpolbul.2005.08.012.

Turner, R. E., N. N. Rabalais, and D. Justic. 2008. "Gulf of Mexico hypoxia: Alternate states and a legacy." *Environmental Science & Technology* 42 (7):2323-2327. doi: 10.1021/es071617k.

Turner, R. E., N. N. Rabalais, E. M. Swenson, M. Kasprzak, and T. Romaire. 2005. "Summer hypoxia in the northern Gulf of Mexico and its prediction from 1978 to 1995." *Marine Environmental Research* 59 (1):65-77. doi: 10.1016/j.marenvres.2003.09.002.

Ulloa, O., and S. Pantoja. 2009. "The oxygen minimum zone of the eastern South Pacific." *Deep-Sea Research Part Ii-Topical Studies in Oceanography* 56 (16):987-991. doi: 10.1016/j.dsr2.2008.12.004.

Kiselkova, V. 2008. "Effect of instabilities in the buoyancy-driven flow on the bottom oxygen: applications to the Louisiana Shelf." PhD diss., Texas A&M University.

Waldhauer, R., A. F. J. Draxler, D. G. McMillan, C. A. Zetlin, S. Leftwich, A. Matte, and J. E. Oreilly. 1985. "Biological, physical and chemical-dynamics along a new-york bight transect and their relation to hypoxia." *Estuaries* 8 (2B):A129-A129.

Wang, W., W. D. Nowlin, and R. O. Reid. 1998. "Analyzed surface meteorological fields over the northwestern Gulf of Mexico for 1992-94: Mean, seasonal, and monthly patterns." *Monthly Weather Review* 126 (11):2864-2883. doi: 10.1175/1520-0493(1998)126<2864:asmfot>2.0.co;2.

Wei, H., Y. C. He, Q. J. Li, Z. Y. Liu, and H. T. Wang. 2007. "Summer hypoxia adjacent to the Changjiang Estuary." *Journal of Marine Systems* 67 (3-4):292-303. doi: 10.1016/j.jmarsys.2006.04.014.

Welsh, B. L., and F. C. Eller. 1991. "Mechanisms controlling summertime oxygen depletion in western long-island sound." *Estuaries* 14 (3):265-278. doi: 10.2307/1351661.

Williams, P. J. L., and N. W. Jenkinson. 1982. "A transportable microprocessor-controlled precise winkler titration suitable for field station and shipboard use." *Limnology and Oceanography* 27 (3):576-584.

Wiseman, W. J., N. N. Rabalais, R. E. Turner, S. P. Dinnel, and A. MacNaughton. 1997. "Seasonal and interannual variability within the Louisiana coastal current: stratification and hypoxia." *Journal of Marine Systems* 12 (1-4):237-248. doi: 10.1016/s0924-7963(96)00100-5.

Wong, K. C. 1990. "Sea-level variability in long-island sound." *Estuaries* 13 (4):362-372. doi: 10.2307/1351781.

Yin, K. D., Z. F. Lin, and Z. Y. Ke. 2004. "Temporal and spatial distribution of dissolved oxygen in the Pearl River Estuary and adjacent coastal waters." *Continental Shelf Research* 24 (16):1935-1948. doi: 10.1016/j.csr.2004.06.017.

Zhang, X. Q., S. F. DiMarco, D. C. Smith, M. K. Howard, A. E. Jochens, and R. D. Hetland. 2009. "Near-Resonant Ocean Response to Sea Breeze on a Stratified Continental Shelf." *Journal of Physical Oceanography* 39 (9):2137-2155. doi: 10.1175/2009jpo4054.1.

Zhang, X. Q., D. C. Smith, S. F. Dimarco, and R. D. Hetland. 2010. "A Numerical Study of Sea-Breeze-Driven Ocean Poincare Wave Propagation and Mixing near the Critical Latitude." *Journal of Physical Oceanography* 40 (1):48-66. doi: 10.1175/2009jpo4216.1.